Master Thesis of Science

Modelling Soil Damping for Suction Pile Foundations

TU Delft

Priyanka Raikar

September, 2016

SPT Offshore

Modelling Soil Damping for Suction Pile Foundations

MASTER OF SCIENCE THESIS

For the degree of Master of Science in Offshore and Dredging Engineering at Delft University of Technology

Priyanka Raikar

September 29, 2016

TU Delft Faculty of Mechanical, Maritime and Materials Engineering (3ME)

The work in this thesis was sponsored by SPT Offshore. Their contribution is hereby gratefully acknowledged.

Cover photo courtesy of SPT Offshore

Summary

In pursuit of saving mother nature, man has been extending his boundaries to find renewable sources of energy. Wind being one of them, has been exploited in the past years with offshore wind gaining high popularity in the recent years. Owing to the high capital costs of the offshore wind sector, research has been directed to focus on technology and science that could ultimately contribute in cost reduction of offshore wind projects. One such science is the mechanism of damping.

Damping, which is often described as 'dissipation of energy stored in a dynamic system', can indirectly play an important role in determining the structural configuration of the support structure and the foundation of an offshore wind turbine. A higher value of overall damping can be associated with either an increase in fatigue life or a reduction in overall structural weight. In both the cases there is significant aid to foundation cost cutting.

Currently, a typical value of 2-3% (of critical) is used within the industry as an overall damping estimate with little understanding about the contribution of soil damping. This thesis focusses on developing a methodology to compute soil damping coefficients for the case of suction pile foundations, using PLAXIS, an advanced geotechnical software. The developed method is further applied to a Suction Installed Wind Turbine (SIWT) structure, in order to find the soil damping in form of modal damping percentage.

The thesis objective is tackled by using two case studies from projects executed by SPT Offshore. The first case study proposed a method to calculate the vertical damping coefficient (C_v) for an individual suction pile from the phase-shift calculated from forced vibration analysis conducted in PLAXIS. Two interesting conclusions were drawn from this case-study;

- C_v increased with an increase in the forcing amplitude. This effect was justified by the fact that higher force amplitudes correspond to higher strain amplitudes which further corresponds to higher values of the soil damping ratio.
- C_v decreased with increasing loading frequency (ω), while the product of C_v and ω increased with increasing ω. The observed nature of these plots seemed to comply with existing literature and experimental data. However, the accuracy of

the value of C_v is highly dependent on the PLAXIS outputs and hence adequate validation of the PLAXIS output was highly recommended.

The second case study implemented the proposed methodology (of the first case study) to a SIWT structure in order to calculate the modal soil damping percentage for the first two modes of the structure using modal analysis. The results when compared with logarithmic decrement percentages, gave similar estimates. The found influence of soil on the damping of this particular structure (modal soil damping in the range of 5-7%) was significantly larger than the order of magnitude used in the industry today. However, one should realize that the modal soil damping percentage is highly sensitive to C_v derived from PLAXIS and hence in depth investigation of the PLAXIS model is highly recommended.

The applicability of the modal analysis method for the second case-study was mainly justified since the generalized damping matrix $\boldsymbol{C}_{gen}$ was diagonalizable for the considered mode shapes. Moreover, this method allowed for straightforward reuse of undamped eigen frequencies and mode shapes, which was fairly easy to obtain with a standard eigen solution software.

Acknowledgements

I would like to express my gratitude to my thesis committee;

Marijn, my daily supervisor, for guiding me so well throughout my thesis and answering all my doubts with patience.

OJ for giving me the opportunity to do my thesis at SPT Offshore and for encouraging me to enjoy the process more than the end result.

Dr. Joao for giving me sufficient time and the critical discussions we had during our meetings.

Dr. Metrikine for his valuable inputs and especially for teaching Structural dynamics so well that I could build my thesis around it.

Dr. Federico for assuring the quality of my thesis content and his lectures, for making me understand soil better.

Furthermore, I would like to thank my colleagues at SPT Offshore for always being interested and enthusiastic about my thesis.

Francisco Marques from PLAXIS helpdesk requires a special mention for solving my queries on time.

Finally, I would also like to thank my parents for their love and support. Special thanks to my friend Ewoud for his constant support and critical comments on my thesis.

"Nine months of master thesis and I am reborn"

-Priyanka Raikar

Table of Contents

List of Figures

1 Introduction

This chapter begins with the motivation behind this thesis topic. The subjects under motivation form the foundation steps leading to the main problem statement. Under the second section of this chapter, the objective is formulated along with the approach and scope. Finally, the chapter ends with an easy-to-follow reading guide to make this report a comfortable read.

1.1 Motivation

In pursuit of saving mother nature, man has been extending his boundaries to find renewable sources of energy. Wind being one of them, has been exploited in the past years with offshore wind gaining high popularity in the recent years. Owing to the high capital costs of the offshore wind sector, research has been directed to focus on technology and science that could ultimately contribute in cost reduction of offshore wind projects. One such science is the mechanism of damping, which could indirectly play an essential role in the cost cutting.

The following subtopics are the foundation steps leading to the main subject.

1.1.1 Offshore Wind Industry: The future

In 2007 the European Commission introduced the 2020 package which is a set of binding legislation to ensure the EU meets its climate and energy targets for the year 2020. The package sets three key targets:

- 20% cut in greenhouse gas emissions (from 1990 levels)
- **20% of energy from renewables**
- 20% improvement in energy efficiency

According to the EU 2020 target, 230GW (of which 40GW offshore) needs to be achieved from wind energy in order to produce 581 TWh of electricity, meeting 15.7% of electricity consumption (estimated EU electricity consumption for 2020 is 3689.5TWh).

Offshore wind in Europe currently represents one of the most stable sources of renewable energy. The current installed capacity of offshore wind is now capable of producing approximately 40.6 TWh in a normal wind year which covers around 1.5% of the EU electricity consumption(EWEA 2015). The figure below gives the offshore wind installed capacity for each contributing country for the year 2015.

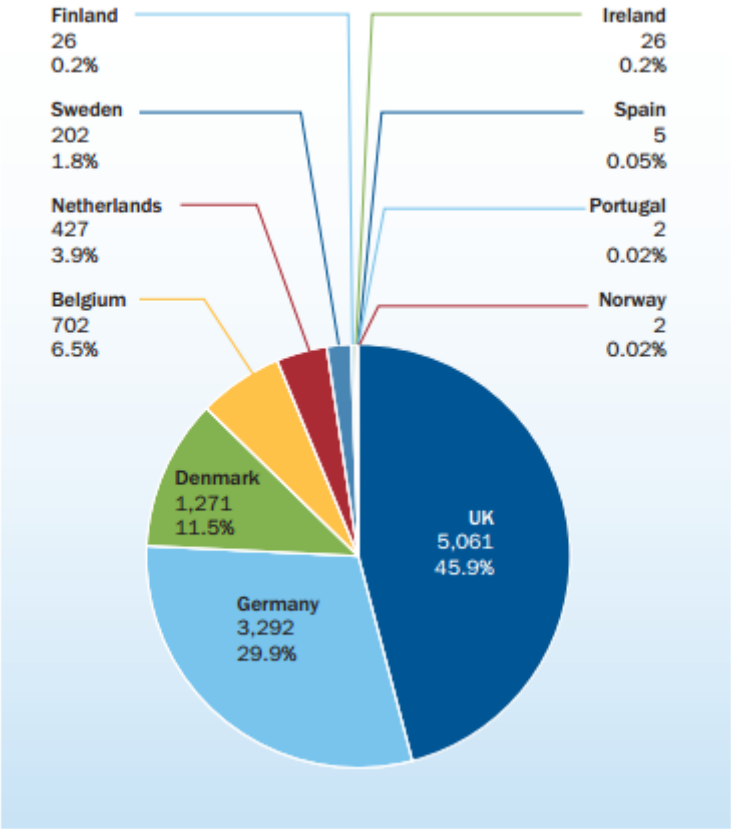

Figure 1 Installed capacity -cumulative share by country in MW; Source : EWEA European offshore statistics 2015(EWEA 2015)

An increased energy capture of offshore wind is expected due to Europe's leading position in offshore wind R&D. More than **1250 scientific publications** were published on offshore wind in Europe between 1994 and 2010 (Wieczorek et al. 2013). European governments and private companies invest significant sums in R&D and have built a leadership position in the offshore wind market. SPT offshore being one of them, invests in research on suction pile foundations for offshore wind structures.

The bright future of the offshore wind industry relies largely on innovation of the existing technology and thus provides the necessary motivation for the author to dig deeper into the subject.

1.1.2 Damping: A boon

Offshore wind might have a bright future provided it conquers one of its biggest challenges: the relatively high levelized cost of electricity (LCOE). The costs of offshore foundations, construction, installations and grid connection are significantly higher than for onshore. For example, offshore turbines are generally 20% more expensive and towers and foundations cost more than 2.5 times the price of a similar onshore project(Association 2009).The cost breakdown for an OWTG is shown below;

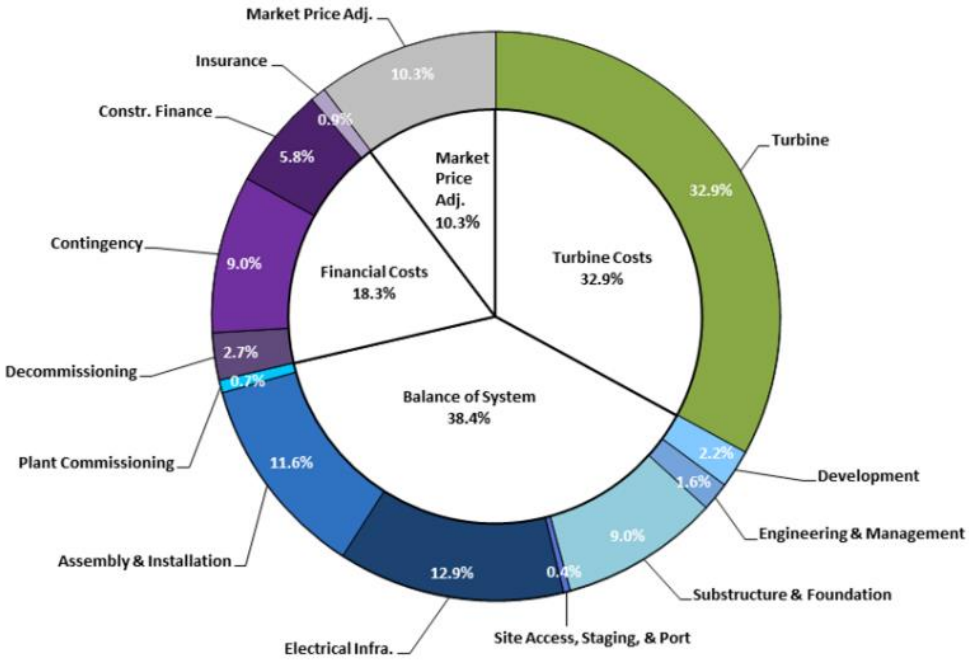

Figure 2 Cost breakdown of an OWTG; Source: (NREL 2014)

The **foundation cost** contributes to around **9% of the total cost**. Any contribution towards reduction of the foundation cost could be beneficial.

Damping, which is often described as '**dissipation of energy stored in a dynamic system**', can indirectly play an important role in determining the structural configuration of the support structure and the foundation. A higher value of overall damping can be associated with the following **either ways**;

- **Increase in fatigue life**

  The Offshore wind turbine structure (OWTS) is designed to survive at least 20 years of harsh environmental conditions. In many cases, the fatigue

lifetime is a crucial design driving factor. The fatigue damage in steel is a function of the number of loading cycles at a particular stress range during the structure's lifetime. The S-N curve formula is given by;

$$N = \frac{a}{S^m}$$

Where N is the fatigue life, S is the stress range and both a and m depend on the material. For steel m, mainly ranges from 3 to 5 (Veritas 2010).

Thus in the most conservative case, fatigue life is inversely proportional to the cube of the stress amplitude. **Reduction in the stress amplitude leads to a cubic increase in fatigue life.** Higher value of damping lead to reduction in stress amplitudes and thus favors increment of fatigue life.

- **Structural weight reduction**

  The steel sections are designed based on the loading/stress amplitude. Larger the value of stress, bigger the section. Reduction in stress amplitude due to increased damping could further reduce the steel sections, leading to reduction in structural weight.

In **either of the cases** there is significant **aid to foundation cost cutting**.

1.1.3 Why focus on soil damping?

Acknowledging the benefits of damping, one needs to further examine various forms of damping experienced by an OWTS. Following are the different damping mechanisms faced by OWTS(Versteijlen 2011);

- **Aerodynamic damping:** caused due to the turning rotor and due to the movement of tower in the air.
- **Sloshing damper:** a recently developed damping mechanism which uses tuned counter moving mass to dampen the vibrations.
- **Structural damping**: structural vibrations cause friction in the micro-cracks of the steel leading to energy dissipation in the form of heat.
- **Hydrodynamic damping:** radiation as well as viscous damping offered by the fluid around the OWTS.

- **Soil Damping**: a combined phenomenon of radiation as well as material damping in soil.

According to (Lloyd 2005), the structural, hydrodynamic and soil are grouped together into additional offshore damping $D_{add,offsh}$(as fraction of critical damping);

$$D_{add,offsh} = D_{radiation,hydro} + D_{viscous,hydro} + D_{steel} + D_{soil}$$

The document states that soil damping contributes with the biggest share of damping while it also creates the highest uncertainty as it presently results in the largest differences between theoretical solutions and measurements. For monopiles, the value may range from 0.56% to 0.87 %.

The ISO : 19902:2007 (DIN 2007)code for fixed steel offshore structures states that in the absence of substantiating information for damping values for a specific structure, a damping coefficient of **2 % to 3 % of critical** may be used for the global dynamic analyses in extreme wave conditions. There is no definite mention for the contribution of soil damping and **a scientifically proven damping value thus attracts the research focus.**

1.1.4 Why this topic?

The USP of this thesis lies in the fact that it addresses two progressive ideas in the offshore wind industry -**suction pile foundation** and **jacket support structure**.

- **Suction pile foundation**

  Until now the researches have been mainly devoted to monopile structures where the pile is idealized to behave like a bending beam while interacting with the soil. Very limited knowledge is available on the soil-structure interaction of other foundation types, especially suction piles. Owing to their structural configuration, suction piles more or less behave like rigid bodies. Applying the science of flexible piles to the so called 'rigid' suction piles for soil structure interaction could lead to an improper analysis.

Hence a thorough study of soil-structure interaction for suction pile foundation needs serious attention.

- **Jacket support structure**

  With increasing demand for offshore wind, offshore wind farms have moved further from shore and into deeper waters. Monopiles may not be the most practical option in deeper waters and thus a number of support structure concepts are being investigated. The **jacket substructure** concept, being one them, seems to **perform very well** in the transition-water depth due to its comparably lighter structural mass, while exhibiting **higher transparency** to the wave loading, **greater structural stiffness**, and **lower soil dependency**(De Vries 2011). However the installation at greater water depths poses greater challenges ,not only in the technical and practical aspects, but also in the viability of the overall technology to lower the cost of energy in the current ,highly-competitive energy market(Chew et al. 2014).

This thesis combines the two by studying the damping caused due to soil-structure interaction of the suction piles that support the offshore jacket support structure. SPT offshore offers the offshore jacket support structure concept under the name Self Installing Wind Turbine (SIWT). The Figure 3 depicts the SIWT model;

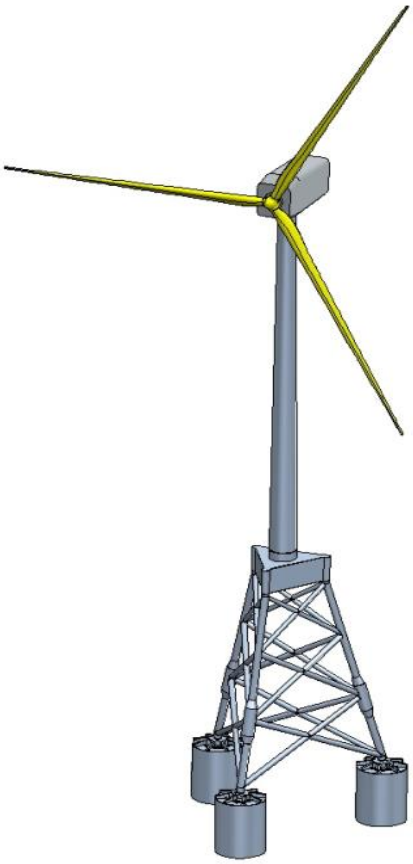

Figure 3 Self Installing Wind Turbine; Source: SPT Offshore

1.2 The 'Thesis'

This section gives insight into the thesis by describing the problem statement, objective, approach and scope of the thesis. With an aim to ease the maneuvering over this thesis report, an easy to follow report guide had been attached in the end.

1.2.1 Problem Definition

With offshore wind farms moving to deeper waters, a huge responsibility lies with the engineers to design substructures and foundations that fulfill the three important aspects: **Economic feasibility**, **Installation viability** and **Structural serviceability**. SPT's SIWT is one such concept which has a great potential in fulfilling the aforementioned aspects.

The suction piles at the foundation of the SIWT, provide huge benefits in terms of **fast** and **noise free installation** and **decommissioning** of offshore structures. An untapped potential of the SIWT could be the damping offered by the Soil-structure interaction (SSI). Currently SPT uses 2-3% of damping for the entire structure while it is unclear how large the contribution of soil damping exactly is.

SSI of the suction pile is yet considered to be an area of significant uncertainty. The existing knowledge available on SSI of flexible piles is questionable in its application to rigid foundations like suction piles. Therefore, a better understanding of the damping behavior of rigid structures such as suction pile is much needed.

1.2.2 Thesis objective

The objective of this thesis is to develop a methodology to calculate the soil damping coefficients using PLAXIS and further apply it for the case of SIWT structure to find the soil damping in the form of modal damping.

1.2.3 Approach

A brief overview of the approach can be seen in Figure 4. To promote clear understanding of the content and the process, the author believes in backing up the theory with examples and hence two case studies are considered from SPT Offshore's project database.

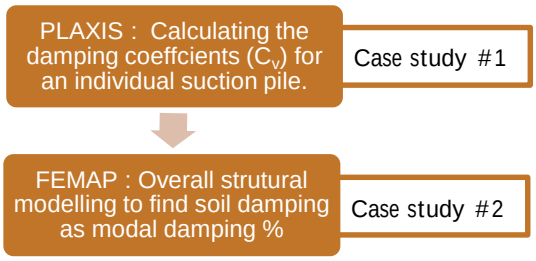

Figure 4 Thesis approach overview

- **Case study 1:** To study how PLAXIS works with soil dynamics and to get damping coefficient for a single suction pile.

  This case study is used to study and show the working of PLAXIS in a dynamic setting. A method is hence developed to calculate the damping coefficients using PLAXIS output data.

- **Case study 2**: To implement the developed method to a SIWT and to find modal soil damping (%) for the first two modes of the structure using modal analysis.

  The SWIT is relatively a **stiffer structure**. It responds to the lateral loading of the wind turbine with its 'push-pull' mechanism. With the 'push-pull' action at its foundation, the suction piles are dominantly exposed to **vertical vibrations**. In order to ease the complexity of the problem, only vertical motion of the suction piles has been considered. Hence each individual pile has been idealized as a **single degree of freedom system**.

  Forced vibration analysis is carried out on a single suction pile in **PLAXIS,** an advanced geotechnical FEM based software. The frequency of vibration is chosen close to the first Eigen frequency of the SIWT (the first two modes have same frequency due to symmetry of the structure). The output is analyzed to give the **phase-shift** with respect to the harmonic vertical forcing. **Vertical damping coefficient** is then derived from this phase-shift.

The entire structure is modelled in **FEMAP** (a FEM based structural analysis software) and using modal analysis, a method to calculate modal soil damping (%) for the first two modes of a SIWT is developed.

1.2.4 Scope

The scope of the thesis is as follows;

- This thesis only deals with vertical degree of freedom. In theory, the method can be used to find all the damping coefficients for vertical (V), horizontal (H) and rotation (M) mode of the suction pile, including the coupled terms (H-M) (refer Appendix D). Although in practice, the calculation of the coupled terms requires more development in the current software.
- Both the case studies mostly deal with clayey soil and hence undrained analysis has been studied and used in PLAXIS.
- The assumption of idealizing the suction pile as a single degree of freedom system was viable in the case of SIWT due to the dominant 'push-pull' mechanism shown by the structure. For flexible structures, all the three degrees of freedom (VHM) for suction pile will have to be considered.
- Since the main focus of the thesis is on soil damping, hence predefined foundation loads (calculated from wind and wave loading) has been used directly.

1.2.5 Report structure

The report structure is as follows;

Chapter 1

- This chapter discusses the motivation, objective ,scope and approach of the thesis.

Chapter 2

- The chapters covers the literature study on jacket substructure, suction foundations and soil damping.

Chapter 3

- Relevant features of the PLAXIS software used for the case-studies is explained in this chapter for a clear understanding of the back end.

Chapter 4

- Case-study #1 which deals with deriving a method to calculate the damping coeffcient using PLAXIS , is presented in this chapter.

Chapter 5

- This chapter discusses Case study #2 in which a methodeology is derived for calculating the modal damping of SIWT structure.

Chapter 6

- Conclusions along with reccomendations for future research is presented in this chapter.

2 Literature Study

Soil damping in a three legged jacket structure with suction pile as its foundation forms the core of this thesis. This chapter is dedicated to the literature study carried out on the three important topics (from top to bottom): Jacket Substructure, Suction Pile Foundation and Soil Damping.

2.1 Jacket Substructure

The jacket substructure for offshore wind applications is gaining quite some popularity in the recent years due to the wide range of benefits it could potentially offer. The sections below discuss these benefits by first comparing it to an existing substructure concept-the monopile and then providing good reasoning as to why a symmetric three legged jacket was chosen for the SIWT concept. The section also provides in-depth information on SIWT.

2.1.1 Support structure: Offshore Wind

Support structure can be defined as the structure that supports the turbine and holds it in place and transfers the loads from turbine to the ground. The three main components of the support structure include;

- Tower: supplied by the turbine manufacturer
- Substructure: part of structure between the tower and the seabed
- Foundation: part which is directly in contact with the soil

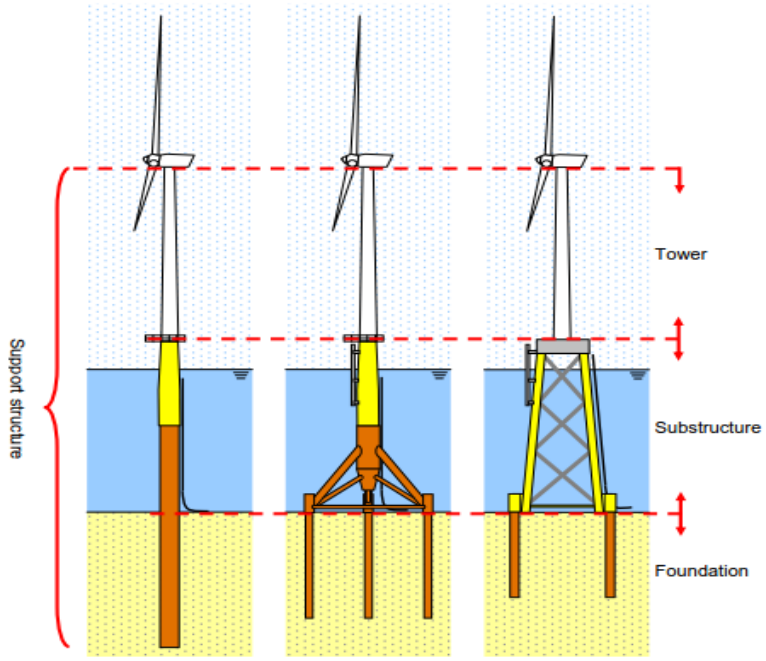

Figure 5 Definition of 'support structure' and main components, Source:(De Vries 2011)

The loading regime for offshore wind turbine(OWT) structures is dominated by cyclic lateral loading and bending moments while vertical and torsion loading dominate in case of offshore oil and gas structures. For instance, in contrast to oil and gas structures, the dead weight of the OWT is so small that resulting horizontal load from wind and sea state can reach up to 150% of the vertical loading(Lesny 2010).

Dynamic considerations for the design of the OWT are crucial to the structure. As a result of their slender nature, offshore wind-turbines are dynamically sensitive at low frequencies, the first modal frequency of the system (less than 1Hz) being very close to the excitation frequencies imposed by environmental and mechanical loads(Bhattacharya et al. 2013). The designer is usually provided with the load frequency graph like the one below;

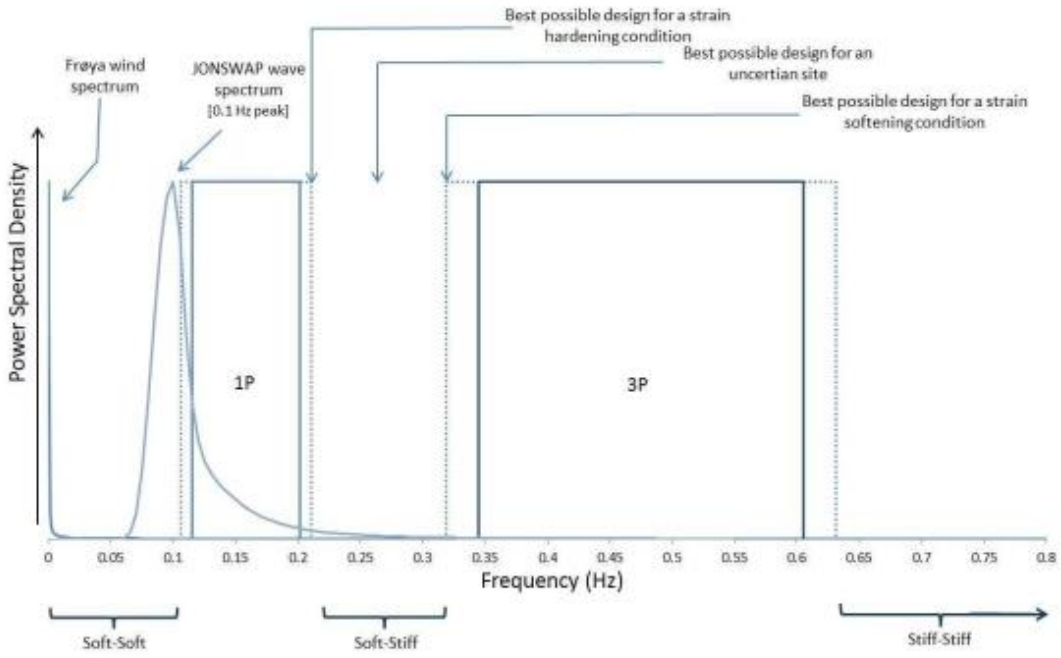

Figure 6 Forcing frequencies plotted against the power spectral densities for a 3 bladed NREL standard 5W Wind turbine. 3P stands for blade passing frequency; Source : (Bhattacharya et al. 2013)

In the figure, 1P interval is the range of the minimum and maximum rotational speed, while 3P refers to the three blade passing frequency interval (=3 x interval of 1P).

The OWT requires a design such that its global frequency lies outside the load frequency ranges in order to avoid resonance. The DNV Guideline (2002) also specify that the global frequency of the system should be at least $\mp 10\%$ away from operational 1P and 2P/3P frequencies, as indicated by the dotted lines in Figure 2. This leaves the designer with three options;

- **Soft-soft**

  Design concepts that have very low natural frequency. Only extremely low stiffness can make it achievable which might not be practical for extreme aerodynamic and hydrodynamic loads. Soft-soft solutions for bottom-mounted offshore structures have so far been applied mainly in the offshore oil & gas industry whereas soft-soft solutions in the offshore wind industry have mainly been discussed in relation to floating structures.

- **Soft-stiff**

  Most of the OWT structures lie within this interval because it ensures safe distance from the frequency range of high wave energy contents as well as a sufficiently high stiffness of the structure.

- **Stiff-stiff**

  Structures having natural frequency beyond the 3P interval lie in this range. The support structure is required to be extremely stiff resulting in significantly larger amounts of material compared to soft-stiff design.

One also needs to pay attention to the fact that the natural frequency of a OWT changes with cycles of loading. The reason being: alteration in foundation stiffness due to strain hardening or strain softening behavior of soil supporting the foundation. (Bhattacharya et al. 2013) drew main conclusions from the past study and summarized it as follows;

- For strain-hardening sites (for example, loose to medium dense sand) where the stiffness of the soil increases with cycles of loading, the natural frequency of the overall system will increase. (referring to drained loading conditions)
- For strain-softening sites (clay sites) where the stiffness of the soil may decrease with cycles of loading, the natural frequency of the overall system will also decrease correspondingly. Of course, this depends on the strain level

in the soil next to the pile and the number of cycles. (referring to undrained loading condition)

Overall soft-stiff interval seems to be the most amicable option and hence SIWT is designed within the limits of this frequency interval.

2.1.2 The Reign of Monopiles

A monopile is a simple structure, made of cylindrical steel tube, which is often used to support the wind turbine tower, either directly or through a transition piece. The structural capacity is achieved from its penetration depth, which is adjusted to suit the actual environment and sea bed conditions. It is installed by either lifting or floating the structure into position and then driving it into the seabed using a steam/hydraulic powered hammer. The handling of piles and hammers requires the use of crane vessel (revolving or shear leg crane), while jack-up are the most commonly used vessels for installation of the monopiles in general. A typical monopile structure has been shown in the figure below (refer Figure 7;

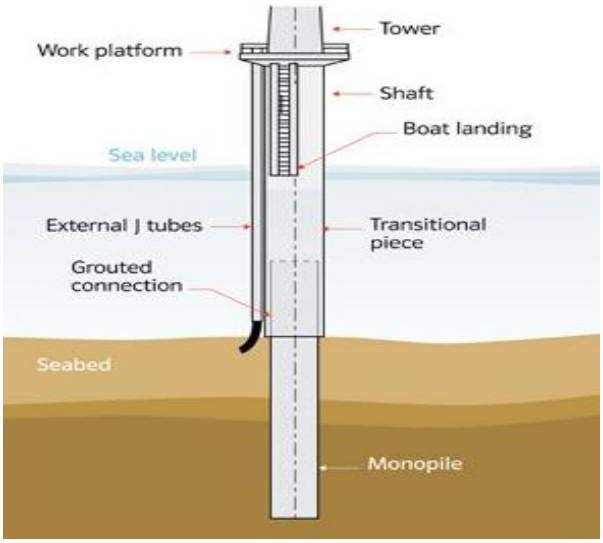

Figure 7 Monopile Foundation; Source: 4C Offshore

Monopile has ruled the offshore wind industry due to its relatively simple design and ease of installation in shallow to medium water depths (0-30m). The annual report commissioned by EWEA for year 2015 clearly highlighting the monopile's reign can be seen in Figure 8;

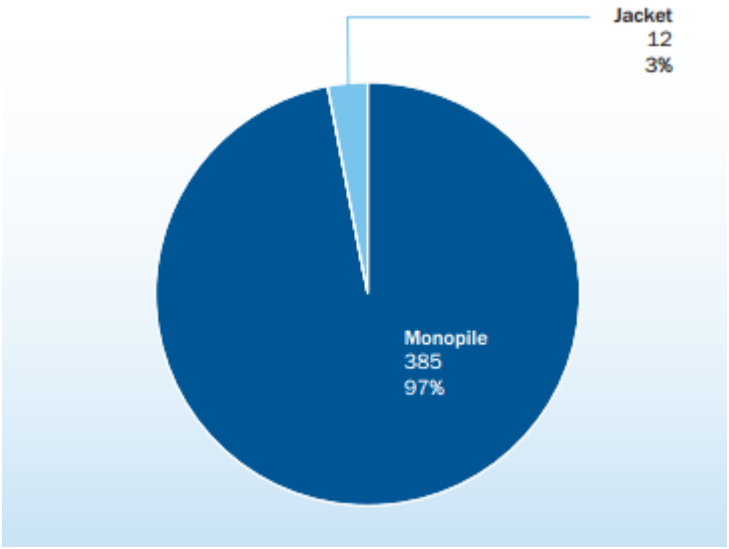

Figure 8 Foundation types share of 2015 annual market; Source: European Offshore Statistics 2015, EWEA

Monopile substructures remain by far the most popular substructure type.

2.1.3 Jacket substructure: The possible game changer

A jacket substructure consists of minimum three legs connected by slender braces, making it a highly transparent structure. The load transfer is mainly in the axial direction. This concept is an extension of the traditional offshore jackets used in the oil and gas industry. The substructure can possibly have four foundation options;

- Piles driven through the pile sleeves at the base of the jacket
- Piles driven from the top, through the jacket legs
- Suction pile foundations
- Gravity base

The large base of the jacket offers a large resistance to the overturning moment. The structure is assembled by welding the prefabricated tubulars together at the fabrication yard. Most commonly it is installed by transporting it to the offshore location on a barge and upending or lifting the structure to its upright position. The piles are then driven into the seabed. In case of jackets with suction foundation, the suction piles are welded prior to positioning the jacket on the seabed. Once on the seabed, the suction piles first penetrate due to the self-

weight of the structure and later due to water being pumped (facilitated by individual pumps on the piles) out of the suction piles.

12 jacket foundations were installed in 2015, representing 3% of all newly installed substructures (EWEA-European Offshore Statistic,2015).

2.1.4 Deep waters: The trouble maker

This sub section discusses the viability of conventional monopile and jacket substructure in deeper waters.

Monopiles have served as reliable and cost effective support structures for offshore wind turbines at shallow water depths (up to 30 m). The limiting condition of this type of support structure is the overall deflection and vibration, when subjected to large cyclic lateral loads and moments caused due to current and wave loads. The loads are subsequently transferred laterally to the soil. Sufficient stiffness for the monopile comes from its diameter. Then again, larger diameter attracts relatively high hydrodynamic loads.

With increasing water depth, the overturning moment experienced by the structure increases. This leads to thicker sections of the monopile , which is not very convenient, both from an economic point of view and in relation to practical aspects such as fabrication and installation(De Vries 2011).

Jackets on the other hand allow for relatively light and efficient construction. With a positive testimony from the oil and gas industry, jacket structures have performed well in greater water depth up to about 520 m.

2.1.5 Why a Three Legged Jacket (TLJ)?

In the UP Wind report published by (De Vries 2011), a comparison on overall required structural mass and hydrodynamic loads was made between different soft-stiff substructure concepts for a water depth of 50m. The substructures were- monopile, monopile truss hybrid, tripod, TLJ and FLJ. The results are shown in the figure below;

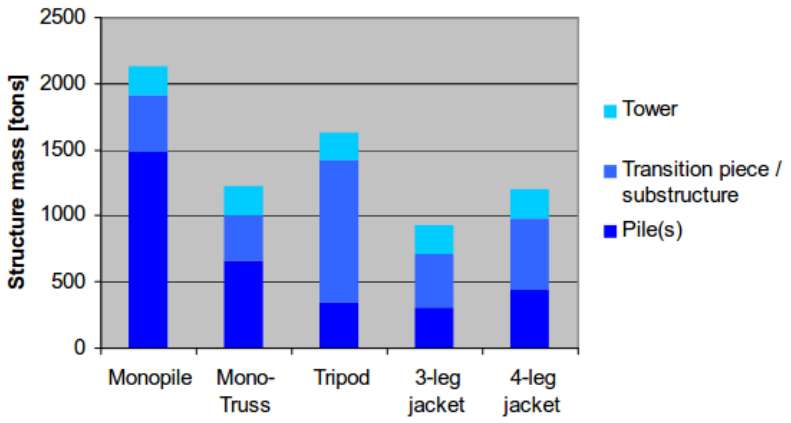

Figure 9 Overview of structural mass for the five concepts Source:(De Vries 2011)

The TLJ concept had the lowest structural mass among the other concepts.

More recently in a parametric study comparing TLJ with four legged jackets conducted by (Chew et al. 2014), the following points were reinforced in favor of the TLJ structure ;

- For similar base radius and load conditions, the TLJ had its first and higher-mode natural frequencies outside the excitation frequencies interval.
- Reduction of the structural mass requirement. (Approximate reduction of 17% for the parametric study)
- Reduction in the number of welded joints. (Around 25% for the parametric study)

SPT Offshore had also performed a feasibility study on a wind turbine substructure design with suction pile foundations for OWT applications in water depths from 25 m to 55 m. TLJ was chosen for SIWT concept design as the most suitable and serviceable design. The design considerations that led to this choice are as follows;

- **Symmetric shape:** allows for equal distribution of environmental load and relatively clear dynamic behavior (making it less sensitive to fatigue).
- **Tripod structure:** statically determinate and hence less sensitive to irregular seabed or non-uniform soil conditions. It allows for easier vertical

position control during installation without inducing detrimental stresses in the structure.

- **Reduced mass:** minimum no of legs leads to the least possible structural mass along with a reduction in total number of joints.

Overall, the TLJ can be more cost efficient support structure design in the transition water depth.

2.1.6 Suction Installed Wind Turbine (SIWT)

The SIWT concept is basically a symmetric three legged jacket substructure founded on three identical suction piles. The important features of this concept are discussed below;

- **Easy offshore installation**

  SIWT can be fully assembled and commissioned in yard. The transportation and installation is described in four easy steps using real captures of first ever installed SIWT concept in Borkum Riffgrund 1 windfarm project;

Step 1

Towing to the field (The SIWT is suspended partly by the sea fastening and grillage on the barge and partly by the twin cranes)

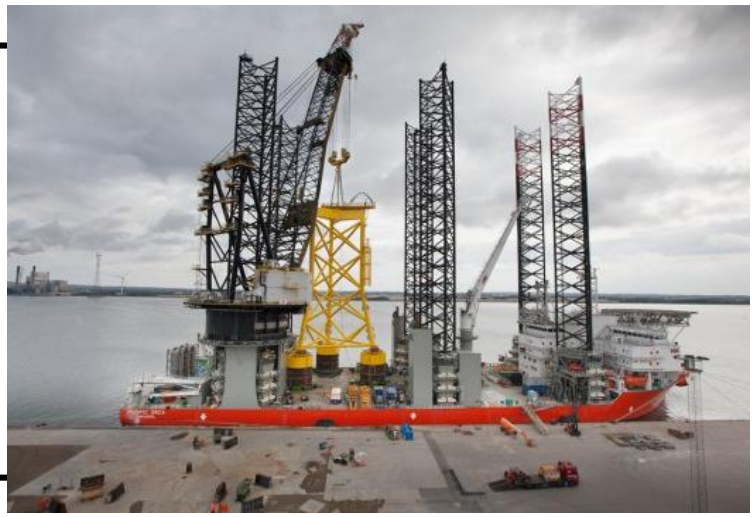

Source: SPT Offshore

Step 2

Positioning and lowering to the seabed

Source: SPT Offshore

Step 3

Installing the suction piles

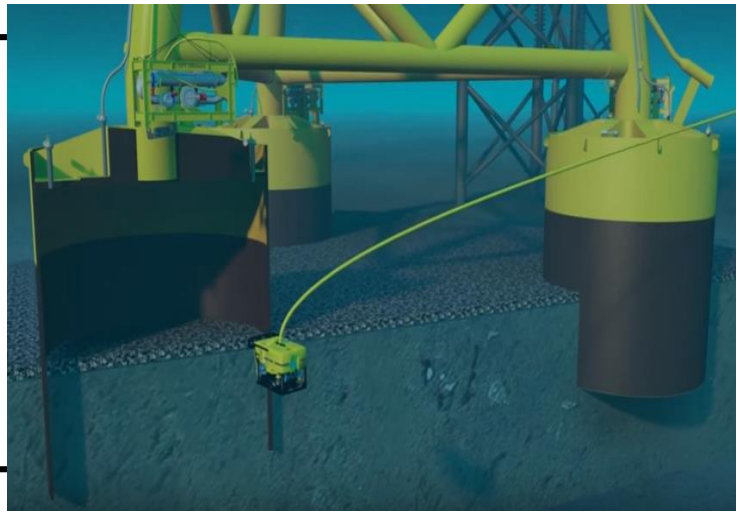

Source: SPT Offshore

Step 4

Disconnecting the rigging

Source: SPT Offshore

- **Maximum water depth of 60m**

  The SIWT design is well suited for water depths ranging from 30 to 60 m that are difficult to achieve using conventional monopile sub structure.

- **Easy decommissioning**

  For decommissioning the entire process can be simply reversed. Water can be pumped into the suction piles creating the required uplift force for the SIWT to be easily removed in one piece, leaving nothing behind.

- **Noise-free installation**

  Piling in general involves hammering for driving the piles into the seabed. The hammering mechanism leads to noise pollution creating nuisance for the marine life. Suction piles on the other hand use suction pressure as the driving force which is indeed noise free. Projects that involve pile hammering need to ensure that they lawfully abide by the noise regulations set up by various certifying bodies. Nowadays additional investments are being made in noise mitigation systems adding to the installation costs. SIWT hence provides a better solution to noise related issues.

The SIWT concept had its full scale trial in the German offshore windfarm project-Borkum Riffgrund 1, 37 km off the North West coast of Germany. In 2014 SPT Offshore successfully installed the SIWT for a 3.6 MW Siemens wind turbine, in a water depth of 25 m, with pile dimensions of 8 m (diameter) x 8 m (height). As compared to the conventional installation by parts, the jacket substructure along with the transition piece and the suction cassion foundation was lifted and lowered to the seabed in one piece (refer to the figures above).

A better understanding of the dynamics of the SIWT would thus play a significant role in its optimization.

2.2 Suction Pile Foundation

Suction foundations have been used extensively since mid-1990's for safely securing large offshore installations to the seafloor worldwide. This section talks about the important features of the suction pile.

2.2.1 Suction foundation: What is it?

A suction foundation can be literally picturized as an upside-down bucket that is embedded into the sea bed. Structurally, it consists of two important components; **top plate** and **skirting**.

The skirt length (L) to diameter (D) ratio of a suction foundation is usually less than 6. A suction foundation can be referred to as;

- **Suction pile** for L/D>1 and typically < 6. Generally used for moorings and subsea structures.
- **Suction bucket** for L/D ≤ 1. It mainly exhibits a stiff /rigid body behavior due to its structural configuration and is thus preferred for jacket and gravity based substructures. The focus of this thesis is specifically on suction bucket foundation. **Please note that in this thesis, the term 'bucket' is not been used explicitly.**

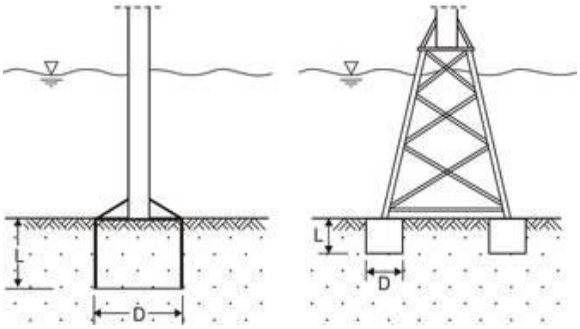

Figure 10 Definition of D and L

Figure 11 gives an overview of typical values of L/D and D, for different applications.

Application	Typical diameter (m)	Examples
Moorings: L/D < 5	4–6	Suction anchors/ suction piles
Subsea structures: 1 < L/D < 4	5–10	Suction pile/ "suction foundation" – Mono-bucket – Suction caisson – Bucket foundation – Skirt compartments – Skirt foundation (self-weight penetration)
Jackets: Typical L/D < 1	8–15	Bucket foundation – Skirted foundations
Gravity Base Structures: L/D << 1 to 1	25–35	Skirt/skirt-piles
Monopod tower	15–20	Bucket foundation – Mono bucket

Figure 11 Suction Foundation and their L/D ratios ; Source :(Tjelta 2015)

2.2.2 Why did it become so popular?

Suction foundation was introduced around 35 years ago in the Gorm field as suction anchors. The time spent in the field and the total cost was in excess of comparative systems like piles or marine drag and embedment anchors (Tjelta 2001). It took around 10 years for the concept to develop further and overcome its shortcomings so that it could reappear for the Gullfaks C Large Scale Penetration Test. The test data provided valuable insight to the further development of suction foundation technology. It led to incorporation of special features such as water injection at the skirt tip, effect of "cyclic penetration", monitoring principles, ample pump capacity etc.(Tjelta 2015)

Key factors which have helped suction foundations gain popularity include;

- Reliable design methods for installation and operational behavior of the suction foundation. Certification bodies such DNV have published codes specially for suction foundations. Eg. DNV-RP-E303.
- Easy and predictable installation in nearly all kinds of offshore soils.
- Noise free installation
- Cost efficiency
- Easy removal if planned for

2.2.3 How are they installed?

A suction foundation is open at the base and closed at the top. The foundation at first is allowed to penetrate under its own self weight until it reaches a point beyond which external pressure is necessary. A suction (relative to seabed water pressure) is applied within the foundation using pumps attached to the foundation. This forces the remainder of the foundation to embed itself, leaving the top flush with the seabed. The figure to follow (Figure 12) gives a clear picture of the stresses acting on the foundation.

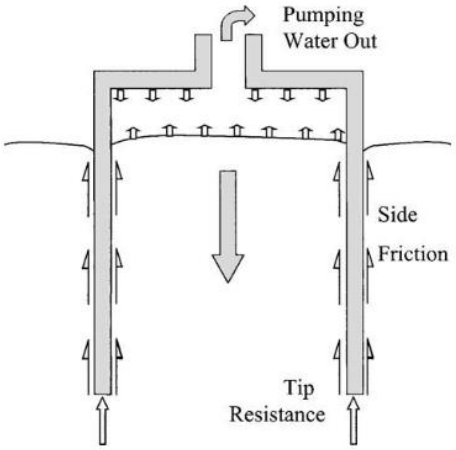

Figure 12 Suction foundation schematic (Chakrabarti 2005)

- **The physics behind installation**

  The total soil resistance to penetration, R_{tot} is the sum of the resistance from the side friction, R_{side} and the resistance from the tip including any stiffeners that may be present R_{tip};

  $R_{tot} = R_{side} + R_{tip}$

  The amount of under-pressure, Δu, needed to penetrate the pile into the soil is;

  $$\Delta u = \frac{R_{tot} - W}{A}$$

  Where,
  W is the submerged weight of the foundation,
  A is the projected horizontal area inside the pile.

- **Installation in clay v/s installation in sand**

  (Housby and Byrne 2005) provides a clear design procedure for installation of suction cassion in clay as well as in sand. The strength of the clay can be characterized by its undrained strength (linearly increasing with depth). The resistance for clay is then calculated as sum of adhesion on the outside and inside of the cassion and the end bearing on the annular rim. Similarly, for sand, the resistance is calculated using its friction properties.

2.3 Soil Damping

Damping in soil can be contributed due to three phenomena: Viscous damping offered by the pore water, Hysteretic damping due to friction of the system and its surroundings and Radiation damping due to geometric spreading of energy. This section sheds light on the abovementioned phenomenon.

2.3.1 Hysteretic Damping

Hysteretic damping is a form of internal damping caused by energy dissipation due to friction in soil elements. In the course of energy dissipation, some of elastic energy stored in soil elements is consumed for destroying edges and structures of soil grains or transform into energy of sound, heat etc.(Tatsuoka, Iwasaki, and Takagi 1978a). This type of damping is not frequency dependent and is in phase with the velocity and proportional to the displacement of the system.

Hysteretic damping is measured in the form of a damping ratio. This ratio is fundamentally defined as the ratio of the damping energy or dissipation energy in a soil element per cyclic loading to (ΔW) the elastic energy or stored energy in the soil element per cyclic loading (W). (Refer Figure 13)

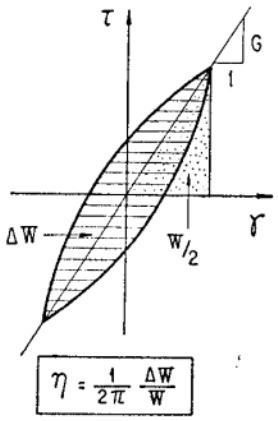

Figure 13 Definition of hysteretic damping ratio (Tatsuoka, Iwasaki, and Takagi 1978a)

Determination of the damping ratio

The damping ratio for soil is obtained from laboratory tests depending on the range of the strain amplitudes. The dependence on strain amplitude is due to the fact that shear moduli of soil reduces with increasing shear strain. For shear strains less than 10^{-4} , the shear moduli values can be accurately captured by **Resonant-Column method**. At shear strain level larger than 10^{-4}, soil behaves

as non-elastic material and has larger damping. For this range of strain, the **Resonant-Column method** is not a proper one in evaluating soil properties.

Cyclic loading tests are deployed to study dynamic properties of soil at medium to large strain levels ($10^{-4} - 10^{-2}$). The **Cyclic torsion shear test** is one of most powerful and versatile tests as the torsional loads and torsional displacements in this test can be measured directly.

- **Resonant-Column method**

  The cyclic resonant column test is based on the analytical relationship of the dynamic modulus of a column of soil to its resonant frequency. In this test, a column of soil is excited either longitudinally or via torsion in one of its normal modes. The common end conditions for this test are;

  - Fixed-free end
  - Spring-base and free end
  - Partially fixed base and free end

  Figure 13 gives the schematics of a typical resonant column test. The frequency of the electromagnetic drive is gradually increased until all the first mode resonant conditions are encountered. After measuring the resonant column, the drive system is cut off and the system is brought to a state of free vibration. The damping ratio is then calculated from observing the logarithmic decay pattern.

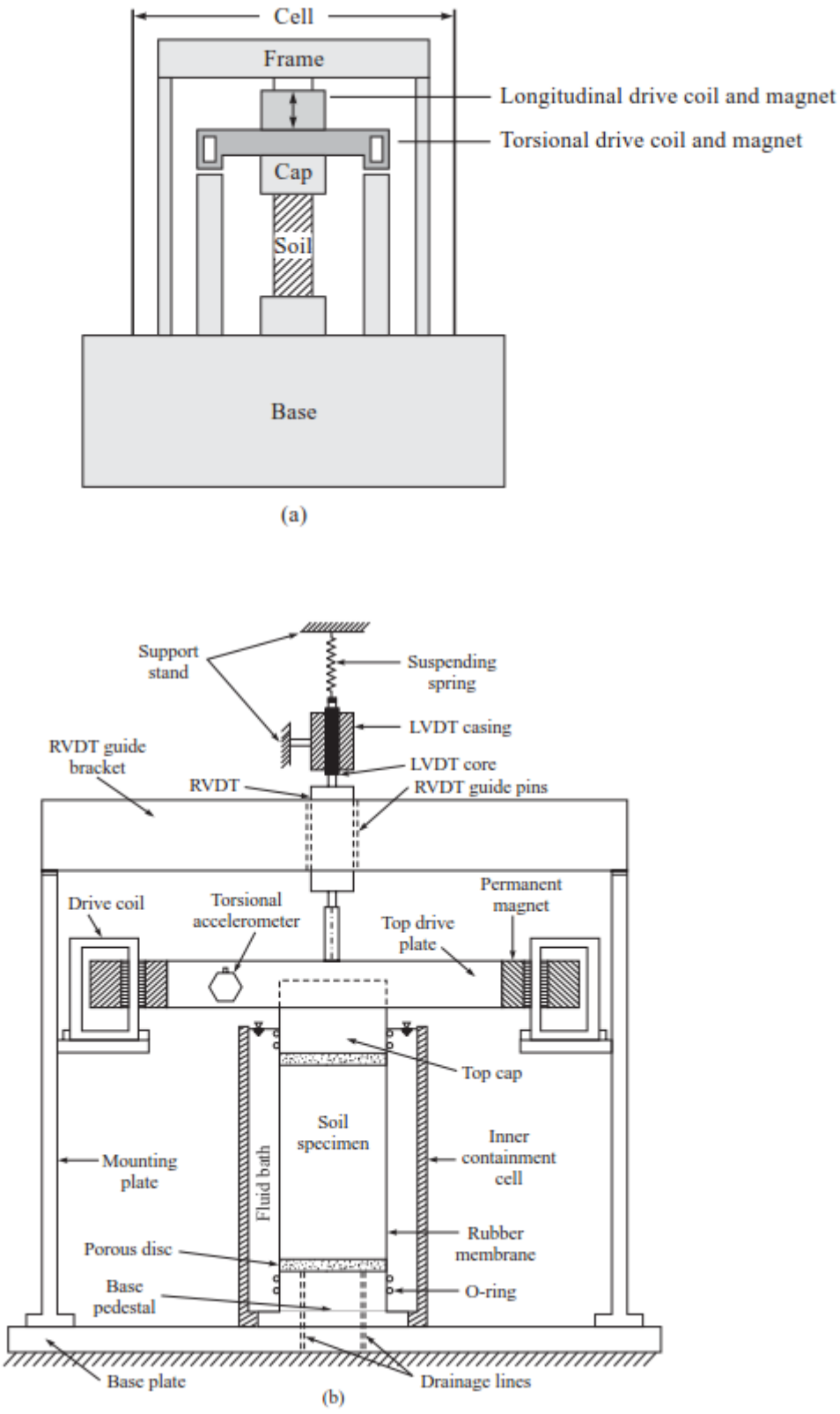

Figure 14 Resonant-column test apparatus (Bhushan 2011)

- **Cyclic torsion shear test**

  Figure 15 depicts the schematic of the test.

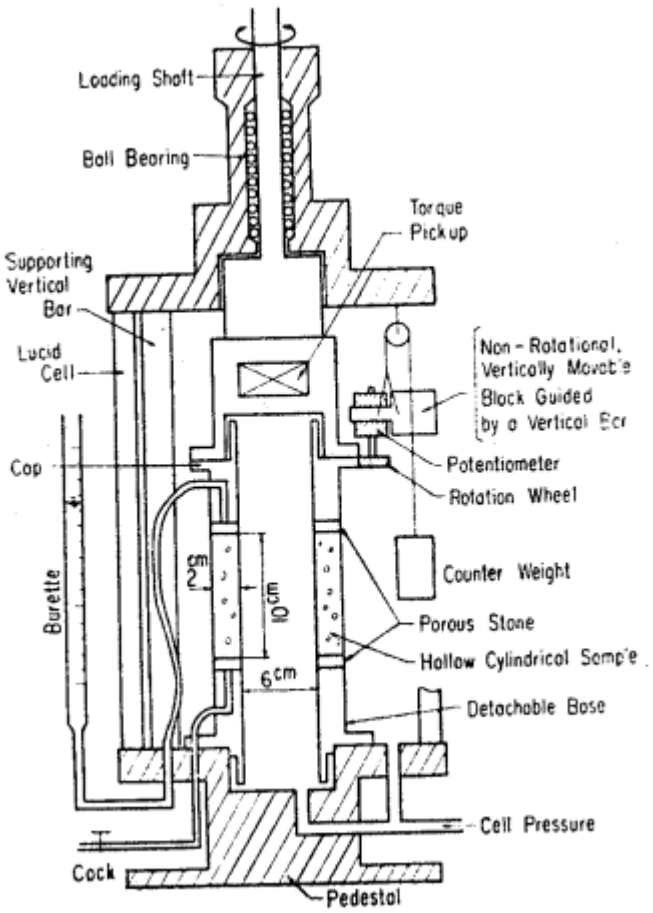

Figure 15 Schematic diagram of torsional shear device, (Tatsuoka, Iwasaki, and Takagi 1978b)

The hollow cylinder soil sample is fixed at bottom and is subjected to loads/pressure exerted by a torsional shear apparatus. Four independent loads/pressures act on the sample (Refer Figure 16);

- Outer chamber pressure p_o
- Inner chamber pressure p_i
- An axial load W
- A torque T

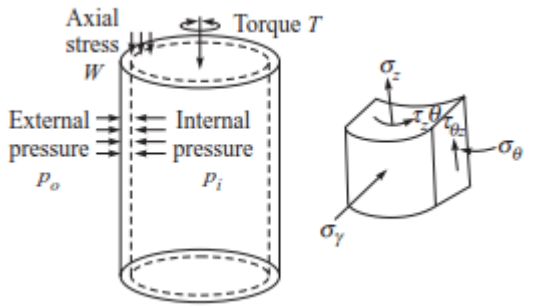

Figure 16 Loads subjected on the hollow sample (Bhushan 2011)

The torsional loads are measured by a torque pickup which is located in the loading shaft just above the sample to eliminate errors due to the friction. The torsional displacements at the top of the sample are monitored by a potentiometer placed just above the sample. The relational between these torsional forces and displacement is recorded in the form of time histories and hysteresis loops to further compute the damping ratio.

In order to get the feel of the magnitude of the damping ratios, one could compare the damping ratios of other frequently used materials. (Refer Figure 17)

material	material damping [5.2] [5.6]	structural damping material damping included (indication)
Steel	0.004	0.005 – 0.01
reinforced concrete	0.009	0.01 – 0.02
pre-stressed concrete	0.009	0.01
pine wood	0.021	0.05
beech wood	0.025	0.05
natural rubber	0.03	-
natural rubber with canvas	0.08	-
sylomer	0.10	-
aluminium	0.018	0.02
masonry	0.04	0.05
dry sand	0.01 – 0.03	-
sand-gravel	0.03 – 0.07	-
clay	0.02 – 0.05	-

Figure 17 Indication for the magnitude of the damping ratio for a number of frequently used materials (Spijkers, Vrouwenvelder, and Klaver 2005)

2.3.2 Radiation Damping

Stress waves are generated at the interface of the foundation and the soil. As these stress waves propogate in the form of compression (P-waves) and shear waves (S-waves),the energy in these waves gets distributed over a growing volume of the soil environment. This phenomena is called as Radiation Damping,also popularily known as Geometric Damping.

Research on radiation damping is majorly done in the field of machine foundation and seismic analysis. Earlier researchers came up with the concept of frequency independent radiation damping coefficient (C_{rad}) using the anolgy between one dimensional wave propogation in an elastic space and a visocus dashpot. Lysmer

and Richart suggested frequency independent "dashpot" coefficients to model vertical,horizontal ,rocking and torsional oscillations of a rigid circular plate on the surface of elastic halfspace(Lysmer and Richart 1966). Later on it was proved that C_{rad} varies with the frequency and that only at high frequencies it asymptotically reaches a constant value (Gazetas and Dobry 1984).Gazetas along with his co authors, did extensive research on developing simple models for radiation damping in arbitrarily shaped surface and embedded foundations for the case of homogeneous halfspace.

Simple models by them were based on Huygen's Principle showing that waves are generated at every point on the soil-foundation interface.

For the case of embedded foundation, two possible foundation-soil interfaces exist: the vertical sidewalls and the horizontal basement.

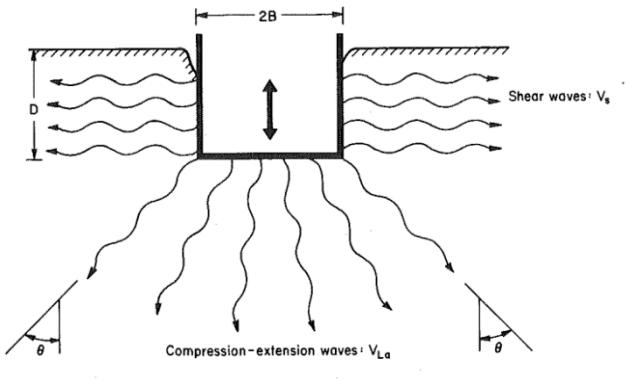

Figure 18 Proposed Radiation Damping Model: Vertical vibration (Gazetas, Dobry, and Tassoulas 1985)

Considering the case of vertical vibration of the pile, S waves are generated at the sidewalls of the foundation while compression extension waves are generated at the basement.The latter waves travel with a velocity close to the "Lysmer's analog" velocity. The formulae for which is given by ;

$$V_{La} = \frac{3.4 \times V_s}{\pi\,(1-v)} \qquad (1)$$

Where V_s is the shear wave velocity and v is the Poisson's ratio of the soil. V_{La} originates in Lysmer's study of a circular foundation vibrating on a half-space(Lysmer and Richart 1966).

The radiation energy is summed up at the two interfaces which yeilds the following equation;

$$C_{rad} = (\rho V_{La} A_b)\tilde{c}_z + \rho V_s A_s \qquad (2)$$

In which $\tilde{c}_z = \tilde{c}_z(a_0; \frac{L}{B}, v)$ where $a_0 = \omega B/V_s$ is the dimensionless frequency, A_b and A_s represent the area of the basement and the sidewall respectively.

Based on the above mentioned concept, (Gazetas 1991) published a complete chart to compute the radiation damping coefficient for the other degrees of freedom which include horizontal and rocking movement of the foundation. The figure to follow shows the tabulated chart for the case of embedded foundations.

TABLE 2. Dynamic Stiffness and Damping of Foundations Embedded in Half-Space with Arbitrary Basemat Shape

Vibration mode (1)	Static stiffness, K_{emb} (2)	Dynamic stiffness coefficient, $k_{emb}(\omega)$ (3)	Radiation dashpot coefficient, $C_{emb}(\omega)$ (4)
Vertical (z)	$K_{z,emb} = K_z[1 + (1/21)(D/B)(1 + 1.3\chi)][1 + 0.2(A_w/A_b)^{2/3}]$ where $K_z = K_{z,surface}$ is obtained from Table 1. A_w = actual sidewall-soil contact area; for constant effective-contact height, d, along the perimeter: $A_w = (d) \times$ (perimeter); $\chi = A_b/4L^2$	($\nu \leq 0.40$): fully embedded: $k_{z,emb} \cong k_z[1 - 0.09(D/B)^{3/4}a_0^2]$ in a trench: $k_{z,tr} \cong k_z[1 + 0.09(D/B)^{3/4}a_0^2]$ ($\nu \simeq 0.48$): fully embedded with $L/B = 1 - 2$: $k_{z,emb} \cong k_z[1 - 0.09(D/B)^{3/4}a_0^2]$ fully embedded with $L/B > 3$: $k_{z,emb} \cong k_z[1 - 0.35(D/B)^{1/2}a_0^{3.5}]$ in a trench: $k_{z,tr} \cong k_z$, where $k_z = k_{z,surf}$ from Table 1.	$C_{z,emb} \cong C_z + \rho V_s A_w$ where $C_z = C_{z,surface}$ is obtained from Table 1 and the associated chart of Fig. 2.
Horizontal (y) and (x)	$K_{y,emb} = K_y[1 + 0.15(D/B)^{0.5}]\{1 + 0.52[(h/B)(A_w/L^2)]^{0.4}\}$ $K_{x,emb} = K_x \cdot (K_{y,emb}/K_y)$ where $K_y = K_{y,surface}$ and $K_x = K_{x,surface}$ are obtained from Table 1.	All ν, partially embedded: interpolate $k_{y,emb}$ and $k_{x,emb}$ can be estimated in terms of L/B, D/B, and d/B for each value of a_0 from the plots in Fig. 3	$C_{y,emb} = C_y + 4\rho V_s Bd + 4\rho V_{La} Ld$ $C_{x,emb} = C_x + 4\rho V_{La} Bd + 4\rho V_s Ld$ where $C_y = C_{y,surface}$ and $C_x = C_{x,surface}$ are obtained from Table 1 and the associated chart of Fig. 2.
Rocking (rx) and (ry)	$K_{rx,emb} = K_{rx}\{1 + 1.26(d/B)[1 + (d/B)(d/D)^{-0.2}(B/L)^{0.5}]\}$ $K_{ry,emb} = K_{ry}\{1 + 0.92(d/L)^{0.6}[1.5 + (d/L)^{1.9}(d/L)^{-0.6}]\}$ where $K_{rx} = K_{rx,surface}$ and $K_{ry} = K_{ry,surface}$ are obtained from Table 1.	$k_{rx,emb} \cong k_{rx}$ $k_{ry,emb} \cong k_{ry}$ The surface-foundation k_{rx} and k_{ry} are obtained from Table 1.	$C_{rx,emb} = C_{rx} + \rho I_{bx}(d/B)\{V_{La}(d^2/B^2) + 3V_s + V_s(B/L)[1 + (d^2/B^2)]\} \cdot \eta_r$ where $\eta_{rx} = 0.25 + 0.65\sqrt{a_0}(d/D)^{-a0/2}(D/B)^{-1/4}$ $C_{ry,emb}$ is similarly evaluated from C_{rx} after replacing x by y, and interchanging B with L in the foregoing two expressions. In both cases $a_0 = \omega B/V_s$.
Swaying-rocking (x-ry)(y-rx)	$K_{x\text{-}ry,emb} \cong (1/3)dK_{x,emb}$ $K_{y\text{-}rx,emb} \cong (1/3)dK_{y,emb}$	$k_{x\text{-}ry,emb} \cong k_{y\text{-}rx,emb} \cong 1$	$C_{x\text{-}ry,emb} = (1/3)dC_{x,emb}$ $C_{y\text{-}rx,emb} = (1/3)dC_{y,emb}$
Torsion (t)	$K_{t,emb} = K_t \cdot \Gamma_w \cdot \Gamma_{tre}$ where $K_t = K_{t,surface}$ is obtained from Table 1. $\Gamma_w = 1 + 0.4(D/d)^{0.5}(j_x/j_y)(B/D)^{0.6}$ $\Gamma_{tre} = 1 + 0.5(D/B)^{0.1}(B^4/I_{bz})^{0.13}$ $j_x = (4/3)d(B^3 + L^3) + 4BLd(L + B)$ $j_y = (4/3)BL(B^2 + L^2)$	$k_{t,emb} \cong k_{t,surface}$	$C_{t,emb} = C_t + 4\rho d[(1/3)V_{La}(L^3 + B^3) + V_s BL(L + B)] \cdot \eta_t$, where $C_t = C_{t,surface}$ is obtained from Table 1 and Fig. 2 $\eta_t \cong (d/D)^{-0.5} \cdot a_0^2/[a_0^2 + (1/2)(L/B)^{-1.5}]$

Figure 19 Chart from(Gazetas 1991)

In order to compute the total damping coefficient, material damping of hysteretic nature is added to C_{rad} using a frequency independent damping ratio, β. For most soils β typically ranges from 0.02-0.05. The effective damping coefficient is thus written as;

$$C_{total} = C_{rad} + \frac{2\widetilde{K}}{\omega}\beta \tag{3}$$

Where ω is the frequency of vibration and $\widetilde{K}$ is the dynamic stiffness of the foundation.

(Wolf 1994) describes a three-parameter model (refer Figure 20) to analyze the dynamic behavior of surface and embedded footings. It consists of spring K that equals to the static-stiffness coefficient of the soil's half space. The other two free parameters are the dashpot C and mass M. These are specified based on the dimensionless coefficients γ and μ as;

$$C = \frac{r}{V_s}\gamma \mathrm{K} \qquad (4)$$

$$M = \frac{r^2}{{V_s}^2}\mu \mathrm{K} \qquad (5)$$

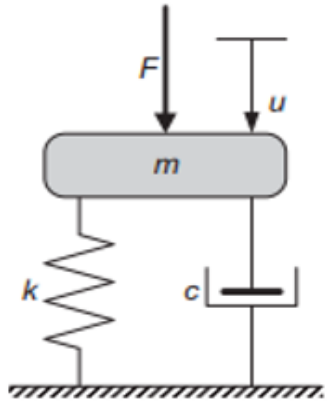

Figure 20 Wolf's three parameter model

Where V_s is the shear wave velocity of the soil. The three parameters are calculated using the table published by Wolf in his book (refer Figure 21).

	Static Stiffness K	Dimensionless Coefficients of Dashpot γ	Mass μ
Horizontal	$\frac{8Gr_0}{2-\nu}$	0.58	0.095
Vertical	$\frac{4Gr_0}{1-\nu}$	0.85	0.27
Rocking	$\frac{8Gr_0^3}{3(1-\nu)}$	$\frac{0.3}{1+\frac{3(1-\nu)m}{8r_0^5\rho}}$	0.24
Torsional	$\frac{16Gr_0^3}{3}$	$\frac{0.433}{1+\frac{2m}{r_0^5\rho}}\sqrt{\frac{m}{r_0^5\rho}}$	0.045

Figure 21 Static stiffness and dimensionless coefficients of three parameter model in homogenous half space (Wolf 1994)

Futhur in this thesis, the results obtained for the case of suction pile has been compared with the Gazetas charts and Wolf's three parameter model for the case of vertical vibration.

In very recent research paper published by (Carswell et al. 2015) it is stated that geometric dissipation is negligible for frequencies less than 1Hz and the majority of wind and wave loads have frequencies below 1 Hz. The difficulty lies in uncoupling the contribution in total damping due to radiation and hysteresis in soil. For instance, (Richart, Hall, and Woods 1970) writes that radiation damping is principle factor for energy dissipation. This assumption is commonly adopted in engineering applications because the practise is based on the assumption that soil is perfectly elastic medium, where material damping is negligibly small. On the contrary, (Wolf 1985) states that in case of shallow layer soils, radiation

damping can be drastically reduced leaving material damping as dominant source of energy dissipation.

2.3.3 Viscous Damping

The offshore soil is fully submerged due to which the water trapped in the saturated granular soil structure could cause viscous damping forces on the suction pile embedded in it. The magnitude of this viscous damping force is proportional to the relative velocity of the oscillatory motion of the suction pile and the pore water. As it is velocity dependent, it is also dependent on the combination of amplitude and frequency.

(Bolton and Wilson 1990) in their research had desired to have an order-of-magnitude estimate of the possible effects of viscous damping due to the pore fluid. They conducted resonant column test to derive the damping in dry and fluid-saturated sand. The results confirmed that the water filling the pores of sand in the resonant column tests had a negligible effect on the damping ratio. They further concluded that water-saturated sand is purely hysteretic at typical earthquake frequencies (1Hz-10Hz).

Limited information is available on behavior of viscous damping for lower frequencies (<1Hz). Given the ambiguity, viscous damping could play a role in the soil-foundation interaction of an OWT.

2.3.4 Damping in Suction Piles

Very limited literature and research is available for soil damping specially for the case of suction pile foundation. In 2005, field trials of suction caisson foundations in clay was conducted at the Bothkennar test site (Houlsby et al. 2005). The tests were relevant to the design of foundations for offshore wind turbines, in the form of either monopod or tetrapod foundations. In case of monopod foundation, the horizontal forces and the overturning moments from wind and waves are dominant, while the moment loading in tetrapods is carried principally by "push-pull" action by opposing footings. Hence for tetrapods, it is the variation of vertical load that is most important. Field trails were conducted for the following scenarios;

- Installation of the cassions
- Cyclic moment loading under dynamic and quasi-static ocnditions
- Cyclic inclined vertical loading
- Pullout test for cassion

With regard to damping, the cyclic moment loading test gave outcomes that when compared to Wolf's three parameter model, gave a resonable fit. Further in Section 4.3.2, the nature of the plots obtained from of this experiments have been compared with findings of Case study 1.

Recently in 2014, DONG energy has installed a Suction Pile Jacket foundation at its German offshore wind farm, Borkum Riffgrund 1. The full-scale trails inorder to investigate the dynamic behaviour of the structure, are being conducted. Uptil now, the only information available regarding damping is from measurements of the transition piece accelerations when subjected to accidental boat impact. A free decay analysis on the transition piece accerleration gave a damping value of around 2.17 %. This value is inclusive of the wave, structure and soil damping(DONG 2014). Hopefully in the near future these field trials will provide valuable information for soil damping in suction piles.

3 The Black-Box

PLAXIS is a Finite Element based software used for the case studies in this thesis. This chapter attempts to showcase what exactly runs inside the 'black-box' by explaining the thesis relevant analytical/empirical theories this FEM software is based on. Both PLAXIS 2D and 3D was used for the two case studies respectively. The content of this chapter is based on the latest version of the PLAXIS manuals.

3.1 PLAXIS: Material Models

Plaxis is an advanced geotechnical software based on the finite element method. The latest edition offers a range of material models that can be used to model soil at various degrees of accuracy. HSsmall which is one of the existing advanced models for simulation of soil behavior, has been used in this thesis. This section talks about the various available materials models in Plaxis with focus on the HSsmall model. Please note that both PLAXIS 2D and 3D offer the same material models.

3.1.1 What is a material model?

Soil is a complicated material given its non-linearity, anisotropy and time dependent behavior when subjected to stresses. In order to deal with soil numerically, one needs a mathematical model of soil that can define its mechanical behavior in a continuum framework of soil layers, rock masses or material volume in general. Hence material models (also known as constitutive model) provide a qualitative description of deformation behavior of the soil.

A material model is defined by its model parameters. These parameters are a quantification of the deformation behavior of the soil and can be determined on the basis of;

- Soil investigation (Laboratory test, in-situ tests)
- Rules of thumb
- Experience

(Brinkgreve 2005) discussed in depth about the five basic aspects of soil behavior;

1. Influence of water on the behavior of soil in terms of effective stresses and pore pressures.
2. Factors which influence the soil stiffness such as the stress level, stress path (loading and unloading), strain level, soil density, soil permeability, consolidation ratio and the stiffness anisotropy of the soil.
3. Irreversible deformation as a result of loading.

4. Soil strength with its influencing factors; loading speed of the tested specimen, age and soil density, undrained behavior, consolidation ratio and strength anisotropy.
5. Other factors such as compaction, dilatancy and memory of pre-consolidation stress.

Developing a single soil material model for all the above mentioned characteristics can be complex and complicated to use. Hence different soil models are available whose applicability depends on the project/case study at hand.

3.1.2 Available material models in PLAXIS

Plaxis currently offers 11 material models. The frequently used ones are as follows;

- **Linear Elastic model (LE)**

  This model is based on Hooke's law of isotropic elasticity. It involves two basic elastic parameters: Young's modulus E and Poisson's ratio v. This model is too unrealistic to model soil; however, it can be used to model stiff volumes in the soil (e.g. concrete walls).

- **Mohr-Coulomb model (MC)**

  This model emulates linear elastic-perfectly plastic Mohr-Coulomb model involving five input parameters: E and v for soil elasticity, φ and c for soil plasticity and ψ as an angle of dilatancy. It gives a fairly good 'first order 'approximation of soil or rock behavior.

- **Hardening Soil model (HS)**

  Along with the model parameters from the MC model, soil stiffness is defined much more accurately with this model. This model requires three different input stiffnesses: the triaxial loading stiffness (E_{50}), the triaxial unloading stiffness(E_{ur}) and the oedometer loading stiffness (E_{oed}). This model also accounts for stress-dependency of stiffness moduli and initial soil conditions.

- **Hardening Soil model with small-strain stiffness (HSsmall)**

As an extension to the HS model, this model accounts for the increased stiffness of soil at small strains. It only demands two extra parameters compared to the original HS model: the small-strain shear modulus (G_0) and the shear strain at which the secant modulus has reduced to 0.7 times G_0 ($\gamma_{0.7}$). The advanced features of this model are most apparent in working load conditions. This model also accounts for hysteretic material damping when used for dynamic applications. Given its capabilities for dynamic calculations, HSsmall model has been used for the case-studies in this thesis. The subsections to follow shall explain this model in depth.

- **Soft Soil model (SS)**

  This model is specially meant for primary compression of near normally-consolidated clay type soils. In comparison to the HS model, this model is better capable to model the compression behavior of very soft soils.

- **Soft Soil Creep model (SSC)**

  All soils exhibit some creep, and primary compression is thus followed by a certain amount of secondary compression. This model has been developed primarily for application to settlement problems of foundations, embankments etc.

- **Jointed Rock model (JR)**

  The JR model is an anisotropic elastic-plastic model, specially meant to simulate the behavior of rock layers involving stratification and particular fault directions.

- **Modified Cam-Clay model (MCC)**

  This model is primarily meant for the modelling of near normally-consolidated clay-type soils. This model has been added to PLAXIS to allow for a comparison with other codes.

3.1.3 Why HSsmall was chosen?

The principle goal of this thesis is to study soil damping. Damping requires a model that can accurately model the dynamic behavior of soil. Soil damping can be broadly divided into **radiation damping** and **hysteretic (material)damping**. It is difficult to decouple these, however one can safely say that PLAXIS accounts for radiation damping by the virtue of its finite element modelling. Hysteretic damping on the other hand can be further divided based on elastic and plastic strains. The soil models (except for LE) are able to generate plastic strains if stress points reach the failure criterion (of the respective soil model), which will lead to damping in dynamic calculations. However, when it comes to calculation of damping within the failure contour the following can been concluded;

- The **HSsmall** model calculates the hysteresis in cyclic loading using the formulation based on modulus reduction curves. The amount of hysteresis depends on the applied load amplitude and the corresponding strain amplitudes. For dynamic calculations, this model uses the varying wave velocities caused by the stress-dependent stiffness.
- **Other soil models** when used for dynamic calculations require the user to input the elastic stiffness parameter for the model to correctly predict the wave velocities in the soil. This stiffness prediction demands expertise from the user which may not be the case always. Moreover, the stress cycles within the failure contours (of the respective soil models) will only generate elastic strains and no hysteretic damping. For such models, Rayleigh damping may be defined in order to simulate the soil's damping characteristics in cyclic loading. As mentioned before, prediction of these Rayleigh damping parameters once again demands geotechnical expertise of the user.

In short, the HSsmall model has the capability to model hysteretic damping in dynamic application with the help from modulus reduction curves (where shear modulus G, is plotted as a logarithmic function of the shear strain).

3.1.4 And finally……. HSsmall

Shear modulus of soil is known to decay nonlinearly with increasing strain amplitude. Hence, the strain range in which soils can be considered truly elastic

is very small. The original HS model assumes elastic material behavior during unloading and reloading. This reduction of shear modulus is taken into account by the HSsmall model, which is formulated using the stiffness reduction curve. The stiffness when plotted against the shear strain amplitude, gives a characteristic S shape stiffness reduction curve (refer Figure 23).

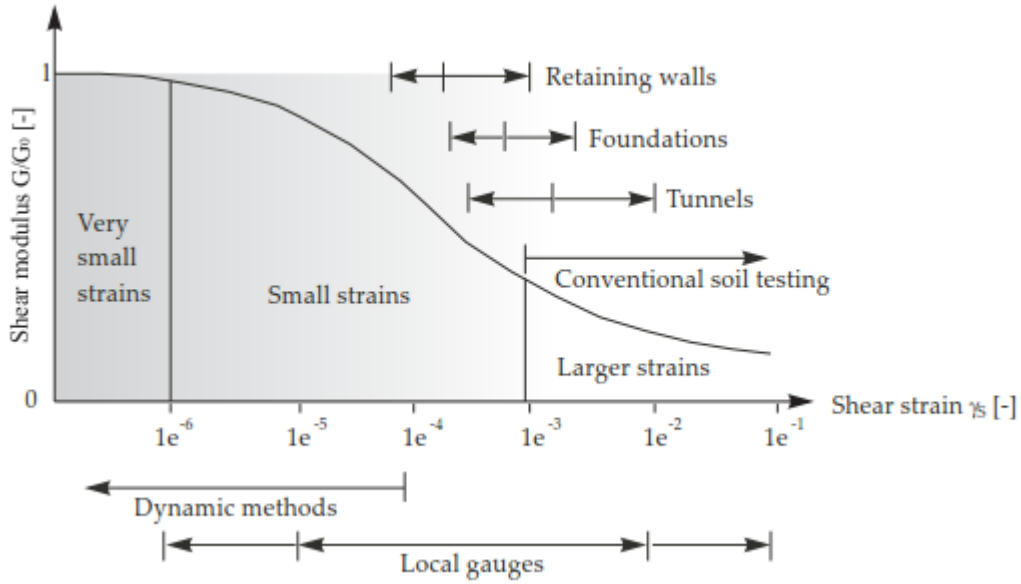

Figure 23 Characteristic stiffness-strain behavior of soil with typical strain ranges for laboratory tests and structures

Figure 22 summarizes the list of parameters required as an input for HSsmall soil model.

c	:	(Effective) cohesion	[kN/m^2]
φ	:	(Effective) angle of internal friction	[°]
ψ	:	Angle of dilatancy	[°]
σ_t	:	Tension cut-off and tensile strength	[kN/m^2]
m	:	Power for stress-level dependency of stiffness	[-]
E_{50}^{ref}	:	Secant stiffness in standard drained triaxial test	[kN/m^2]
E_{oed}^{ref}	:	Tangent stiffness for primary oedometer loading	[kN/m^2]
E_{ur}^{ref}	:	unloading / reloading stiffness from drained triaxial test	[kN/m^2]
ν_{ur}	:	Poisson's ratio for unloading-reloading	[-]
G_0^{ref}	:	reference shear modulus at very small strains ($\varepsilon < 10^{-6}$)	[kN/m^2]
$\gamma_{0.7}$	:	threshold shear strain at which $G_s = 0.722G_0$	[-]

Figure 22 Model parameter for HSsmall model

- **Stiffness moduli E_{50}^{ref} , E_{oed}^{ref}, E_{ur}^{ref} and power m**

The graph (refer Figure 24) gives a clear understanding of the stiffnesses. The stress-strain relationship of the model uses a hyperbolic stress-strain curve instead of a bi-linear curve (as used in MC model). In order to incorporate the control of stress level dependency of the soil stiffness, the stiffnesses are defined for a reference stress p^{ref} . As a default value, the program uses $p^{ref} = 100\ kN/m^2$.

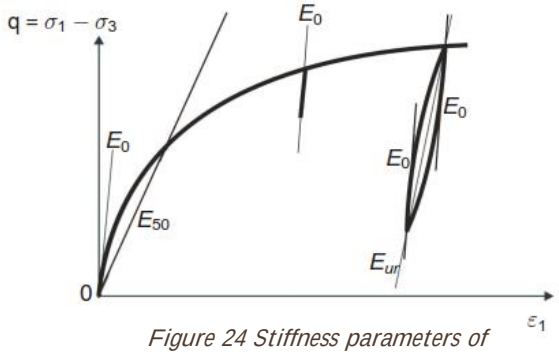

Figure 24 Stiffness parameters of HSsmall in a triaxial test

$\boldsymbol{E_{50}}$ and $\boldsymbol{E_{oed}}$ are calculated using the following equations;

$$E_{50} = E_{50}^{ref}\left(\frac{c\ cos\varphi - \sigma'_3 sin\varphi}{c\ cos\varphi + p^{ref} sin\varphi}\right)^m \quad (6)$$

$$E_{oed} = E_{oed}^{ref}\left(\frac{c\ cos\varphi - \sigma'_1 sin\varphi}{c\ cos\varphi + p^{ref} sin\varphi}\right)^m \quad (7)$$

Where σ'_3 is the confining pressure in a triaxial test.

The value of m, should be taken equal to 1.0 for soft clays and around 0.5 for Norwegian sands and silts. In general, its value varies in the range 0.5 $< m <$ 1.0.

- **Parameters G_0 and $\gamma_{0.7}$**

The small state parameters $\boldsymbol{G_0}$ **and** $\boldsymbol{\gamma_{0.7}}$ are mainly influenced by the material's actual state of stress and void ratio ***e.*** In the HSsmall model, the stress dependency of the shear modulus $\boldsymbol{G_0}$ is taken into account with the power law:

$$G_0 = G_0^{ref}\left(\frac{c\ cos\varphi - \sigma'_3 sin\varphi}{c\ cos\varphi + p^{ref} sin\varphi}\right)^m \quad (8)$$

One can derive $\boldsymbol{G_0^{ref}}$ based on many correlations that are offered in the literature. A good estimation for many soils is for example the relation given by Hardin and Black (1969);

$$G_0^{ref} = 33.\frac{(2.97 - e)^2}{1 + e} \quad for \quad p^{ref} = 100\ [kPa] \tag{9}$$

In absence of data, the threshold shear strain $\boldsymbol{\gamma_{0.7}}$ can be calculated using available correlations. One such correlation could be using the original Hardin-Drnevich relationship, by relating it to the model's failure parameter. Applying the Mohr-Coulomb failure criterion, $\boldsymbol{\gamma_{0.7}}$ can be calculated as;

$$\gamma_{0.7} \approx \frac{1}{9G_0}[2c'(1 + \cos(2\varphi')) - \sigma'_1(1 + K_0)sin(2\varphi')] \tag{10}$$

Where K_0 is the earth pressure coefficient at rest and σ'_1 is the effective vertical stress (pressure negative).

3.1.5 Hysteretic damping in HSsmall

(Brinkgreve, Kappert, and Bonnier 2007) in their paper have a given detailed description of how local hysteretic damping ratio $\boldsymbol{\xi}$ can be obtained using HSsmall model. The secant stiffness (G_S) reduction curve (refer Figure 25) is first fitted into a good approximation given by the following equation;

$$G_S = \frac{G_0}{1 + \frac{a\gamma}{\gamma_{0.7}}} \tag{11}$$

The constant $\boldsymbol{a}$ is fitted to 0.385 to arrive at the best fit (central line of Figure 25).

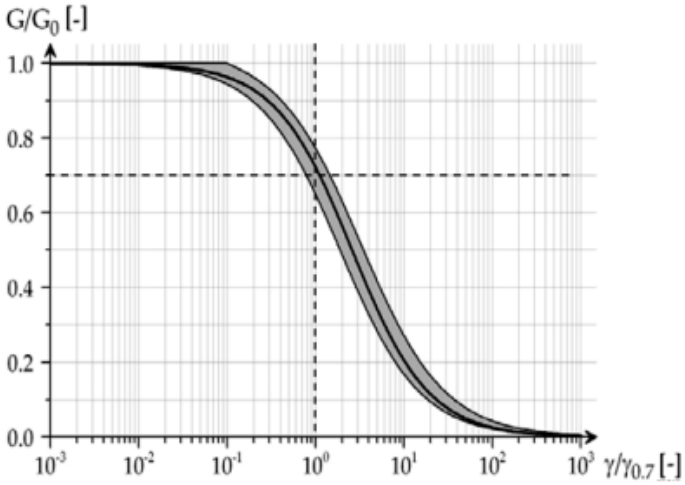

Figure 25 Reduction of secant shear modulus with shear strain (Brinkgreve, Kappert, and Bonnier 2007)

The tangent shear modulus (G_t) can be thus derived as;

$$G_t = \frac{G_0}{(1 + \frac{a\gamma}{\gamma_{0.7}})^2} \geq G_{ur} \tag{12}$$

As HSsmall model is an overlay model, the tangent shear modulus is bounded by a lower limit, G_{ur} of the original HS model.

When subjected to cyclic shear loading, the HSsmall model will show typical hysteretic behavior as visualized in Figure 26. Considering a case of particular magnitude of γ_c, the dissipated energy (E_D) in a load cycle is equivalent with the area of the closed loop which can be formulated as;

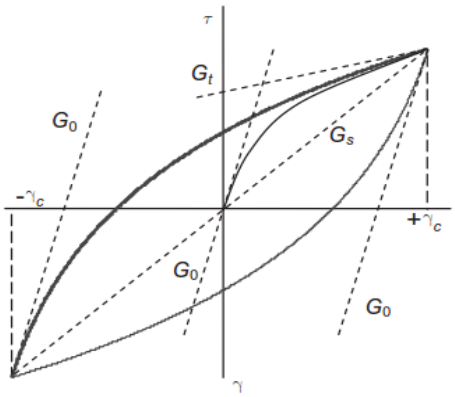

Figure 26 Hysteretic behavior in HSsmall model (Brinkgreve, Kappert, and Bonnier 2007)

$$E_D = \frac{4G_0\gamma_{0.7}}{a}[2\gamma_c - \frac{G_0}{1+\frac{\gamma_{0.7}}{a\gamma_c}} - \frac{2\gamma_{0.7}}{a}\ln(1 + \frac{a\gamma_c}{\gamma_{0.7}})] \tag{13}$$

The local hysteretic damping ratio ξ can be defined as;

$$\xi = \frac{E_D}{4\pi E_S} \tag{14}$$

Where E_S is the energy stored at maximum strain γ_c;

$$E_S = \frac{1}{2}G_S{\gamma_c}^2 = \frac{G_0{\gamma_c}^2}{2 + \frac{2a\gamma}{\gamma_{0.7}}} \tag{15}$$

This holds as long as G_{ur} has not been reached, i.e;

$$\gamma_c \leq \frac{\gamma_{0.7}}{a}(\sqrt{\frac{G_0}{G_{ur}}} - 1) \tag{16}$$

The above damping ratio in the HSsmall model only applies as long as the material behavior remains elastic and the shear modulus decreases according to the small-strain formulation. As soon as G_{ur} is reached the damping does not further increase.

3.2 PLAXIS: Modelling

The modelling process in PLAXIS is done steps starting from defining the project boundaries, the soil polygon, the structure, the loads and finally meshing the whole model to the required accuracy. This section discusses each of the aforementioned step in depth.

3.2.1 The project properties

The project properties define the basics of each project. The project property screen of PLAXIS 2D is given in Figure 27.

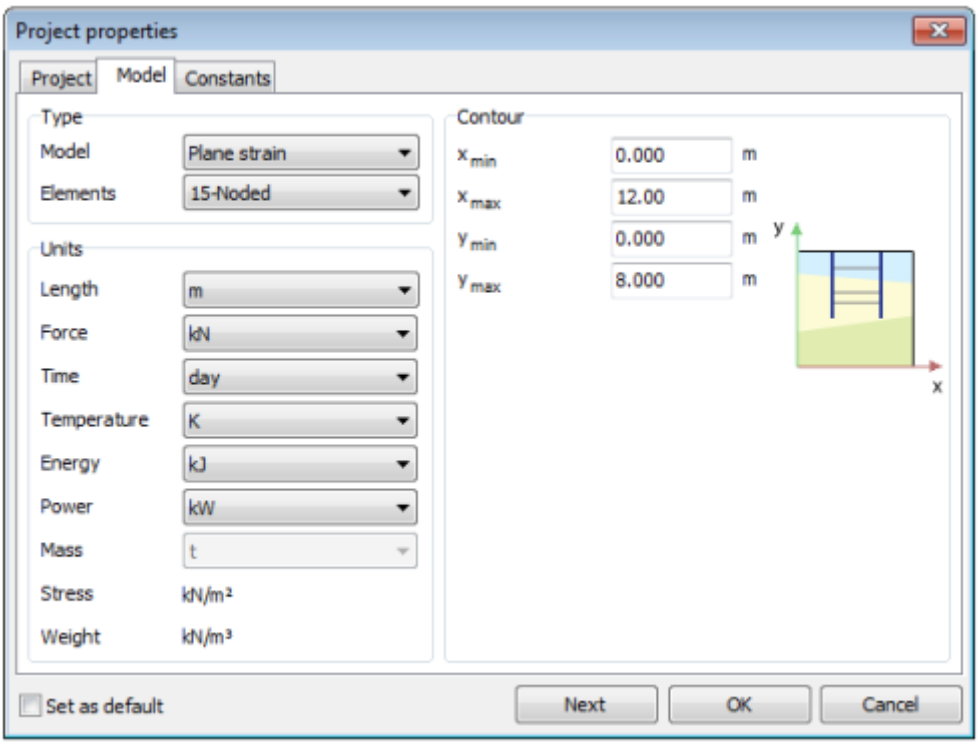

Figure 27 Project properties window

A brief description of these properties with regard to the thesis is given below;

- **Model type**

  In PLAXIS 2D, the real situations may be modelled either by a plane strain or an axisymmetric model. A vertically loaded suction pile is best modelled by an axisymmetric model while plane strain model is generally used in case of structures like dykes where one of the dimensions is very large as compared to the others. Figure 28 gives a clear understanding of the two model types.

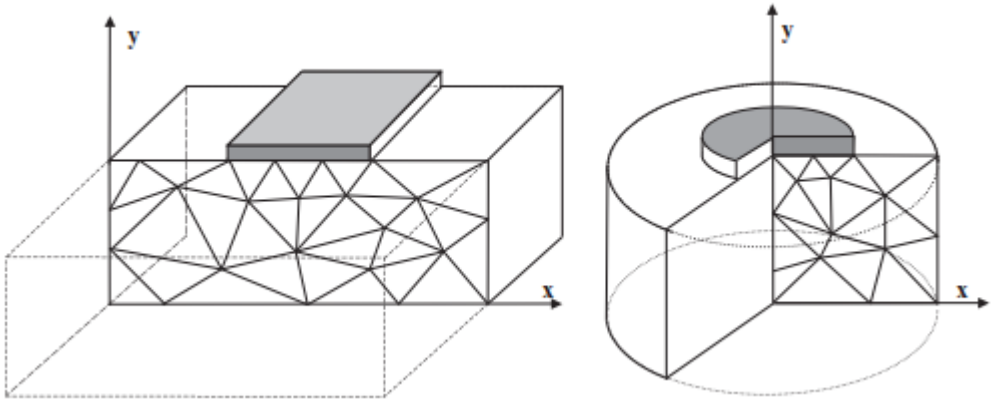

Figure 28 Example of a plane strain (left) and axisymmetric problem (right)

In PLAXIS 3D, the suction pile can be modelled as a half model, owing to the model and the loading symmetry.

Note: For horizontal and rotational loading, different modelling conditions prevail. Such cases should be handled by plane strain models in PLAXIS 2D.

- **Element type (for soil)**

  In PLAXIS 2D, a choice of 15-node triangle element and 6-node triangle is available. The 15-node element provides a fourth order interpolation for displacements and the numerical integration involves 12 Gauss points (stress points) while, the 6-node node element provides a second order interpolation for displacements and the numerical integration involves 3 Gauss points. Failure loads or safety factors are generally over predicted using 6-noded elements. The 15-node element is particularly recommended for axisymmetric analysis even though it consumes more memory and exhibits slower calculation and operation performance.

  In PLAXIS 3D only an option of 10-noded tetrahedral element is available.

- **Units**

  The user can choose the units in accordance to his/her convenience. For this thesis the default units were chosen. The default units, as suggested by the program are, m(meter)for length, kN (kilo Newton) for force, day for time, (kelvin) for temperature, (kilojoule) for energy, kW(kilowatt) for power and t(tonne) for mass.

- **Contours**

  The contours define the boundaries for the model. In static analysis, the boundary distance for the case of axisymmetric model is recommended to be at least five times the diameter of the structure(Pisanò 2015). In case of dynamic analysis, greater value is recommended.

3.2.2 Soil modelling

The soil stratigraphy is defined in the soil mode using the Borehole feature of the program. In reality, the soil layers are not perfectly horizontal and every project has a number of boreholes from which data is collected in order to predict the site conditions. PLAXIS provides the facility to define multiple boreholes, which are further interpolated to derive the positions of the soil layers from the borehole information. For simplicity, both the case studies in this thesis have used data from a single borehole.

The following information can be input while defining a borehole;

- Number of soil layers and their thickness
- Assigning the material models to the soil layers
- Information regarding the hydraulic head level
- Defining the water conditions
- Defining the initial conditions of soil

PLAXIS also provides the option of generating soil stratigraphy from CPT logs. However, this feature has not been explored in this thesis.

3.2.3 Structure modelling

PLAXIS 2D provides various geometric entities that are the basic components of the physical model. Figure 29 gives the list of available geometric entities. Structures and loads can be assigned to the geometric entities. The suction pile in PLAXIS 2D can be modelled using plate elements. Plates are generally used to simulate the influence of walls, shells or linings extending in z-direction. The material properties of plates are contained in material data sets. The most important parameters are flexural rigidity (bending stiffness) EI and the axial

stiffness *EA*. From these two parameters an equivalent plate thickness d_{eq} is calculated from the equation:

$$d_{eq} = \sqrt{12 \frac{EI}{EA}} \tag{17}$$

Since a suction pile can be idealized as a rigid body, it is wise to model the pile as a 'stiff' structure, with an arbitrary stiffness that is sufficiently large compared to the stiffness of the soil. However, in such situations, care should be taken since considering an arbitrarily large stiffness may deteriorate the condition of the global stiffness matrix.

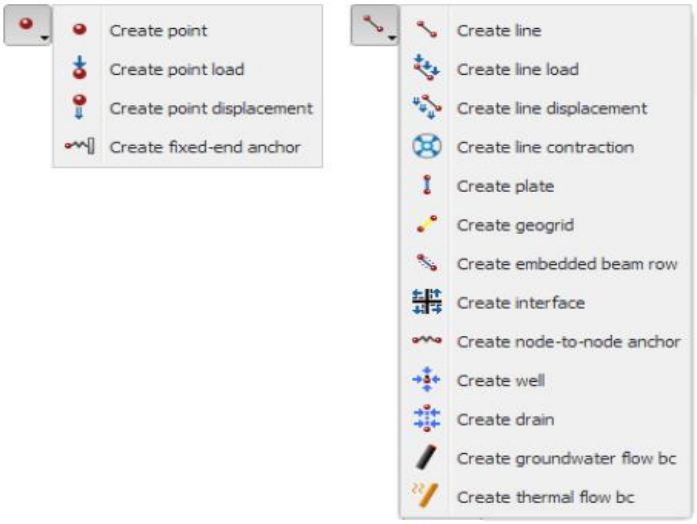

Figure 29 Geometric entities and structural elements in PLAXIS 2D

As an alternative to modelling 'stiff' structures, PLAXIS 3D provides an option to create 'rigid body' objects based on predefined geometry components (surfaces and volumes). Each rigid body has a reference point associated to it and it should be given a combination of forces/moments and/or displacements/rotations in x, y, z - direction (refer Figure 30), in order to apply external forces and to set its boundary conditions. When using rigid body element, it is not possible to calculate internal stresses and structural forces, however contact stresses and forces between the rigid body and the soil can be calculated as long as there are interface elements between the rigid body and the soil.

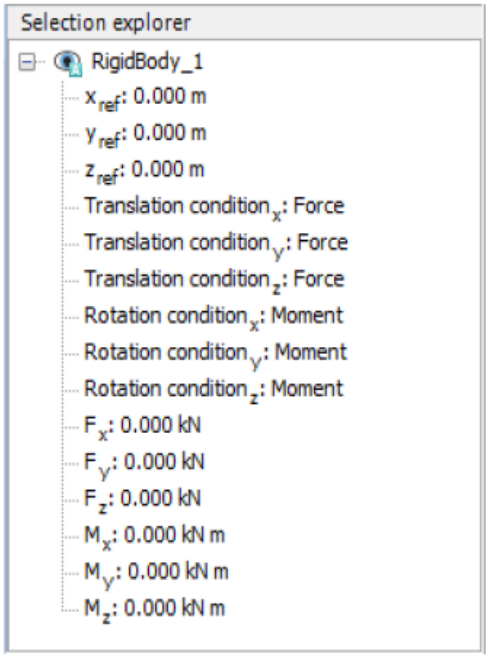

Figure 30 Rigid body features in PLAXIS 3D

3.2.4 Loads

PLAXIS offers load controlled analysis as well as displacement controlled analysis. Hence one can either add a direct load or a prescribed displacement.

In this thesis, load controlled analysis is done for the axisymmetric model in PLAXIS 2D by application of line load whose magnitude is derived by dividing the total force by the area of the top plate of the suction pile. Similarly, in PLAXIS 3D, surface loads have been used.

PLAXIS also enables application of dynamic loads by means of an input value and a multiplier. The actual dynamic value at each time step equals to the product of input value and the multiplier. Harmonic loads have been applied in

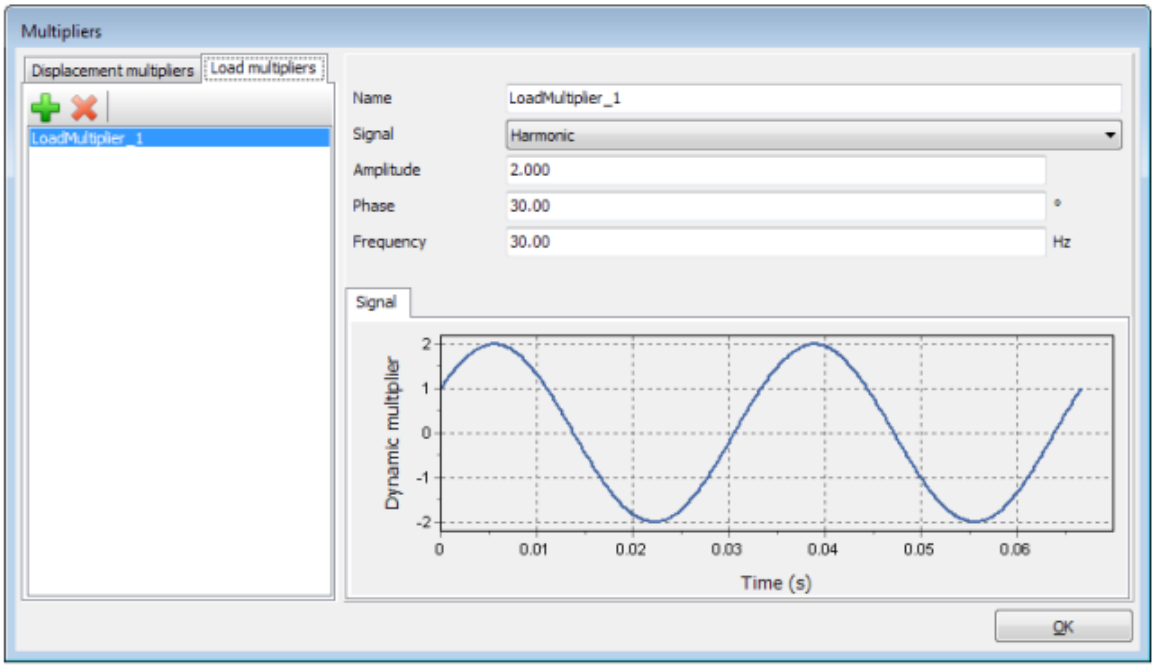

Figure 31 Definition and display of a Harmonic signal in PLAXIS

the case-studies. Figure 31 gives a clear definition of how a load multiplier looks for the case of harmonic loading.

PLAXIS also offers a possibility to define a signal by specifying a set table values or by importing data from a digitized load signal.

3.2.5 Applying Interfaces

Interfaces are joint elements which when added to plates, allow for proper modelling of soil-structure interaction. The properties of interface elements are related to the soil model parameters of the surrounding soil. In case of HSsmall model, the strength reduction factor R_{inter} is the main interface parameter. The interface can be set to rigid in cases where the interface should not have a reduced strength with respect to the strength in the surrounding soil (e.g. extended interfaces around corners of structural objects). The value of R_{inter} can also be entered manually. In reality, the interface in soil-structure interaction is weaker and more flexible than the surrounding soil. Hence, the value of R_{inter} should be

less than 1. A value of 0.65 (for clay) is usually used for analysis (Andersen and Jostad 2002).

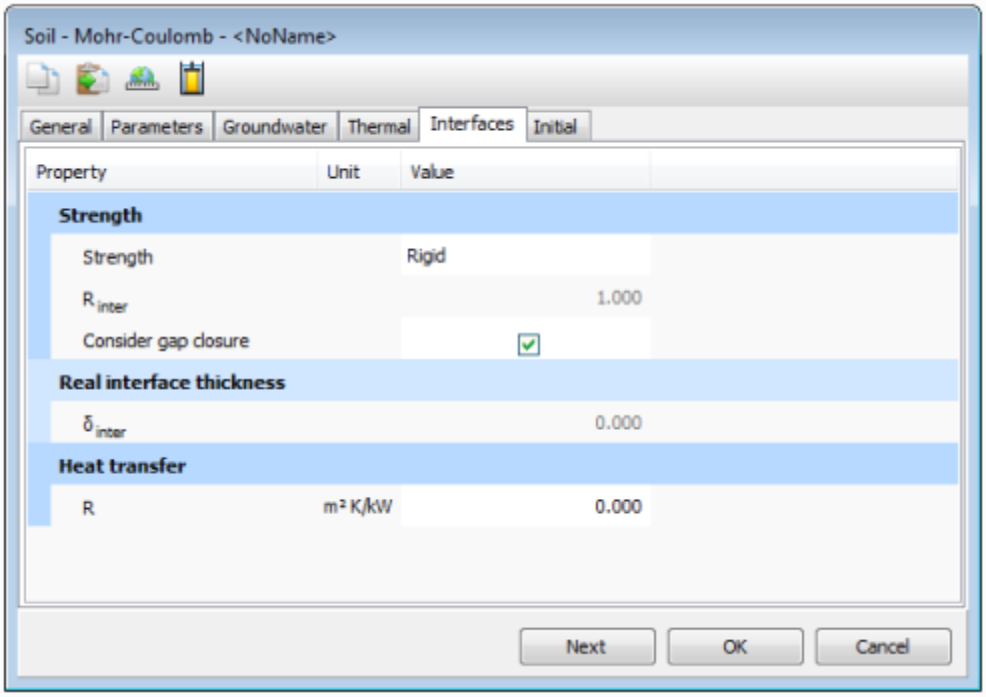

Figure 32 Interface properties

Along with reduced soil-structure interface strength, the interface also helps to avoid the occurrence of non-physical peak stresses at plate ends.

3.2.6 Meshing

Once the geometry has been completely modelled, it can be meshed according to the level of accuracy (in the form of predefined element distributions ranging from very coarse to very fine mesh) expected by the user. Two important parameters are used to define the meshing in PLAXIS;

- **Relative element size factor (r_e)**

  The values of the parameter r_e for the predefined element distributions are as follows;

  Very coarse: $r_e = 2.0$

  Coarse: $r_e = 1.5$

  Medium: $r_e = 1.0$

  Fine: $r_e = 0.7$

  Very fine: $r_e = 0.5$

- **Average element size (I_e)**

  The average element size is calculated from the outer geometry dimensions (x_{min}, x_{max}, y_{min}, y_{max}, z_{min}, z_{max}) and is defined by the following formula;

$$I_e = \frac{r_e}{20} \cdot \sqrt{(x_{max} - x_{min})^2 + (y_{max} - y_{min})^2 + (z_{max} - z_{min})^2} \qquad (18)$$

Finer the mesh, more is the computation time and the memory consumption. Therefore, a convergence study was performed for the case studies in this thesis, in order to optimize the mesh.

3.2.7 Boundary Conditions

This thesis deals majorly with dynamic analysis and PLAXIS provides different boundary conditions than the standard fixities in order to represent the far-field behavior of the soil medium. The reality is characterized by an infinite domain

which has to be reduced to a finite domain when creating a geometry model. Appropriate boundary conditions can simulate the far-field behavior by absorbing the increment of stresses caused by dynamic loading and avoiding spurious wave reflections inside the soil body. PLAXIS provides an option to use **viscous boundaries** for dynamic calculations.

Viscous boundary

These boundaries absorb the outgoing wave energy. The condition corresponds to a situation in which viscous dampers are applied in the x-y-z directions along the boundary providing a resistant force in the normal and tangential direction at the boundary that is proportional to the velocity in the near -boundary material. The Relaxation coefficients C_1 and C_2 are used to improve the wave absorption on these boundaries. C_1 corrects the dissipation in the direction normal while C_2 does it for the tangential direction. The standard values that have also been used in this thesis are $C_1=1$ and $C_2=1$.

The normal and shear stress components absorbed by the viscous dampers (for the case of x direction) are formulated as follows;

$$\sigma_n = -\mathrm{C}_1 \, \rho \, V_p \, \dot{u}_x \tag{19}$$

$$\tau = -\mathrm{C}_2 \, \rho \, V_s \, \dot{u}_y \tag{20}$$

Where ρ is the density of the materials and V_p and V_s are the pressure wave and the shear wave velocities respectively.

3.3 PLAXIS: Calculations

In order to calculate soil damping, forced vibration analysis is carried out in the case-studies. PLAXIS conducts this analysis by running the calculation in phases similar to the design approach of the real project. Since this thesis majorly deals with clay type soil, the analysis is carried out for undrained behavior of soil. This section talks about the analysis types used in this thesis.

3.3.1 Undrained analysis

Considering the case of suction pile in offshore clayey soils, the permeability is usually low and in cases of extreme weather conditions the rate of loading can be high. In such scenarios, no water movement takes place leading to build up of excess pore pressures.

PLAXIS provides three possibilities for drainage type parameters;

Undrained (A)

This type enables modelling undrained behavior using effective parameters for stiffness and strength. The characteristic features include;

- The undrained calculation is performed as an effective stress analysis using the effective stiffness and effective strength parameters.
- Pore pressures are generated whose accuracy will depend upon the selected model and parameters.
- Undrained shear strength s_u is not an input parameter but an outcome of the constitutive model. This needs to be checked against the known data.

Undrained (B)

This type enables modelling undrained behavior using effective parameters for stiffness and undrained strength parameters. The characteristic features include;

- The undrained calculation is performed as an effective stress analysis using the effective stiffness and undrained strength parameters.
- Pore pressures are generated, but may be highly inaccurate.

- Undrained shear strength s_u is an input parameter.

When used in HSsmall model, the stiffness moduli in the model are no longer stress dependent.

Undrained (C)

The characteristic of this model include;

- The undrained calculation is performed as a total stress analysis using the undrained stiffness and undrained strength parameters.
- Pore pressures are not generated.
- Undrained shear strength s_u is an input parameter

This drainage type is not available for HSsmall model.

In conclusion, **Undrained (A)** is the most appropriate drainage type for the case-studies in this thesis.

3.3.2 Calculation stages

The analysis in PLAXIS for both the case studies is carried out in three stages;

1. Initial stress generation →For direct generation of initial effective stresses, pore pressures and state parameters.
2. In-place phase → To represent the installation stage of the suction pile.
3. Dynamic phase → To represent the operational stage of the structure.

1. Initial stress generation

The initial stresses in a soil body are influenced by the weight of the material and the history of its formation. This stress state is usually characterized by an initial vertical effective stress ($\sigma'_{v,0}$). The initial horizontal effective stress $\sigma'_{h,0}$ is related to $\sigma'_{v,0}$ by the coefficient of lateral earth pressure K_0 by the equation;

$$\sigma'_{h,0} = K_0 . \sigma'_{v,0} \tag{21}$$

In case of the HSsmall model, the K_0 is based on the K_0^{nc} parameter and is also influenced by the over-consolidation ratio (OCR) or the pre-overburden pressure (POP). The K_0 is thus calculated using the formula;

$$\mathrm{K}_0 = K_0^{nc}\mathrm{OCR} - \frac{v_{ur}}{1-v_{ur}}(\mathrm{OCR}-1) + \frac{K_0^{nc}\mathrm{POP} - \frac{v_{ur}}{1-v_{ur}}POP}{|\sigma_{yy}^0|} \qquad (22)$$

These initial stresses are generated using the feature ***K0 procedure***. When this feature is adopted, PLAXIS generates vertical stresses that are in equilibrium with the self-weight of the soil. Horizontal stresses, however are calculated from the specified value of K_0. At the end of the ***K0 procedure,*** the full soil is weight activated.

2. Installation Phase: Plastic Calculation

A ***Plastic calculation*** is used to carry out an elastic-plastic deformation analysis in which it is not necessary to take the change of pore pressure with time into account. Here the stiffness matrix is based on the original undeformed geometry.

3. Dynamic phase

The dynamic option should be selected as the calculation type when it is necessary to consider stress waves and vibration in the soil.

In PLAXIS the dynamic calculation is based on the basic equation for the time-dependent movement of a volume under the influence of a dynamic load, which is given by;

$$M\ddot{u} + C\dot{u} + Ku = F \qquad (23)$$

Where M is the mass matrix, u is the displacement vector, C is the damping matrix, K is the stiffness matrix and F is the load vector.

- The **M matrix** is implemented as lumped matrix which includes the mass of the materials (soil + water + any constructions).

- The **C matrix** is formulated as a function of the mass and the stiffness matrices if the user provides the Rayleigh damping parameters. In this thesis, no Rayleigh damping parameters have been provided.
- The **K matrix** accounts for the stiffness of the system. In case of undrained analysis, the bulk stiffness of the groundwater is added to this matrix.

Time Integration

In PLAXIS the time integration is carried out using implicit time integration scheme of Newmark. With this method, the displacement and the velocity at the point in time $t+\Delta t$ are expressed respectively as;

$$u^{t+\Delta t} = u^{t} + \dot{u}^{t}\Delta t + ((\left(\frac{1}{2} - \alpha\right)\ddot{u}^{t} + \alpha\ddot{u}^{t+\Delta t})\Delta t^{2} \tag{24}$$

$$\dot{u}^{t+\Delta t} = \dot{u}^{t} + ((1-\beta)\ddot{u}^{t} + \beta\ddot{u}^{t+\Delta t})\Delta t \tag{25}$$

In the above equations, Δt is the time step. The coefficients α and β determine the accuracy of the numerical time integration. For a stable solution the following conditions must apply;

$$\beta \geq 0.5\,, \alpha \geq \frac{1}{4}\left(\frac{1}{2} + \beta\right)^{2} \tag{26}$$

For the thesis, default values of α=0.25 and β =0.50 are utilized.

Critical Time Step

The time step used by Plaxis in a dynamic calculation is constant and is given by;

$$\Delta t = T / (m * n) \tag{27}$$

where ***T*** is the Time interval specified for the relevant phase, ***m*** is the number of Additional steps and ***n*** is the number of Dynamic sub steps.

The result of the multiplication of the Additional step number (m) and the Dynamic sub steps number (n) gives the total number of steps to be used in the time discretization. It is important to define a proper number of steps such that the dynamic signal used in dynamic loading is properly covered. In general, it is recommended to choose T, m and n in such a way that the dynamic sub step time interval Δt is equal to the time interval used in the input signal.

The critical time step ($\Delta t_{critical}$)can be defined by the following equation;

$$\Delta t_{critical} = \frac{I_e}{\alpha\sqrt{\frac{E\,(1-v)}{\rho(1+v)(1-2v)}}\sqrt{1+\frac{B^4}{4S^2}-\frac{B^2}{2S}\left[1+\frac{1-2v}{4}\frac{2S}{B^2}\right]}} \qquad (28)$$

Where the term B and S respectively denote the largest dimension of the finite element and the surface area of the finite element. The factor α depends on the element type (for 15 node element $\alpha \approx 0.748$) .

The $\Delta t_{critical}$ is formulated in such a way that a wave during a single time step does not move a distance larger than the minimum dimension of an element. The user needs to choose $\boldsymbol{T}$ in such a way that $\Delta t \leq \Delta t_{critical}$.

To sum up, the three calculation phases are executed for each load case in the case-studies.

4 Case study # 1

This chapter explores the dynamic capabilities of PLAXIS 2D by running test cases for a reference project executed by SPT Offshore in the past.

4.1 Modelling in PLAXIS 2D

A suction pile can be idealized as a rigid body with four degrees of freedom: vertical, horizontal, rotational and torsional. However, this case-study majorly focuses on the vertical dof of the suction pile, simulation practical scenarios where suction piles are used for jacket structure (with push-pull mechanism) or in the case of anchoring of Tension Leg Platforms, where the vertical dof is the dominant one. This section covers the details of the PLAXIS 2D model.

4.1.1 Project properties

PARAMETER	VALUE/UNIT	COMMENTS
Model type	Axisymmetric model	Refer section 3.2.1
Element type	15-node triangle element	
Units	Length: m Force: kN	
Contours	50 x 50	▪ Boundary sensitivity was carried out (Section 4.1.5). ▪ 50 x 50 → x_{min}=0; x_{max}=50; y_{min}=-50; y_{max}=0

4.1.2 Soil modelling

- **Site conditions**

The site conditions from the reference project is tabulated below;

PARAMETER	VALUE/UNIT
Water depth	55m
Soil type	NC clay
Soil shear strength	35 *kPa*
No. of soil layers	1
Plasticity Index (PI)	40 %

- **Soil parameters for PLAXIS model**

  HSsmall model is used in order to model the soil (refer section 3.1.3). In accordance to the site conditions mentioned above, the soil parameters for the HSsmall model have been calculated based on the plasticity index of the clay.

PARAMETER	VALUE/UNIT	COMMENT
Tangent stiffness for primary oedometer loading (E_{oed}^{ref})	1250 kN/m^2	$E_{oed}^{ref} = \frac{50000}{PI}\ (KPa)$
Secant stiffness in standard drained triaxial test (E_{50}^{ref})	2500 kN/m^2	$E_{50}^{ref} \approx 2E_{oed}^{ref}$
Unloading/reloading stiffness from drained triaxial test (E_{ur}^{ref})	7500 kN/m^2	$E_{ur}^{ref} = 3E_{50}^{ref}$
Reference shear modulus at very small strains(G_0^{ref})	17.2e3 kN/ m^2	▪ G_0 generally, ranges from 10 times G_{ur} for soft soils, down to 2.5 times G_{ur} for harder types. ▪ For this case $G_0^{ref} = 5.5\ G_{ur}^{ref}$ where $G_{ur}^{ref} = \frac{E_{ur}^{ref}}{2(1+\nu_{ur})}$
Shear strain level at which secant shear modulus G_s is reduced to about 70% of G_0 ($\gamma_{0.7}$)	0.15e-3	$\gamma_{0.7}$ is generally between 1 and 2 times 10^{-4}
Poisson's ratio (ν)	0.2	
Reference stress (p^{ref})	100 kN/ m^2	Default
Interface strength factor (R_{inter})	0.65	Generally suggested for the case of NC clays

4.1.3 The structure

In PLAXIS 2D model of the suction pile is axisymmetric. The dimensions of suction pile are taken from the reference project. The following table tabulates the details;

PARAMETER	VALUE/UNIT
Diameter (D)	7 m
Skirt length (L)	8 m

In order to simulate rigid body behavior in PLAXIS 2D, the suction pile has been modelled using plates with an arbitrary stiffness that is sufficiently large compared to the stiffness of the soil. Figure 33 shows the properties defined for the plate element.

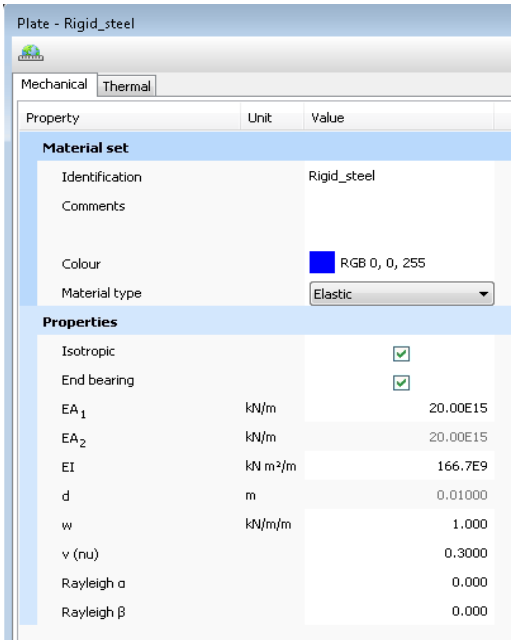

Figure 33 Material property for the plate element

The final model is shown in Figure 34.

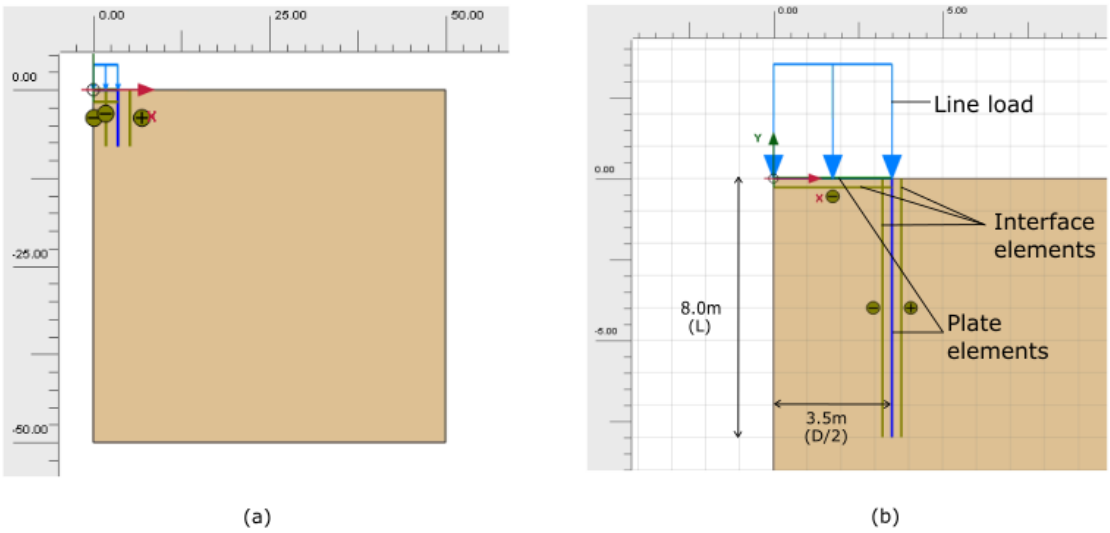

Figure 34 (a) Full model in PLAXIS 2D; (b) Geometric entities used

4.1.4 Loading

The loads from the reference project are as follows;

PARAMETER	VALUE/UNIT	COMMENT
Vertical static load (V_{static})	7 MN	▪ Modeled as line load (pressure) in PLAXIS 2D ▪ 7MN = $\frac{7000}{\pi*3.5*3.5}$=181.89 KN/m^2
Dynamic load amplitude (Ultimate load) (V_{dyn})	±3 MN	▪ Modeled as line load (pressure) in PLAXIS 2D

20 load cases are run in order to execute a parametric study of damping in vertical vibration. A forced vibration analysis is carried by applying harmonic loading at the center of the suction pile. The following range for the harmonic signal is considered;

PARAMETER	RANGE	COMMENT
Loading frequency (freq)	0.2 Hz to 1.0 Hz	Frequently encountered sea state frequencies
Dynamic time	10 cycles	
Dynamic amplitude (dyam)	5% to 20% of Dynamic load amplitude (Ultimate load)	▪ Aligns with the range of operational loads ▪ Modeled as line load (pressure) in PLAXIS ▪ Eg. 5% of 3MN=150 KN 150 KN = $\frac{150}{\pi*3.5*3.5}$=3.89 KN/m^2

Considering the ranges mentioned above, the 20 load cases can be represented in matrix form;

Freq/Dyam	5 % of V_{dyn} [150 kN]	10 % of V_{dyn} [300 kN]	15 % of V_{dyn} [450 kN]	20 % of V_{dyn} [600 kN]
0.2 Hz	Case 1	Case 2	Case 3	Case 4
0.4 Hz	Case 5	Case 6	Case 7	Case 8
0.6 Hz	Case 9	Case 10	Case 11	Case 12
0.8 Hz	Case 13	Case 14	Case 15	Case 16
1.0 Hz	Case 17	Case 18	Case 19	Case 20

4.1.5 Boundary Sensitivity

As mentioned in Section 3.2.1, the contours for the model should be placed in such a way that there are no boundary effects. A boundary sensitivity analysis was thus carried out in this case study for Case 1. The position of the contours/boundaries are defined by x_{min},x_{max},y_{min} and y_{max}. For simplicity let the position of the boundary be defined by the parameter L (refer Figure 35).

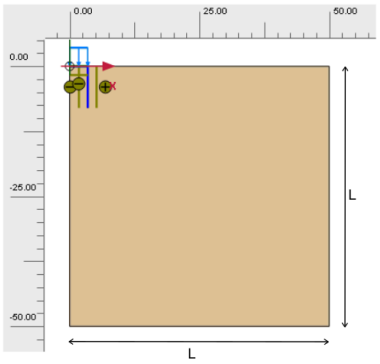

Figure 35 Definition of parameter 'L'

The value of the parameter L was varied from 3 up to 8 times the diameter of the suction pile in order to get a converging solution. The vertical displacement v/s time for the center node (Node A -(0,0)) was plotted for every L. Finally, after L≈ 50, the plots seemed to converge (refer Figure 36). Hence 50 x 50 was chosen as the boundary dimensions for this case-study.

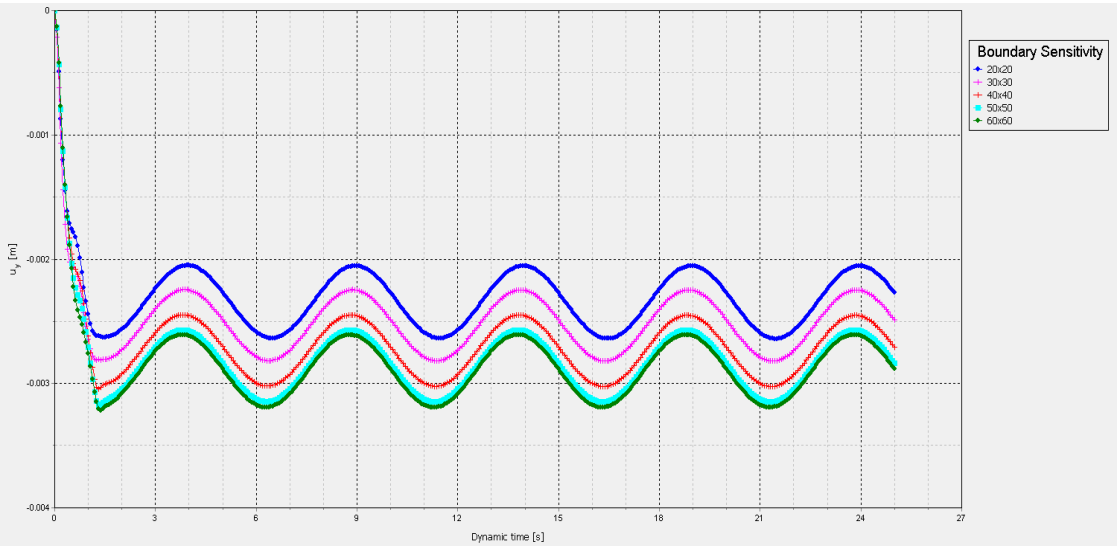

Figure 36 Boundary Sensitivity Analysis

4.1.6 Meshing

A convergence study was carried out for Case 1 by varying the mesh from very coarse to very fine (refer 3.2.6). The vertical displacement v/s time for the center node (Node A -(0,0)) was plotted for every mesh type. The results (refer Figure 37) clearly show that the plots converge after the 'fine' mesh type.

Hence 'fine mesh' was chosen for this case-study. (Refer Figure 37)

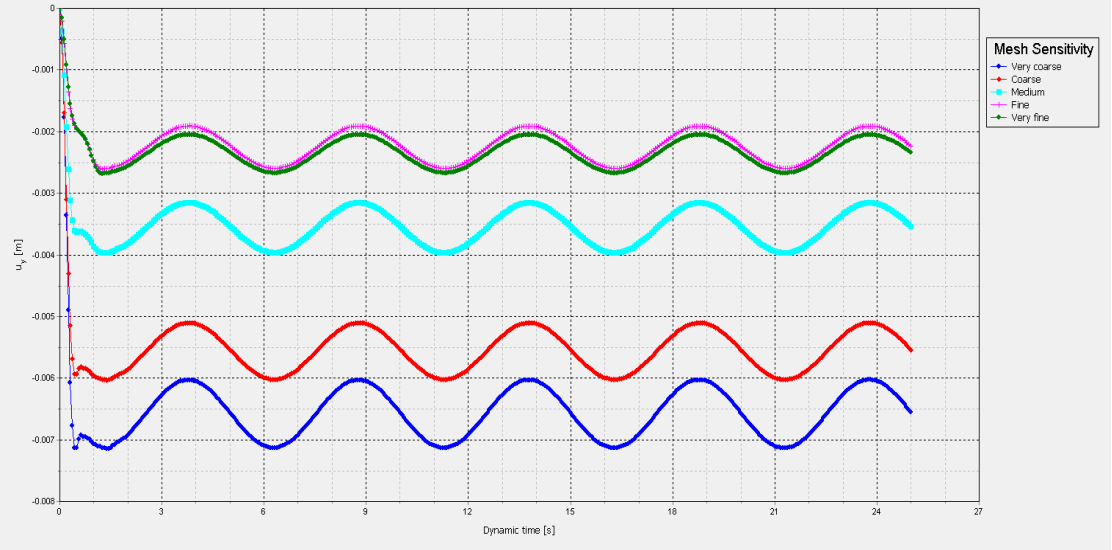

Figure 37 Mesh sensitivity analysis in PLAXIS 2D

4.1.7 Time step calculation

The time step calculation is done according to Section 3.3.2. The formula for critical time step is given below;

$$\Delta t_{critical} = \frac{I_e}{\alpha \sqrt{\frac{E\,(1-v)}{\rho(1+v)(1-2v)}} \sqrt{1+\frac{B^4}{4S^2}-\frac{B^2}{2S}\left[1+\frac{1-2v}{4}\frac{2S}{B^2}\right]}} \qquad (29)$$

The time step Δt should not exceed the $\Delta t_{critical}$. For this case study, B=4.0 m , S=11 m^2 and I_e was calculated for r_e=0.7 (refer 3.2.6).The value of $\Delta t_{critical}$ is thus 0.06 secs. A time step of 0.05 secs was chosen for this case study.

4.1.8 Calculation phases

Every load case has the following calculation phases;

PHASE	CALCULATION TYPE	COMMENT
Initial Phase	K0 procedure	Direct generation of initial effective stresses, pore pressures and state parameters.
Phase 1	Plastic	▪ Activation of the suction pile ▪ Activation of static line load (181.89 KN/m^2)
Phase 2	Dynamic	Forced vibration analysis • Activation of the dynamic load component (eg. Case 1: 3.89 KN/m^2) • The displacement of the Phase 1 is set to zero in order to only plot the dynamic response.

4.2 PLAXIS 2D Output

After running the simulations for all the 20 cases, the output from PLAXIS is further processed in MATLAB in order to calculate the soil damping. This section gives details about the generated output and the results drawn.

4.2.1 Interpreting the PLAXIS 2D output

The center node on the top plate of the suction pile (refer Figure 38)is selected for further calculations in this case-study. In order to calculate damping, the vertical displacement versus the dynamic time plot (for Node A) is extracted for each load case. To get an idea of what to expect, Figure 39, show the plots at Node A for 0.2 Hz frequency.

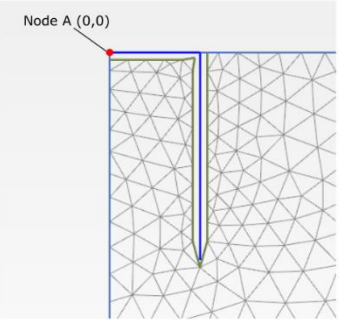

Figure 38 Location of node A

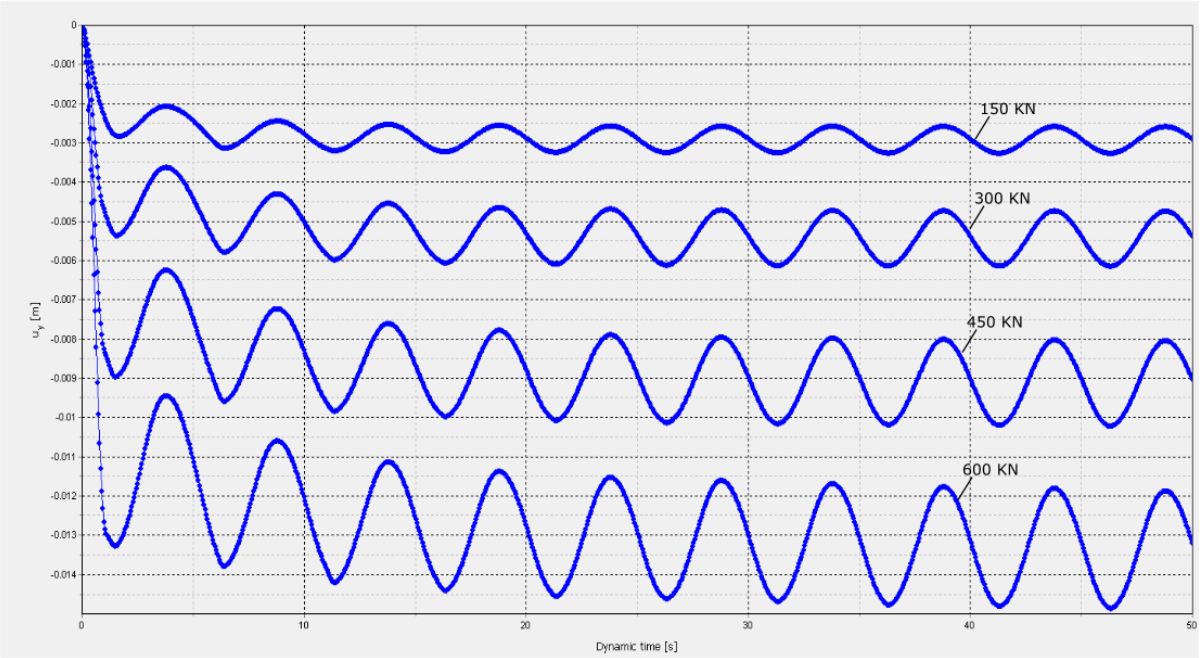

Figure 39 Vertical displacement (u_y) versus dynamic time plot for 0.2 Hz

The total load applied to the suction pile can be expressed as;

$$V_{total} = V_{static} + V_{dyn} \quad (30)$$

Ideally the vertical response should be expressed as;

$$z_{total} = z_{static} + z_{dyn}$$

Where z_{static} refers to the settlement reached in the operational stage of the suction caisson.

Note: In phase 2 the displacement from previous phase is set to zero and hence the plot should only show vertical response due to dynamic load.

Below is the plot (Figure 40) of vertical dynamic response v/s time for Case 1.

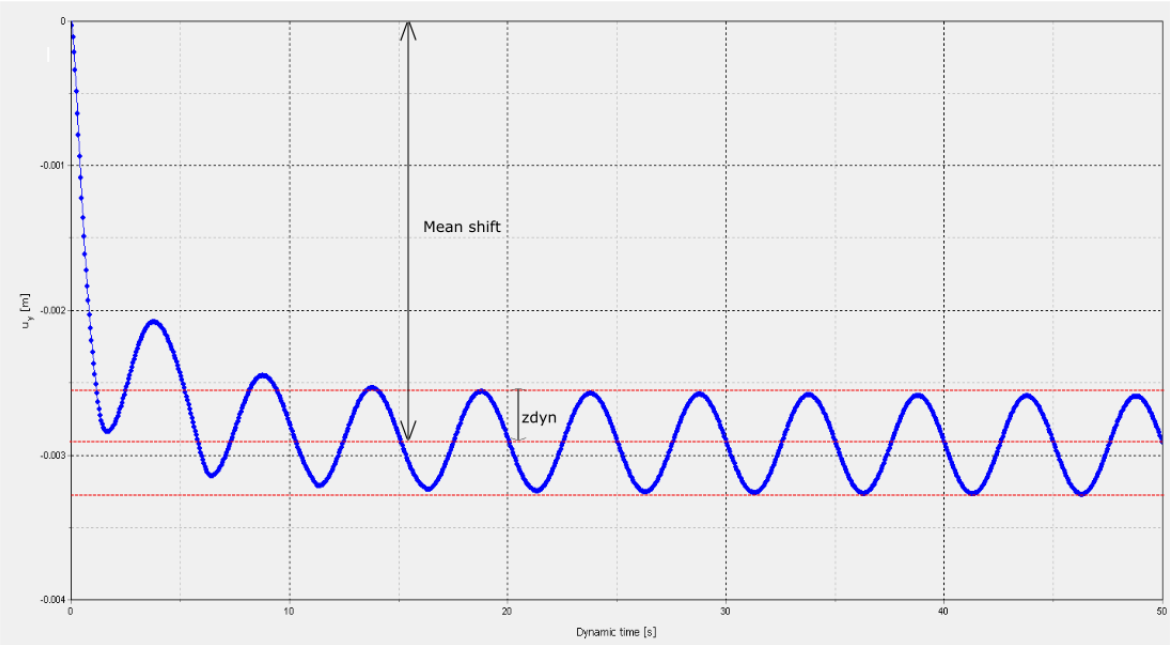

Figure 40 Vertical displacement (u_y) versus dynamic time plot for Case 1

Comments

- An interesting non linearity is observed in the form of mean shift, as shown in Figure 40. This mean shift has been observed for all load cases.
- According to this mean shift, the expression for z_{total} should be modified as

$$z_{total} = z_{static} + z_{dyn} + mean\ shift \quad (31)$$

Further analysis on the mean shift can give idea regarding the degree of non-linearity in the system. Since the focus of the study is damping and the mean shift does not affect the amplitude of the dynamic response, nor the phase-shift one can move ahead with this observation.

4.2.2 Analyzing: The Phase-shift Method

The vertical displacement v/s time response (for Node A) obtained from PLAXIS further is used to calculate the vertical coefficient of damping (C_v) by adopting the Phase-shift method (refer Appendix B).

The following steps were carried out in order to implement the method for the PLAXIS output;

- The 20 load cases are run in PLAXIS 2D
- The vertical displacement v/s time response is imported (for each load case) to MATLAB and fit it to a sine curve in the form of

$$\text{Plaxis response} = mean\ shift + z_{dyn} = m + bt + Asin(\Omega t + \varphi) \tag{32}$$

  - $m + bt$: mean shift
  - A : Dynamic response amplitude
  - φ : Phase shift w.r.t $F\ (F_a \sin(\Omega_1 t))$
  - Ω : Frequency of loading

  The major reason to fit the response into sine curves is to get a constant value of phase shift for a particular load case. In order to get the fit as close as possible, the initial few seconds of the response has not been considered.

- z_{dyn} for every load case is written in the form;

$$z_{dyn} = \tilde{z}_{dyn} e^{i\Omega t} \tag{33}$$

$$\tilde{z}_{dyn} = Ae^{i\varphi t} \tag{34}$$

- C_v is then calculated as a function of frequency using the formula;

$$C = \frac{Im\left(\frac{F_a}{\tilde{z}_{dyn}}\right)}{\Omega} \tag{35}$$

4.3 Results

This section explains the results of the case study.

4.3.1 Variation of C_v with loading amplitude

Using the phase-shift method, the vertical damping coefficient, C_v (Ns/m) is calculated for each load case and presented in a matrix form;

Freq/Dyam	5 % of V_{dyn} [150 kN]	10 % of V_{dyn} [300 kN]	15 % of V_{dyn} [450 kN]	20 % of V_{dyn} [600 kN]
0.2 Hz	2.80E+07	3.22E+07	3.60E+07	3.92E+07
0.4 Hz	1.46E+07	1.52E+07	1.59E+07	1.97E+07
0.6 Hz	1.07E+07	1.18E+07	1.16E+07	1.33E+07
0.8 Hz	9.80E+06	9.59E+06	1.16E+07	1.15E+07
1.0 Hz	1.06E+07	1.10E+07	1.18E+07	1.31E+07

One can examine the variation of C_v with increasing forcing amplitude from the figure below (refer Figure 41);

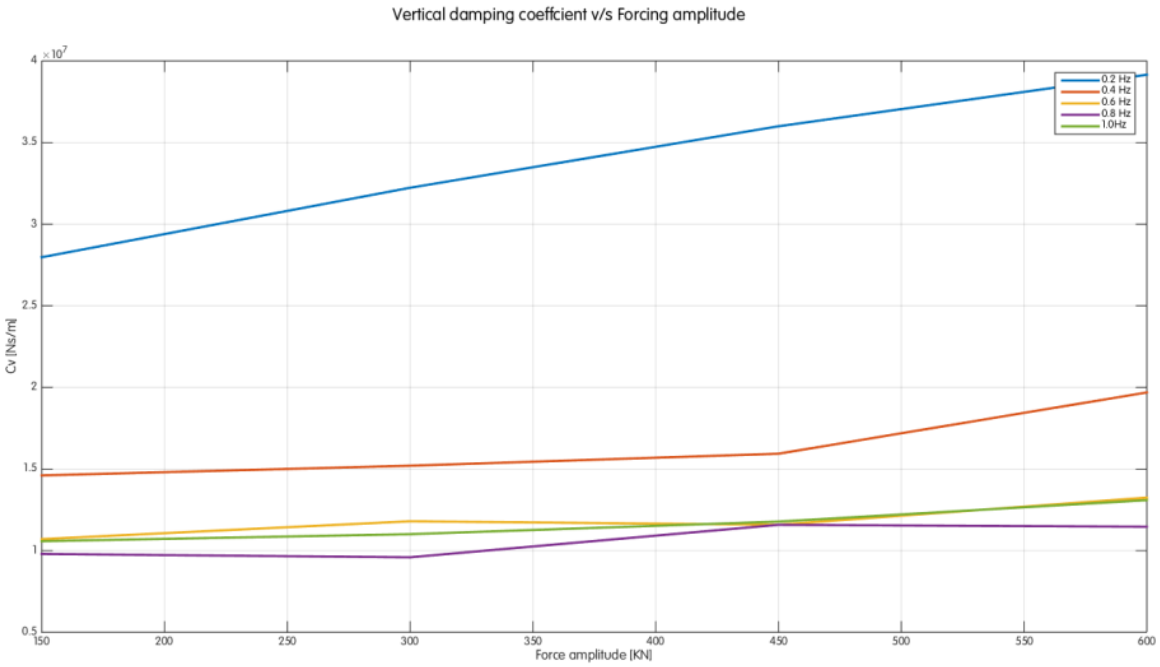

Figure 41 Cv v/s Forcing amplitude

For a particular frequency, a general trend of increase in the value of the damping coefficient with increasing force amplitude can be observed. This variation can be explained by the fact that increase in the loading amplitude leads to an increase of the response amplitude which further leads to increase of the energy dissipated. Figure 42 shows the nature of the force versus response plot of a representative cycle for a particular load case. Damping is equivalent of the dissipated energy which from such plots can be calculated by the following equation;

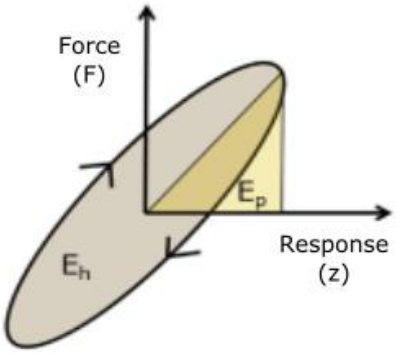

Figure 42 Force v/s Response plot

$$D = \frac{E_h}{4\pi E_p} \qquad (36)$$

Where E_h and E_p are presented in Figure 42.

If plotted for different loading amplitudes, one could clearly see the increased area of the dissipated energy. In reference to this case study, Figure 43 shows the increasing enclosed areas (≈dissipated energy) with increasing load amplitude for frequency of 0.4Hz.

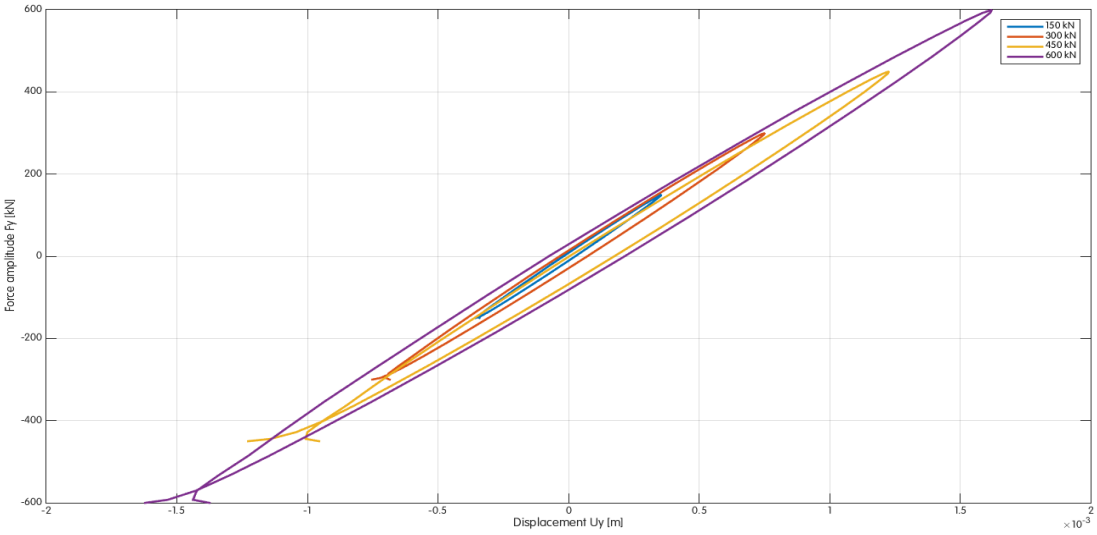

Figure 43 Force v/s response for 0.4 Hz (for 10th cycle)

This explanation can be further extended to the fact that increase in the vertical displacement corresponds to an increase in the shear strain and higher value of shear strains is associated with higher value of the damping factor (refer Figure 44).

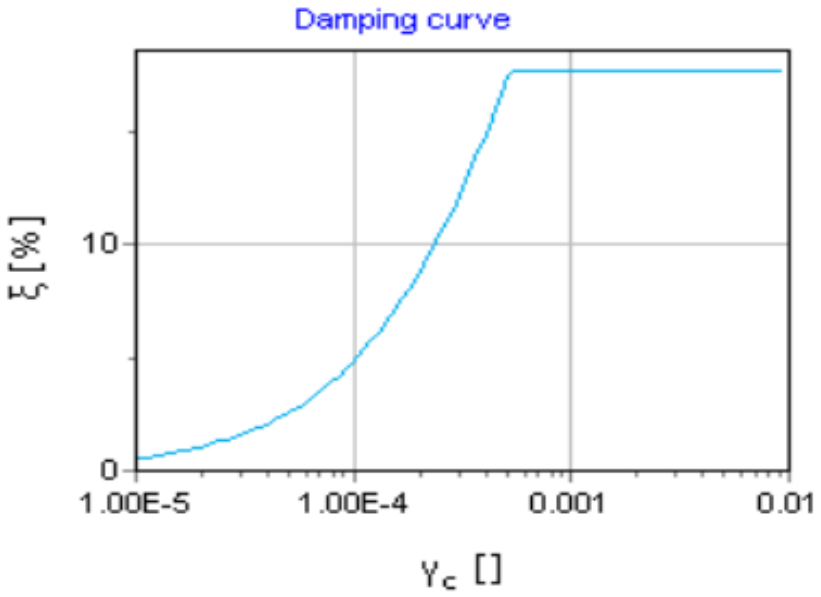

Figure 44 Damping curve for the HSsmall model of the case-study generated by PLAXIS

It is well known that the soil behaves non-linearly resulting in gradual reduction of shear modulus (Figure 45) and increase of hysteretic damping ratio(Figure 44) with increasing amplitude of shear strain(Vucetic and Dobry 1991). This explains the increase of C_v with increasing force amplitude.

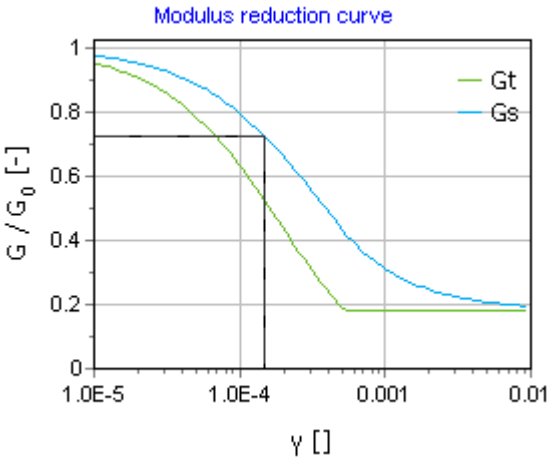

Figure 45 Shear modulus reduction curve for HSsmall model used in Case study#1

4.3.2 Variation of C_v with loading frequency

The plot below (refer Figure 46) gives the variation of C_v with loading frequency for a particular load level;

A general trend of reduction in C_v with increasing frequency is observed in the plot above. One can also see that as the frequency increases, the lines get closer to each other suggesting the fact that at higher frequencies, varying force amplitudes have less influence over the value of C_v.

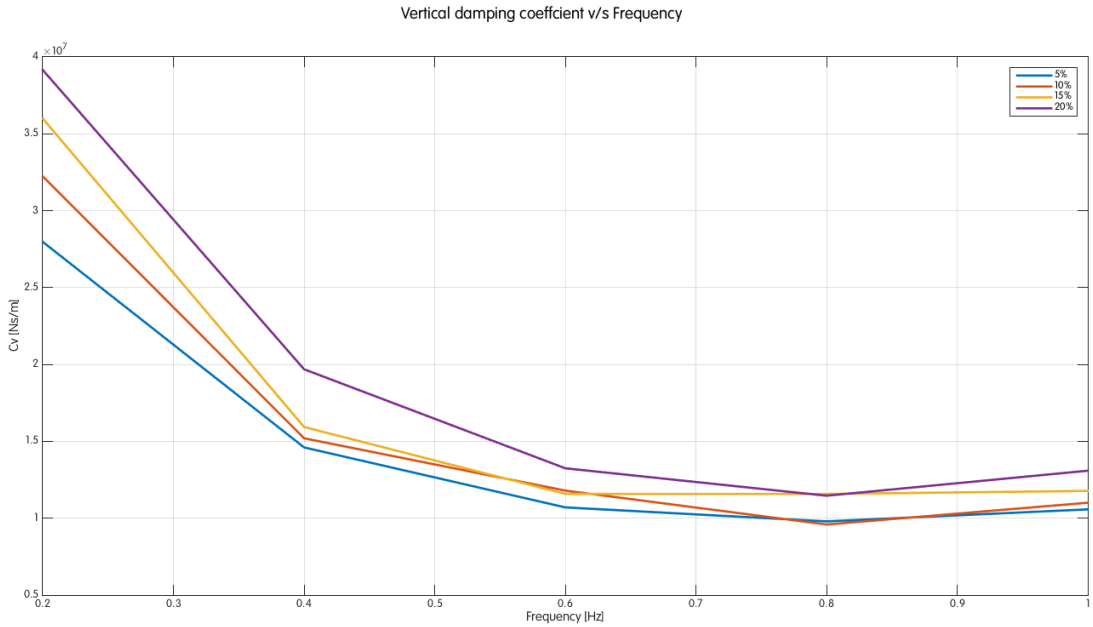

Figure 46 C_v v/s Frequency

- **Comparison with Gazetas**

  As mentioned in Section 2.3.2, the value of C_v ($\equiv C_{total}$) can be calculated using Gazetas charts. The detailed calculation is demonstrated in Appendix C. According to Gazetas charts, C_{total} is a summation of C_{rad} and C_{hys}. It turns out that for the given frequency range ($\leq$1.0 Hz), C_{rad} is constant. It is then interesting to compare the calculated C_v from the case study to the one derived by Gazetas charts. In Figure 47, the green line denotes C_{hys} and the light blue line denotes C_{total} calculated from Gazetas charts.

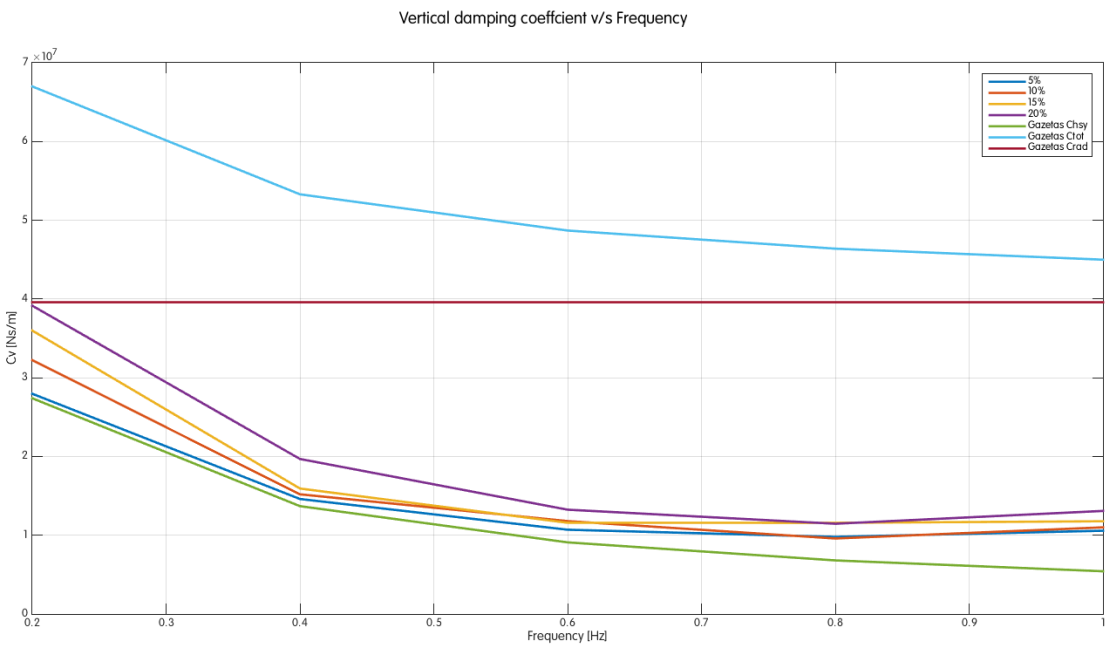

Figure 47 Comparison with Gazetas values

Comments

- In PLAXIS it is not possible to differentiate between damping due to radiation and hysteresis. However, if this clear separation is present as calculated by Gazetas method, the radiation damping predicted by PLAXIS is much lower than C_{rad} derived from Gazetas. This difference might be due to the fact that the Gazetas method was developed for foundation with flat base embedded in homogenous soil, whereas the suction pile in exactly upside down in reality.
- The value of the total vertical damping coefficient C calculated in both the cases display a similar trend of reduction with increasing frequency. In case of Gazetas values, the decreasing trend is attributed to hysteretic damping. It is interesting to observe that C_{hys} provides a reasonable fit to the C_v values for lower load levels.
- C_{rad} derived from Gazetas has a constant value over the given frequency range. This is because, the dynamic damping factor ($\tilde{c}_z = \tilde{c}_z(a_0; \frac{L}{B}, v)$) used in the calculation of C_{rad}, is more or less constant over the specified frequency range ($\leq 1.0\ Hz$).
- C_{tot} is in the range of 1.2-4.8 times the magnitude of calculated C_v. This difference is mainly due to the calculated C_{rad}. However, the formulation

of C_{hys} given by Gazetas, seems to provide a good estimate of damping due to soil hysteresis for the case study at hand.

- **Comparison with Wolf**

The vertical damping coefficient C is calculated for Wolf's three parameter model using the formula;

$$C = \frac{r}{V_s}\gamma \mathrm{K} \tag{37}$$

Where the vertical static stiffness coefficient K ,is given by;

$$K = \frac{4\,Gr}{1-v} \tag{38}$$

Here G is the shear modulus of soil, r is the radius of the suction pile,v is the soil Poisson's ratio, V_s is the shear wave velocity of the soil. Wolf suggests the values γ=0.85 and μ=0.27 for vertical case. Using these values, C is computed and plotted in comparison with the calculated values of C_v (refer Figure 48).

<u>Comments</u>

- The C calculated using the three parameter model is constant with frequency. This is because this model only accounts for loss of energy through radiation damping.
- The three parameter model does not take into account the hysteretic damping in soil. This explains the difference in the nature of the plot for C and C_v.
- The C calculated by Wolf's model seems to give a good approximation of damping due to radiation for the case study at hand.

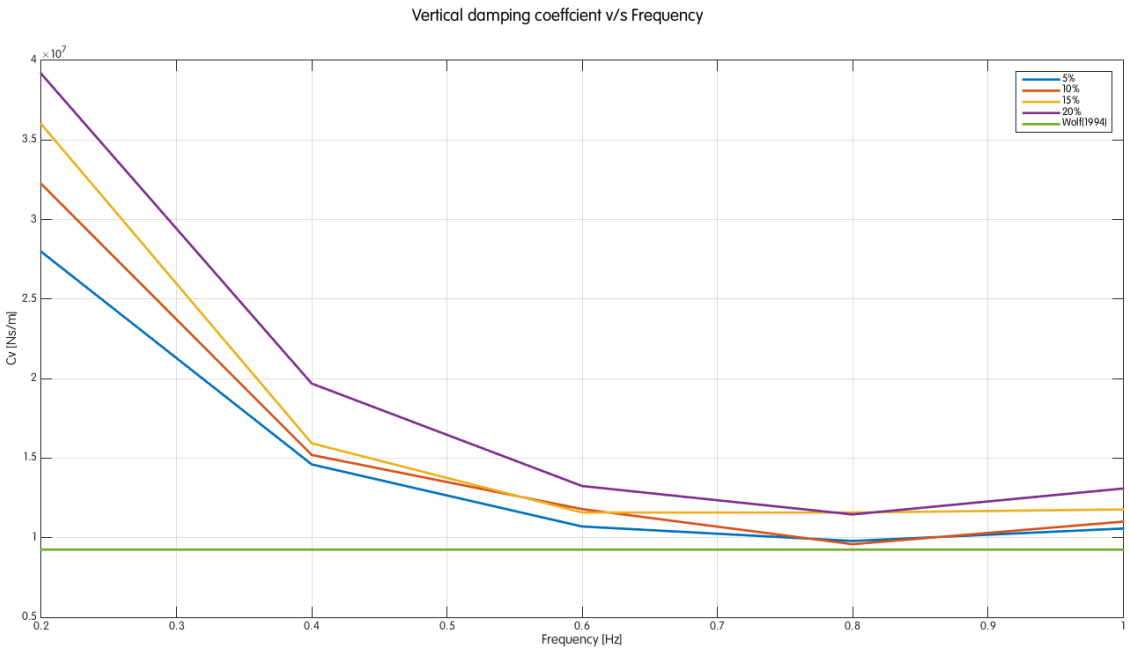

Figure 48 Comparison with Wolf

A comparison with Gazetas charts and Wolf's model shows that the hysteresis part of the calculated C_v seems to adhere to C_{hys} derived from Gazetas charts while the radiation part is approximated better by the three parameter model. Interesting if one could combine the two methods and formulate C_{combi} such that;

$$C_{combi} = C_{hys}\ (Gazetas) + C\ (Wolf's) \tag{39}$$

Comparison of C_v with the newly formulated C_{combi} is depicted in Figure 49. The C_{combi} (plotted in green) provides a reasonable fit for C_v as higher load levels and lower frequencies.

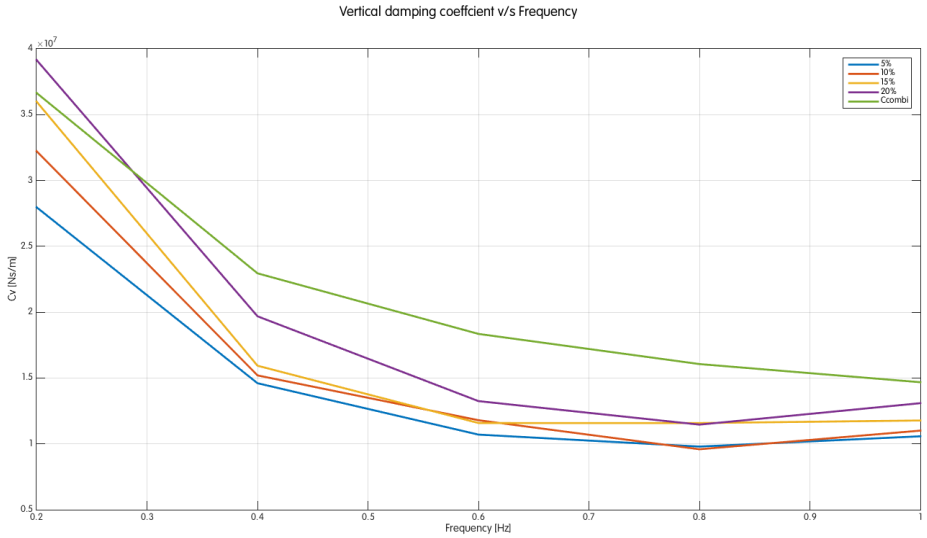

Figure 49 Comparison with Ccombi

A better physical interpretation to the results can be seen in Figure 50, which plots the damping force against the loading frequency. The damping force is calculated as a product of the vertical damping coefficient C_v, the loading frequency and the dynamic response amplitude. A general trend of increase in the

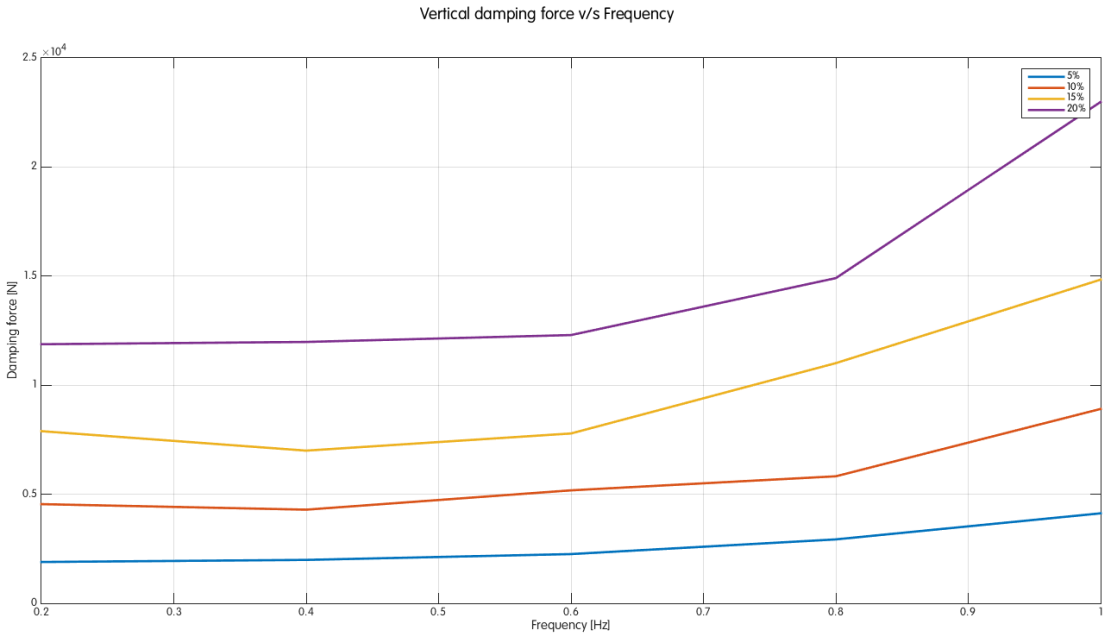

Figure 50 Damping force v/s frequency

damping force with increasing frequency is observed in the plot. For lower force amplitudes, the increase is less steep as compared to the higher load amplitudes.

(Houlsby et al. 2005) conducted field trials of suction caissons in clay for offshore wind turbine foundations. In these trial the cassion was tested for moment loading. The result data was interpreted by first taking the Fast Fourier Transform (FFT) of both the moment and rotation to convert to the frequency domain, and then taking the ratio between the two FFT's to obtain the complex, frequency dependent impedance. The real part of the impedance represents the stiffness and inertial effects, and the imaginary part represents damping. The imaginary part of the impedance is simply the product of damping coefficient (c) and frequency (ω). When compared with Wolf's three parameter model, a reasonable fit was observed (refer Figure 51). The product $c.\omega$ is seen to increase with increasing frequency. A similar graph was plotted for the present case study and compared with Wolf's three parameter model. A reasonable fit was observed at higher frequencies.

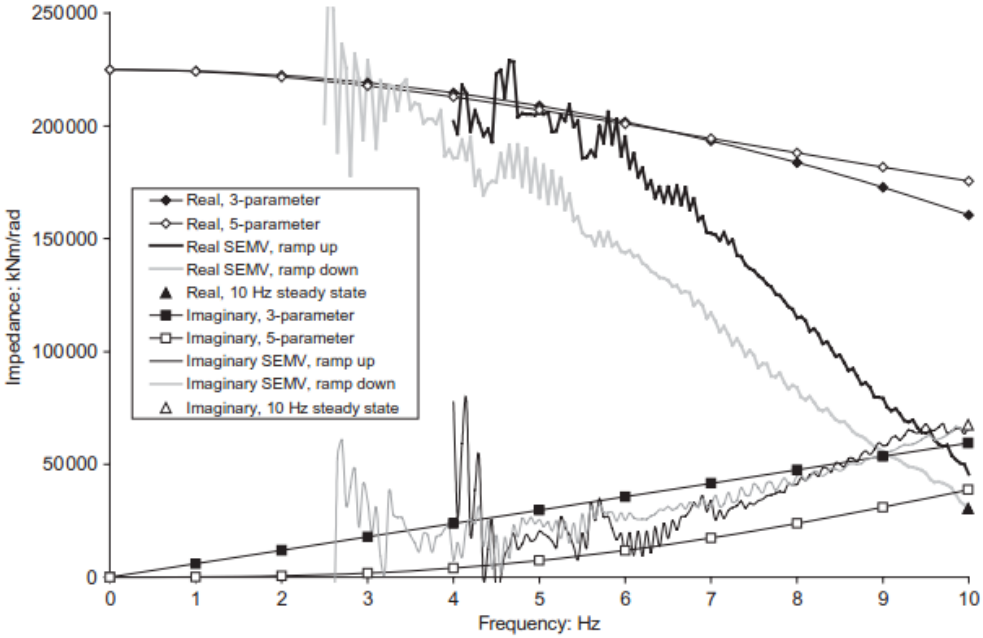

Figure 52 Impedance v/s frequency. Source: (Houlsby et al. 2005)

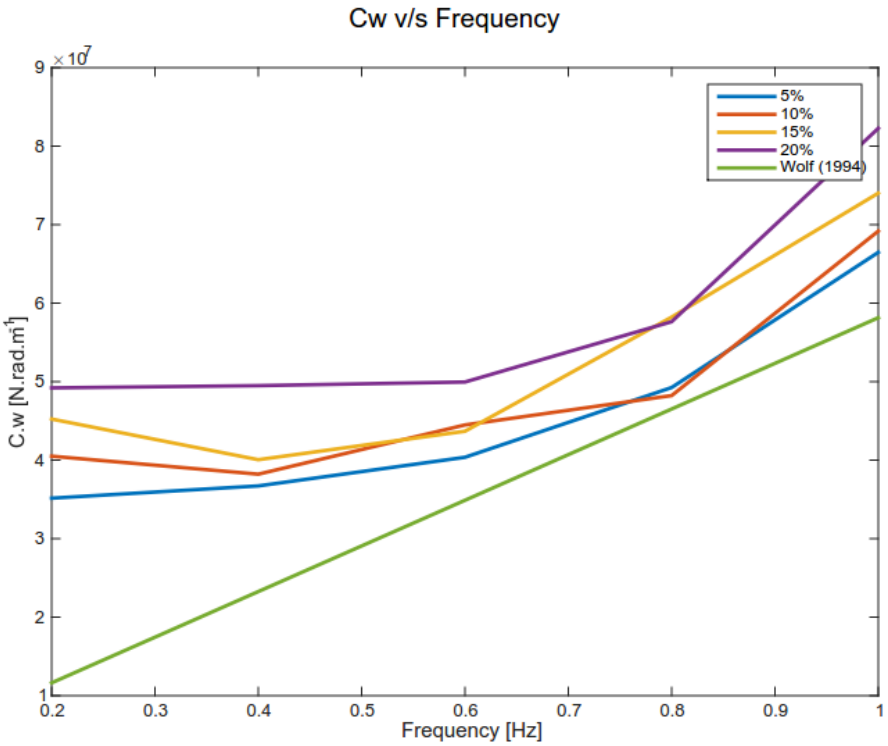

Figure 51 Product of C_v ω against frequency (ω)

Both the graphs show that the value of the product of damping coefficient and frequency, increases with frequency.

5 Case study # 2

A methodology to compute modal damping (due to soil) for the critical modes of a SIWT is formulated in this chapter. Each section in this chapter explains a step of this methodology. The last section of this chapter discusses the usability of the proposed method.

5.1 Eigen Mode Analysis (Step #1)

5.1.1 Modelling in FEMAP

Advanced FEM based softwares makes it easier to model the structure accurately in order to study its dynamic properties. In order to ensure reasonable computational time and memory, the model has optimized such that it is able to capture all the dynamic behavior.

The entire model in FEMAP is mainly built using beam elements except the transition piece (TP), which has been modelled using plate elements. The nacelle and the turbine is modelled as lumped masses on the tower (refer Figure 54). The tower-TP inference along with the TP-leg interfaces are idealized as rigid connections.

The jacket support structure provides **push pull action** in order to accommodate the lateral bending of the entire structure. Consequently, the push-pull movement of the jacket structure causes **vertical vibration of the suction pile**. Owing to the structural properties of the suction pile, the pile more or less behaves like a rigid foundation. By the virtue of this property, one can neglect the horizontal and rotation vibration of the suction pile.

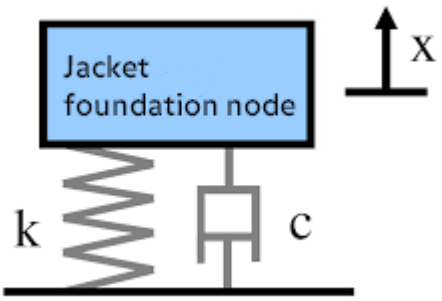

Figure 53 Suction pile idealization

The foundation nodes (the end nodes of all the three leg elements) are therefore modelled with;

- A vertical spring element, to define a stiffness of K=3.5 x10^8 *N/m* (from reference project) in the global Z direction and fixity for global X and Y translation.
- A vertical viscous damper element, whose value will depend on the load case (only modelled when using free decay analysis).

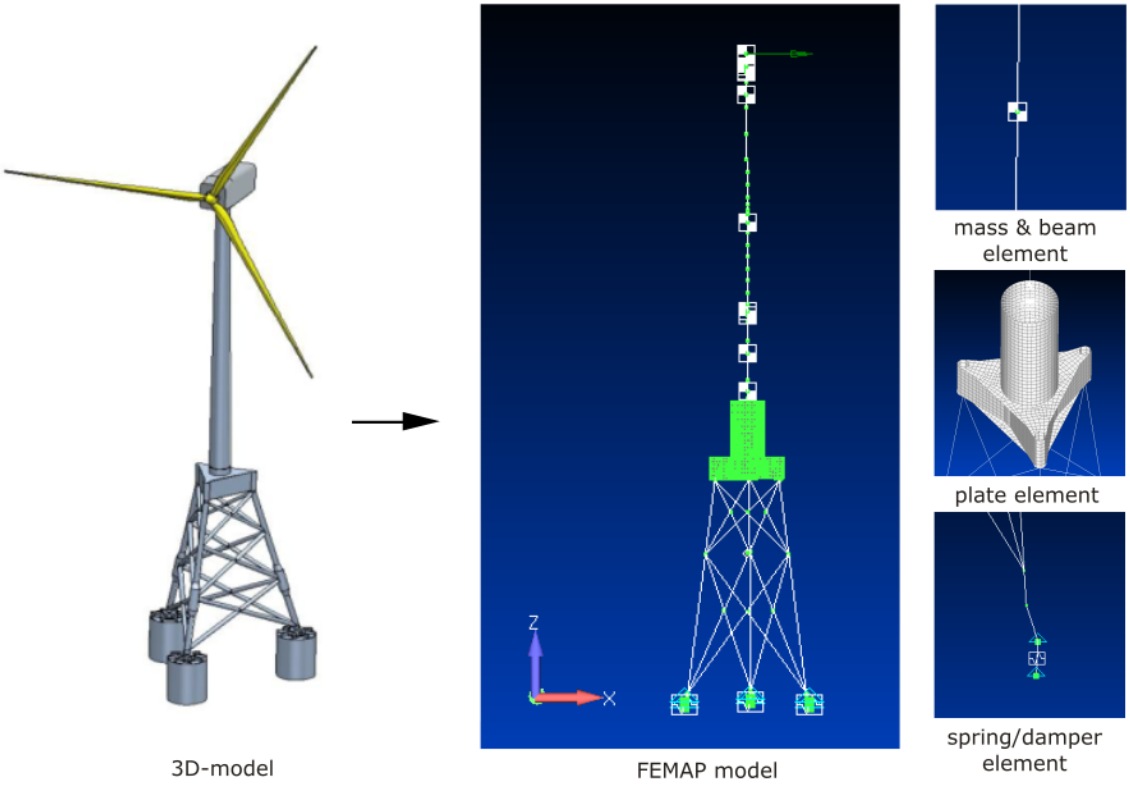

Figure 54 Modelling

5.1.2 Natural Frequencies

Resonance occurs when the loading frequency matches the natural frequency of the system. It is a well-known fact that damping contributes to the total response of a dynamic system only in the vicinity of resonance. Away from resonance, damping is not an important parameter(Ashmawy et al. 1995). Due to this, an eigen mode analysis is the essential first step in order to predict the loading frequency for the PLAXIS input.

Eigen mode analysis is carried for the SWIT in FEMAP. Usually the first three eigen modes are the critical ones but in this case only the first two eigen modes have been considered since the eigen frequencies of these modes fall within the range of the loading spectrum. The following table summarizes the first three modes.

Mode	First mode	Second mode	Third mode
Frequency (Hz)	0.247	0.249	1.011
Mode type	Bending abt global X axis	Bending abt global Y axis	Torsion abt global Z axis
Mode shape	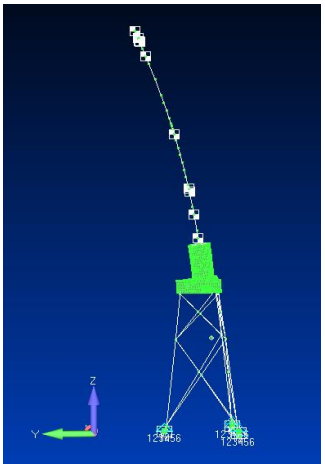	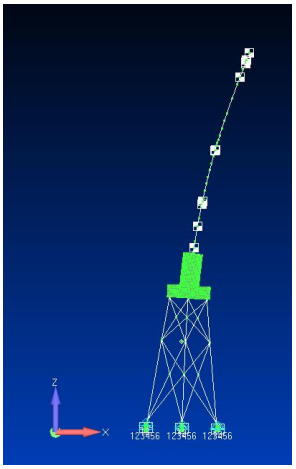	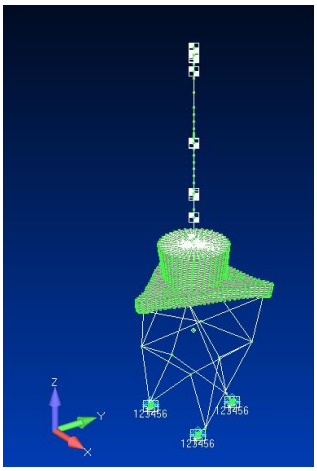

Table 1 Eigen mode analysis

5.2 Analysis in PLAXIS 3D (Step #2)

Ruling out other degrees of freedom (as explained in the previous section), a **forced vertical vibration test** is thus performed in PLAXIS 3D in order to calculate the vertical damping coefficient (C_v). The details of the modelling and the test are as follows;

5.2.1 Soil

- **Soil Model**

  The soil parameters are formulated based on the site specific geotechnical information gathered for this case study (Refer Figure 19). **HSsmall** is chosen as the model type for all the soil layers for the following reasons;

  - It gives more reliable displacements as compared to other existing soil models
  - Hysteretic damping is taken into account making it suitable for dynamic analysis

Soil type	Bottom	γ_{sat}	S_u	c' / φ'	$E_{50;ref}$	$E_{oed;ref}$	$E_{ur;ref}$	m	$G_{0;ref}$	$\gamma_{0.7}$
[-]	[m ML]	[kN/m^3]	[kPa]	[kPa] / [deg]	[MPa]	[MPa]	[MPa]	[-]	[MPa]	[-]
Sand	-2	20	-	0.5 / 38	42	42	126	0.5	168	$1*10^{-4}$
Sand	-8	19	-	0.5 / 30	12	12	48	0.5	72	$1*10^{-4}$
Clay	-15	19	$55+1*z^{1)}$	-	3.4	3.7	26	0.05	41	$2*10^{-4}$

Figure 55 Soil parameters used from the reference project

- **Soil boundary**

  The dynamic boundary conditions are activated. This is done to ensure non-reflecting boundaries for the model. For static cases, it is usually recommended to build soil FEM models with a boundaries measuring five times the diameter of structure. For dynamic cases it is highly recommended to have larger boundaries than that of the static case. In this case the boundaries are 5.5 times the pile diameter.

5.2.2 Structure

Due to the symmetry of the SIWT, the loading scenario for a single suction pile has been analyzed. The pile has been modelled using the available **Rigid Body** feature in PLAXIS 3D. The diameter of the pile is 9.5 m and the skirt length is 12 m.

In order to reduce the computation time, the single suction pile is further modelled as symmetric half-model (refer Figure 56).

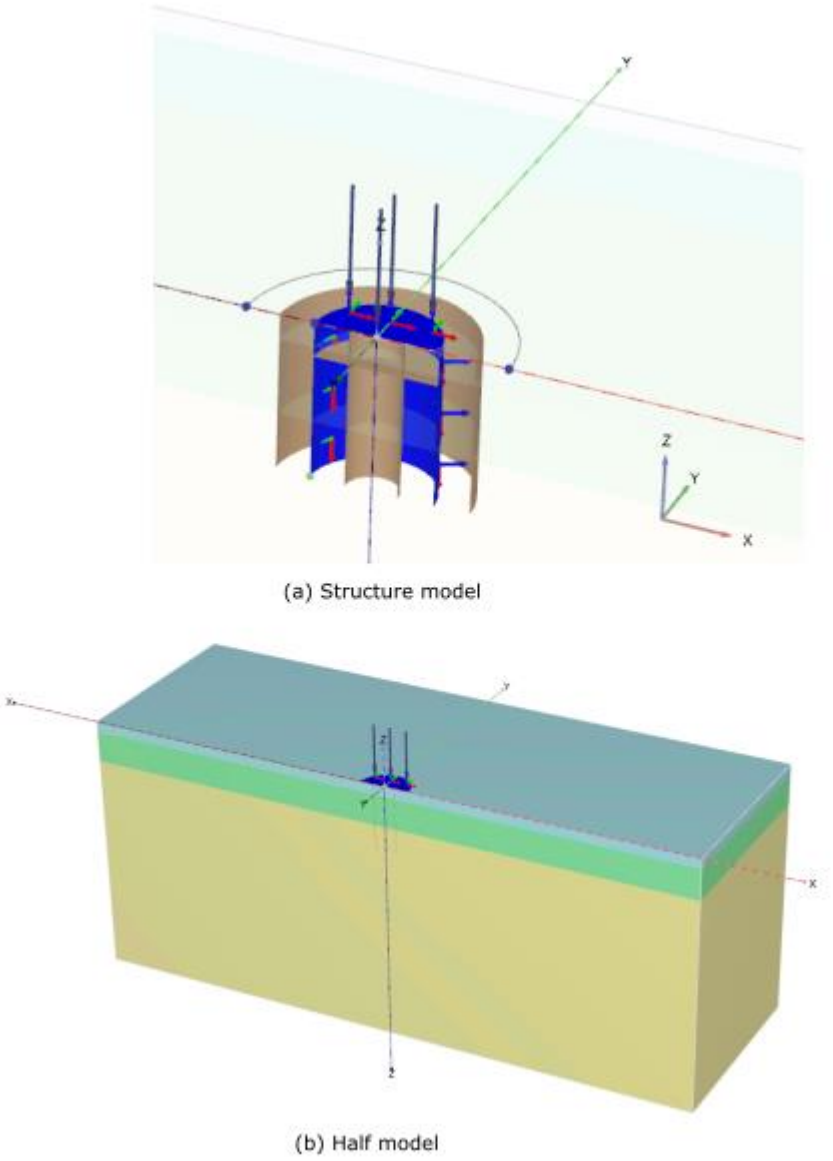

Figure 56 PLAXIS 3D model for Case study#2

5.2.3 Loading

In order to obtain the characteristic graph of C_v varying with the forcing amplitude for a particular frequency, four dynamic load amplitudes ranging from 5% to 50% of the dynamic component of the vertical ULS load amplitude is chosen.

The frequency of the loading is selected such that it matches the natural frequency of the structure. In this case, since the first two mode frequencies are approximately the same ($\approx 0.25Hz$), the loading frequency of 0.25 Hz is chosen. Ten loading cycles is applied for each case.

The dynamic vertical load amplitude (V_{dyn}) = 17.78 MN

Freq/Dyam	5% of V_{dyn}	10% of V_{dyn}	20% of V_{dyn}	50% of V_{dyn}
0.25 Hz	Case 1	Case 2	Case 3	Case 4

5.3 Phase Shift Method (Step #3)

The PLAXIS output of u_z v/s dynamic time for each load case is exported to MATLAB to further calculate C_v using the phase shift method. The table below gives a brief summary of the method;

Fit PLAXIS 2D output to sine curve	$m + Asin(\Omega t + \varphi)$
Consider SDOF system	$M\ddot{z} + C\dot{z} + Kz = F$ $F = F_a e^{i\Omega t}$ $z = \widetilde{z_a} e^{i\Omega t}$ $\widetilde{z_a} = z_a e^{i\varphi}$
Calculate damping coefficient (C)	$C = \frac{Im\left(\frac{F_a}{\widetilde{z_a}}\right)}{\Omega}$

Table 2 The Phase Shift Method

The C_v *(Ns/m)* obtained in this step are as follows;

Freq/Dyam	5% of V_{dyn}	10% of V_{dyn}	20% of V_{dyn}	50% of V_{dyn}
0.25 Hz	1.08E+08	1.17E+08	1.26E+08	1.32E+08

5.4 Modal Damping (Step #4)

5.4.1 Modal Analysis Method

This step has been elaborated in a tabular manner for a better understanding.

Step	Procedure	Equations
1	Equation of motion with damping	$\boldsymbol{M\ddot{u} + C\dot{u} + Ku = F}$
2	Solving for Eigen modes	Substitute $\boldsymbol{C} = 0$ Solve $\boldsymbol{M\ddot{u} + Ku} = 0$
3	Vibration mode shapes obtained	$\boldsymbol{U}_i$ solves $\boldsymbol{KU}_i = \boldsymbol{\omega}_i^2 \boldsymbol{MU}_i$
4	Normalize the vibration mode	$\boldsymbol{U}_i \rightarrow \boldsymbol{\phi}_i$
5	Obtain generalized mass and stiffness matrices	$\boldsymbol{M}_{gen} = \boldsymbol{\phi}_i^T \boldsymbol{M} \boldsymbol{\phi}_i$ $\boldsymbol{M}_{gen} = 1$ (for diagonal terms) $\boldsymbol{M}_{gen} = 0$ (for non-diagonal terms) $\boldsymbol{K}_{gen} = \boldsymbol{\phi}_i^T \boldsymbol{K} \boldsymbol{\phi}_i$ $\boldsymbol{K}_{gen} = \boldsymbol{\omega}_i^2$ (for diagonal terms) $\boldsymbol{K}_{gen} = 0$ (for non-diagonal terms)
6	Obtain generalized damping matrix	$\boldsymbol{C}_{gen} = \boldsymbol{\phi}_i^T \boldsymbol{C} \boldsymbol{\phi}_i$
7	Calculate the modal damping	$\boldsymbol{C}_{modal,\ i} = \frac{\boldsymbol{C}_{gen}}{2\sqrt{\boldsymbol{M}_{gen} \times \boldsymbol{K}_{gen}}}$

From FEMAP one can directly get the $\boldsymbol{K}_{gen}$ and $\boldsymbol{M}_{gen}$ for the required eigen frequency. Since the dampers are external, one can use the T3 translations (≈mode shape) of the foundation nodes in FEMAP to formulate ϕ_i and further calculate the $\boldsymbol{C}_{gen}$. This can be further compared with the modal damping from free vibration analysis. Please note: this method is only applicable for the first

three modes in this case study, since the $\boldsymbol{C}_{gen}$ is a diagonal matrix for these modes.

Sample calculation

Considering the load case 1 for the first mode (0.247 Hz).

On running the eigen analysis in FEMAP one gets the following output;

$$M_{gen,1} = 1 \tag{40}$$

$$K_{gen,1} = {\omega_1}^2 = (2 \times \pi \times 0.247)^2 = 2.4163 \tag{41}$$

The translation in the global Z direction (axial direction of the spring element) gives the mode shape at the foundation nodes;

$$\phi_1 = \begin{bmatrix} -1.49\text{E}-08 \\ 2.86\text{E}-05 \\ -2.86\text{E}-05 \end{bmatrix} \tag{42}$$

Substituting the calculated C_v value from PLAXIS for $\boldsymbol{C}$;

$$\begin{aligned} C_{gen,1} &= {\phi_1}^T \boldsymbol{C} \phi_1 \\ &= \begin{bmatrix} -1.49\text{E}-08 \\ 2.86\text{E}-05 \\ -2.86\text{E}-05 \end{bmatrix}^T \begin{bmatrix} 1.08\text{E}+08 & 0 & 0 \\ 0 & 1.08\text{E}+08 & 0 \\ 0 & 0 & 1.08\text{E}+08 \end{bmatrix} \begin{bmatrix} -1.49\text{E}-08 \\ 2.86\text{E}-05 \\ -2.86\text{E}-05 \end{bmatrix} \\ &= 0.6126 \end{aligned} \tag{43}$$

The modal damping is finally calculated as;

$$C_{modal,\ 1} = \frac{C_{gen,1}}{2\sqrt{M_{gen,1} \times K_{gen,1}}} = \frac{0.6126}{2\sqrt{1 \times 2.4163}} = 0.0571 \tag{44}$$

The modal damping percentages calculated for all the cases is as follows;

Mode No.	Freq/Dyam	5% of V_{dyn}	10% of V_{dyn}	20% of V_{dyn}	50% of V_{dyn}
1	0.247 Hz	5.71 %	6.17 %	6.48 %	6.62 %

2	0.249 Hz	5.90 %	6.29 %	6.69 %	6.74 %

5.5 Discussion

The proposed method is summarized in this section. A comparison is made with the logarithmic decrement method and with past project data. The usability of the modal analysis method is further discussed towards the end of this section.

5.5.1 Method summary

The steps defined in the previous sections of this case-study can be now put together in order to summarize the proposed method.

Step 1: The structure is modelled in a FEM based software and an eigen value analysis is conducted in order to identify the eigen frequencies of the structure. The first two modes are considered to be critical, since these modes fall within the loading spectrum of the structure.

Step 2: The eigen mode frequency calculated in Step 1 is then used as the loading frequency input for PLAXIS along with a specified force amplitude range. A forced vibration analysis is then carried out in PLAXIS using HSsmall soil model for the specified site properties.

Step 3: The output from PLAXIS (displacement v/s time plots) is further analyzed in MATLAB in order to compute the damping coefficients using the Phase -Shift Method. This step finally gives damping coefficient as a function of force amplitude for a particular frequency.

Step 4: Modal analysis is carried out in this step with the help of the generalized stiffness and mass matrices obtained in Step1. The final outcome is the (soil) modal damping percentage for the first two modes of the structure.

5.5.2 Comparison with Logarithmic Decrement Method

Alternatively, the modal damping can be determined using the logarithmic decrement method. For this method, the calculated C_v (from PLAXIS 3D)can be introduced in the FEMAP model using spring/damper element for every suction pile. Free vibration analysis can be carried out for the first two modes by applying a unit pulse load at structure node that can excite the respective mode.

Note: It is very critical to apply the unit pulse loads at appropriate nodes in order to filter out the noise (due to other modes) in the free decay of a particular mode.

The table below shows application of the pulse loads for the two modes. Mode 1 would require a pulse load in the global Y direction while Mode 2 would require one in the global X direction.

Mode 1	Mode 2
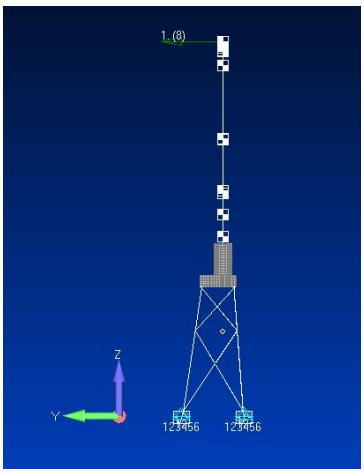	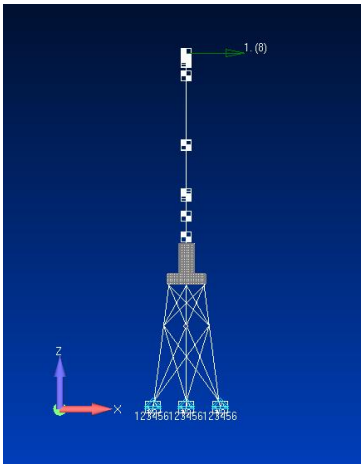

A typical decay plot would look like the figure below (Figure 57).

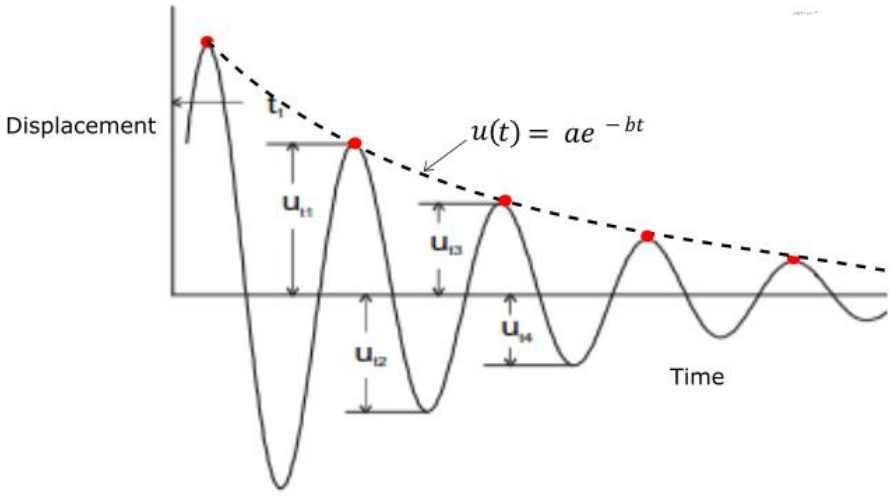

Figure 57 Illustrative decaying displacement time history

One can fit the peaks into an exponential curve of the form $u(t) = ae^{-bt}$ and derive the modal damping ratio **ξ** as $\frac{b}{\omega}$.

The results for the modal damping percentages calculated using logarithmic decrement method are as follows;

Mode No.	Freq/Dyam	5% of V_{dyn}	10% of V_{dyn}	20% of V_{dyn}	50% of V_{dyn}
1	0.247 Hz	5.32 %	5.65 %	5.96 %	5.96 %
2	0.249 Hz	5.06 %	5.37 %	5.66 %	5.65 %

Since the structure is free of any other damping sources (eg. wind, wave, steel etc), **the logarithmic decrement value solely gives the contribution of soil damping.** This can be verified by carrying out the free vibration analysis for

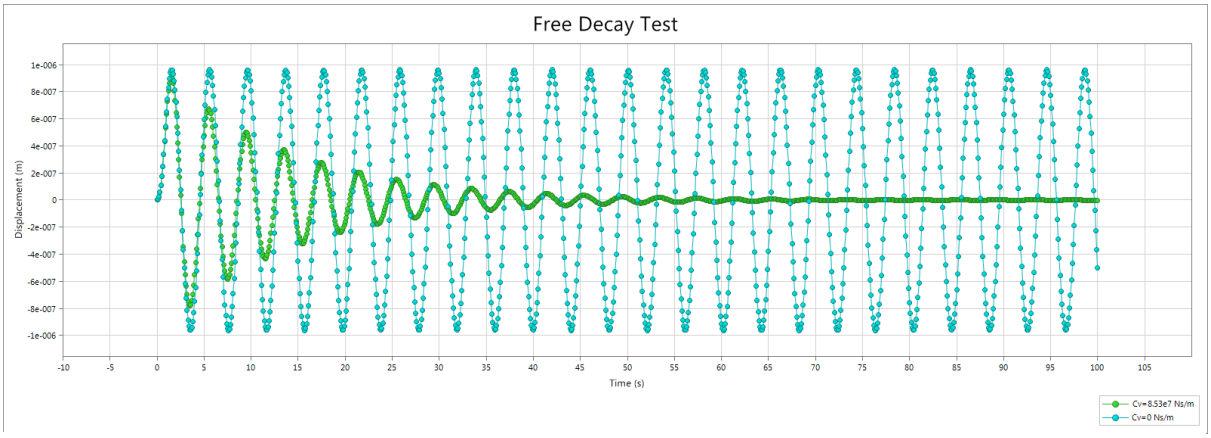

Figure 58 Free vibration analysis with and without the damper

C_v=0 *Ns/m.* No decay is observed for the case of C_v=0 (the blue plot in Figure 58). Hence it is safe to conclude that the external dampers (≈ damping from soil) are the only source of damping for the system.

Comparison

For a better comparison, the ratio of C_v obtained by the two method is calculated and tabulated below;

Mode No.	Freq/Dyam	5% of V_{dyn}	10% of V_{dyn}	20% of V_{dyn}	50% of V_{dyn}
1	0.247 Hz	1.07	1.09	1.11	1.11
2	0.249 Hz	1.17	1.19	1.21	1.21

Both the methods generate modal damping percentages within a difference range of 20%. The logarithmic decrement is however an approximate method and requires manual data logging of the results obtained from free decay analysis for each load case, which otherwise can be easily avoided in the Modal Analysis Method.

5.5.3 Comparison with past projects

The calculated soil modal damping percentages for the first two modes of a SIWT lie in the range of 5-7%. Making a direct comparison with other cases may require a detailed study regarding factors like structure type, dimensions, turbine capacity, soil type etc. Nevertheless, it is worthwhile to mention some benchmarked damping values.

Monopiles

	Tarp-Johansen *et al.* (2009)	Versteijlen *et al.* (2011)	Damgaard *et al.* (2012)	Damgaard *et al.* (2013)	Shirzadeh *et al.* (2013)	Carswell *et al.* (2014)
Method	Experimental	Experimental	Experimental	Experimental	Experimental	Numerical
Analysis	3D FEM	Modified *p-y*	Hysteretic *p-y*	Hysteretic *p-y*	HAWC2, Rayleigh	3D and 2D FEM
Turbine	3.5 MW (Scaled NREL 5 MW)	Siemens 3.6 MW	–	Vestas V90-3 MW	Vestas V90-3 MW (Scaled NREL 5 MW)	NREL 5 MW
Soil profile	Generalized sandy or clayey North Sea	–	Top layer loose sand, very stiff to very hard clay	Medium dense sand and soft clay	Dense sand with layer of stiff clay	Soft, stiff, and hard clay
ξ_{fdn}	0.56%–0.80%	1.5%	0.58%	0.8–1.3%	0.25%	0.17%–0.28%
ξ_{struc}	0.19%	1.5%	0.19%	–	0.6%	1.00%
Sum:	0.75–0.99%	3.0%	0.77%	0.8–1.3%	0.85%	1.17%–1.28%

Figure 59 Damping in monopiles: Source:(Carswell et al. 2015)

In a recent study by (Carswell et al. 2015), the authors have tabulated a summary of monopile-supported offshore wind-turbine damping results from literature (refer Figure 59).

Here ξ_{fdn} represents soil damping and the maximum damping is observed to be 1.5%. The values obtained in this case study are around 4 times the maximum damping that has been bench-marked yet (for monopiles). Many factors like structure type, dimensions, turbine capacity, soil type etc. need to be thoroughly considered in order to justify this comparison.

Borkum Riffgrund 1 Windfarm project

As mentioned before, **Borkum Riffgrund 1** has the first ever installed SIWT structure in a water depth of 24m and with suction piles of (8(L) x 8(D)) dimension. A measuring system was installed to carry test the new concept. The free decay of the transition piece accelerations after accidental boat impact was measured. The damping calculated was around 2.17%. This damping is inclusive of the wave, structure and soil damping(DONG 2014). The findings of the case study are significantly higher than 2.17%. This might be due to the fact that the modal soil damping percentages calculated are highly sensitive to C_v derived from PLAXIS which still needs to be validated.

5.5.4 Method usability

The proposed method is structure specific, i.e., it has been developed for a specific structure (SIWT) and it only caters to the first two eigen modes of the structure. Application of this method to other structures would require critical analysis based on the following points;

- **Diagonalized $\boldsymbol{C}_{gen}$**

  The modal analysis method is applicable only when the non-diagonal terms of the generalized damping matrix are negligible as compared to the diagonal terms. In Case study 2, the following $\boldsymbol{C}_{gen}$ matrix was obtained;

$$\boldsymbol{C}_{gen} = \begin{bmatrix} 0.1769 & 1.478e-07 \\ 1.478e-07 & 0.1844 \end{bmatrix}$$

It can be clearly seen that the non-diagonal terms for this case have an order of magnitude that is negligible as compared to the diagonal terms. In cases where this condition is not satisfied, application of this method is not suggested. In such cases either of the two approaches could be taken (ASEN);

a. Complex eigen system method

This method requires to set up and solve a different (augmented) Eigen problem that diagonalizes two matrices that comprise M, C and K as submatrices. The solution generally leads to frequencies and mode shapes that are complex.

This method is mathematically irreproachable and can solve the equation of motion (EOM) without any approximations. The EOM first needs to be transformed to the so called state space form, which involves a substantial amount of preparatory work. For systems with large number of DOF, this method is cumbersome. Moreover, the physical interpretation of complex frequencies and modes is less immediate and may require substantial expertise in math as well as engineering experiences. The method is also restricted to linear dynamic systems and its applicability to nonlinear system completely depends on any available form of linearization.

b. Direct time integration (DTI)

In this method, the EOM is integrated directly numerically in time, making the method completely general. It can not only handle linear EOM, but also non-linear systems. The main disadvantage is that it requires substantial expertise in computational handling of ODE.

- Rigid body behavior and DOF

Suction piles considered in this case study have an embedment depth to diameter ratio (L/D) ≤ 1. Due to their structural configuration, they mainly exhibit stiff/rigid body behavior. Moreover, in case of the tetrapod the moment loading is carried principally by 'push-pull' action by opposing

footings and it is the variation of vertical load that is most important(Houlsby et al. 2005).Hence an individual suction pile in this case-study could be idealized with a single vertical spring and dashpot system, making it easier to apply the Modal Analysis Method.

On the other hand, horizontal forces and overturning moments are dominant in case of monopiles. Monopiles have a larger L/D ratio (>6) and they exhibit flexible/ bending behavior. A popular model used for such cases is the Winkler foundation model, which comprises a beam attached to distributed springs and dashpots. The proposed Modal Analysis Method might not be a good approximation for such cases due to the existence of coupled horizontal and moment degrees of freedom.

In simpler words, the Modal Analysis Method is hypothesized to work well with piles that can be modelled as a single degree of freedom system or as multi-degree of freedom system with uncoupled DOFs.

- **Modal damping as a function of force amplitude**

  The obtained values of (soil) modal damping percentages, varies with force amplitude. Hence in dynamic loading conditions, as in the case of offshore wind and wave loading, selecting the right modal damping percentage for the required mode can be difficult. In order to be on the conservative side, one could chose the lowest modal damping percentage corresponding to the lowest force amplitude.

The applicability of the proposed Modal Analysis Method thus depends on various factors such as pile type, DOFs involved, loading conditions etc. For the case study at hand, this method allows straightforward reuse of undamped eigen frequencies and mode shapes, which are fairly easy to obtain with standard eigen solution software. The modal damping percentages obtained for the critical modes can be further used in advanced softwares like SACS, which allow the users to input different damping percentages for different modes.

6 The End

This chapter summarizes the conclusions drawn from both the case-studies and also provides recommendations for future research.

6.1 Conclusion

The thesis objective was identified as;

To develop a methodology to calculate the soil damping coefficients using PLAXIS and further apply it for the case of SIWT structure to find the soil damping in the form of modal damping percentage.

The objective consists of two tasks which were dealt by the two case-studies.

Case study #1

The methodology to calculate the damping coefficient from case study #1 can be summarized as follows;

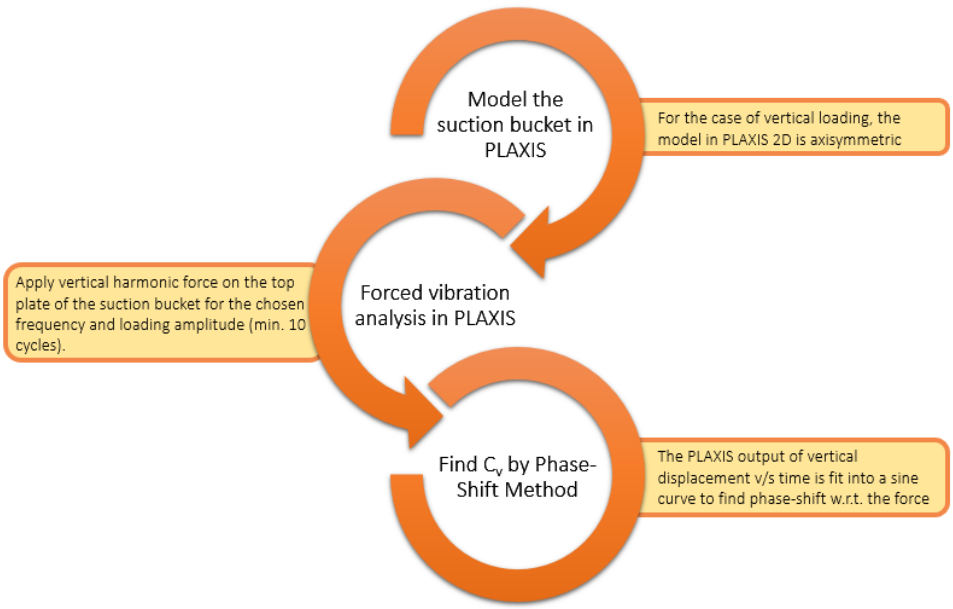

Following conclusions were made from Case-study #1;

- The damping coefficient increases with increase in the force amplitude. This effect is justified by the fact that higher force amplitudes correspond to higher strain amplitudes which further corresponds to higher values of the soil damping ratio.

- The damping coefficient decreases with increasing frequency. The decreasing behavior is due to the influence of hysteretic damping on the total soil damping.
- A comparison with Gazetas charts and Wolf's three parameter model showed that the hysteresis part of the calculated C_v seemed to comply with C_{hys} derived from Gazetas charts while the radiation part was approximated better by Wolf's three parameter model.
- A new damping coefficient C_{combi} ,was formulated by combining the Gazetas method with Wolf's three parameter model. This coefficient provided a reasonable approximation for the calculated C_v, especially at higher load levels and lower frequencies.
- The observed nature of these plots seemed to reasonably comply with existing literature and experimental data. However, the accuracy of the value of C_v is highly dependent on the PLAXIS output and hence adequate validation of the PLAXIS model is highly recommended.

Case study #2

In Case-study #2, the methodology developed in Case-study #1 was applied to the case of SIWT structure to find soil damping in the form of modal damping. The steps are as follows;

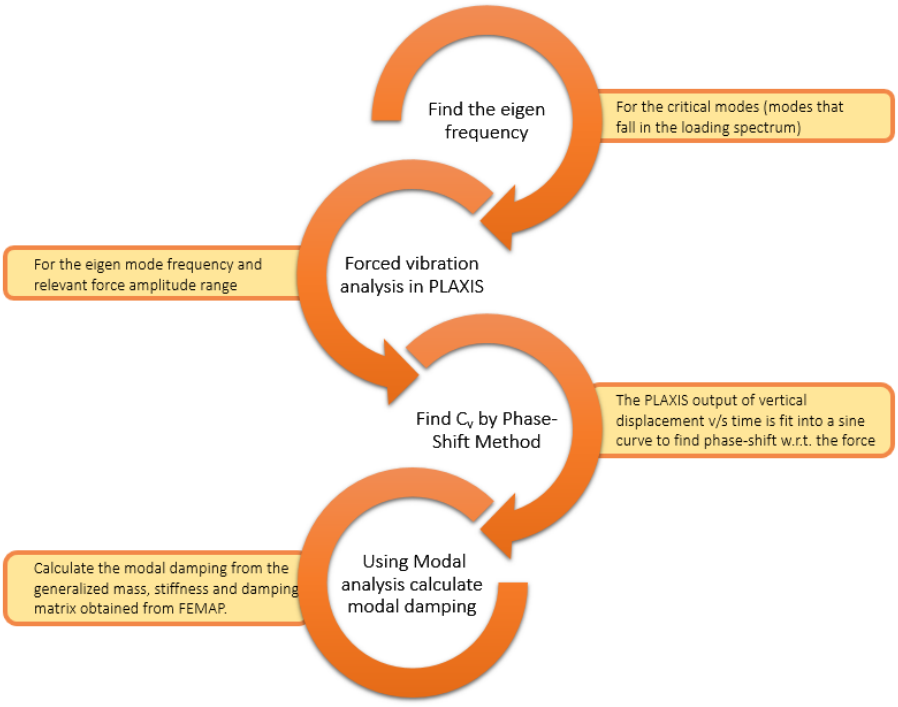

Following conclusions were drawn from Case study #2;

- The suggested method gives the soil modal damping percentages for the first two modes of the SIWT in the range of 5-7% which are significantly larger than the order of magnitude used in the industry today. However, one should realize that the modal soil damping percentage is highly sensitive to C_v derived from PLAXIS and hence in depth investigation of the PLAXIS model is highly recommended.
- Lack of full scale testing for this new concept makes it difficult to validate the obtained values. Since the focus of this thesis was on development of a methodology, the detailing required at each step is reserved for future research.
- In the final step of the method, two ways can be used to compute the modal damping: Modal Analysis and Logarithmic Decrement Method. The Modal analysis is less cumbersome as compared to the latter, since this method this method allows straightforward reuse of undamped eigen frequencies and mode shapes, which are fairly easy to obtain with standard eigen solution softwares.
- The applicability of the proposed Modal Analysis Method depends majorly on the generalized damping matrix. For the second case-study, this method was mainly justified since the generalized damping matrix $\boldsymbol{C}_{gen}$ was diagonalizable for the first two mode shapes.

6.2 Recommendations

Future work can be focused on the following points;

- **Suction pile geometry**

  The dimensions of the suction pile could play an important role in geometric damping. A parametric study based on varying radius and skirt length of the suction pile is further suggested in order to examine the impact of pile dimensions on soil damping.

- **Mean shift requires attention.**

  An interesting non-linearity in the form of mean shift, is observed in the PLAXIS output of displacement v/s time plots. This shift could be due to accumulation of plastic displacements. Further analysis on the mean shift can give an insight into the degree of non-linearity in the system.

- **Other degrees of freedom**

  An analytically background for applying the Phase-shift Method to a two degree of freedom system has been explained in Appendix D. This could provide basis for considering other degrees of freedom that are coupled (especially horizontal and rocking motion) in nature. Since this thesis only focused on the vertical degree of freedom of the suction pile, the other degrees of freedom such as horizontal, rotational and torsional, should also be tested for the proposed methodology. For instance, in the case of monopile suction foundation, the horizontal and the rotational degree of freedom is dominant as compared to vertical. Such cases will require the corresponding damping coefficients.

- **Experimental validation**

  A major part of this thesis is based on the results that PLAXIS generates. Hence it is highly recommended to validate the PLAXIS results against existing experimental data.

References

Andersen, Knut H, and Hans P Jostad. 2002. "Shear strength along outside wall of suction anchors in clay after installation." In *The Twelfth International Offshore and Polar Engineering Conference*. International Society of Offshore and Polar Engineers.

ASEN. 'Modal Analysis of MDOF Forced Damped Systems'. *http://www.colorado.edu/engineering/CAS/courses.d/Structures.d/IAST.Lect22.d/IAST.Lect22.Slides.pdf*

Ashmawy, AK, Rodrigo Salgado, Soumitra Guha, and VP Drnevich. 1995. 'Soil damping and its use in dynamic analyses'.

Bhattacharya, S, N Nikitas, J Garnsey, NA Alexander, J Cox, D Lombardi, D Muir Wood, and David FT Nash. 2013. 'Observed dynamic soil–structure interaction in scale testing of offshore wind turbine foundations', *Soil Dynamics and Earthquake Engineering*, 54: 47-60.

Bhushan, Prasad Bharat. 2011. *Advanced Soil Dynamics and Earthquake Engineering* (PHI Learning Pvt. Ltd.).

Bolton, MD, and JMR Wilson. 1990. *Soil stiffness and damping* (Cambridge Univ., Engineering Department).

Brinkgreve, RBJ, MH Kappert, and PG Bonnier. 2007. 'Hysteretic damping in a small-strain stiffness model', *Proc. of Num. Mod. in Geomech., NUMOG X, Rhodes*: 737-42.

Brinkgreve, Ronald BJ. 2005. "Selection of soil models and parameters for geotechnical engineering application." In *Soil constitutive models: Evaluation, selection, and calibration*, 69-98. ASCE.

Carswell, W, J Johansson, F Løvholt, SR Arwade, C Madshus, DJ DeGroot, and AT Myers. 2015. 'Foundation damping and the dynamics of offshore wind turbine monopiles', *Renewable Energy*, 80: 724-36.

Chakrabarti, Subrata. 2005. *Handbook of Offshore Engineering* (2-volume set) (Elsevier).

Chew, Kok Hon, EYK Ng, Kang Tai, Michael Muskulus, and Daniel Zwick. 2014. 'Offshore Wind Turbine Jacket Substructure: A Comparison Study Between Four-Legged and Three-Legged Designs', *Journal of Ocean and Wind Energy*, 1: 74-81.

De Vries, W. 2011. 'Support structure concepts for deep water sites. EU Project UpWind, final report WP 4.2', *Delft University of Technology*, The Netherlands.

DIN, ENISO. 2007. '19902: 2008-07: Petroleum and natural gas industries–Fixed steel offshore structures (ISO 19902: 2007)', *English version EN ISO*, 19902: 182-202.

DONG Energy. 2014. " The suction bucket jacket-a new wind turbine foundation concept"
ht*tp://www.danskgeotekniskforening.dk/sites/default/files/pdf/pdf2014/Moede%2010/1.%20BKR01-SBJ%20-%20CHMOR-%20Dansk%20geoteknisk%20forening%2020%20nov%202014%20%282%29%20pdf%20-%20Adobe%20Acrobat%20Professional.pdf.*

European Wind Energy Association. 2009. *The economics of wind energy (EWEA).*

European Wind Energy Association. 2015. 'The European offshore wind industry key trends and statistics 1st half 2015', *European Wind Energy Association* (EWEA), 1: 8.

Gazetas, George. 1991. 'Formulas and charts for impedances of surface and embedded foundations', *Journal of Geotechnical Engineering*, 117: 1363-81.

Gazetas, George, and Ricardo Dobry. 1984. 'Simple radiation damping model for piles and footings', *Journal of Engineering Mechanics*, 110: 937-56.

Gazetas, George, Ricardo Dobry, and John L Tassoulas. 1985. 'Vertical response of arbitrarily shaped embedded foundations', *Journal of Geotechnical Engineering*, 111: 750-71.

Houlsby, GT, RB Kelly, J Huxtable, and BW Byrne. 2005. 'Field trials of suction caissons in clay for offshore wind turbine foundations', *Géotechnique*, 55: 287-96.

Houlsby, GT, and BW Byrne. 2005. 'Design procedures for installation of suction caissons in clay and other materials', *Geotech. Eng*, 158: 75-82.

Lesny, Kerstin. 2010. Foundations for offshore wind turbines: tools for planning and design (VGE-Verlag).

Lysmer, JFER, and Frank Edwin Richart. 1966. 'Dynamic response of footings to vertical loading', *Journal of Soil Mechanics & Foundations Div*.

NREL. 2014. 'Cost of Wind Energy Review'.

Pisanò, Federico. 2015. 'Lecture notes for OE4624-15 Offshore Geotechnical Engineering'.

Richart, FE, JR Hall, and RD Woods. 1970. "Vibrations of soils and foundations. International Series in Theoretical and Applied Mechanics." In.: *Englewood Cliffs*, NJ: Prentice-Hall.

Spijkers, J, A Vrouwenvelder, and E Klaver. 2005. 'Lecture notes structural dynamics ct4140', *Delft University of Technology*.

Tatsuoka, Fumio, Toshio Iwasaki, and Yoshikazu Takagi. 1978a. 'Hysteretic damping of sands under cyclic loading and its relation to shear modulus', *Japanese Society of Soil Mechanics and Foundation Engineering*, 18: 25-40.

Tatsuoka, Fumio, Toshio Iwasaki, and Yoshikazu Takagi. 1978b. 'Shear moduli of sands under cyclic torsional shear loading', *Japanese Society of Soil Mechanics and Foundation Engineering*, 18: 39-56.

Tjelta, TI. 2015. 'The suction foundation technology', *Frontiers in Offshore Geotechnics III*, 85.

Appendix A

Mesh convergence study for Case Study#1

The corresponding figures of the mesh convergence study done in Case Study#1 are as follows;

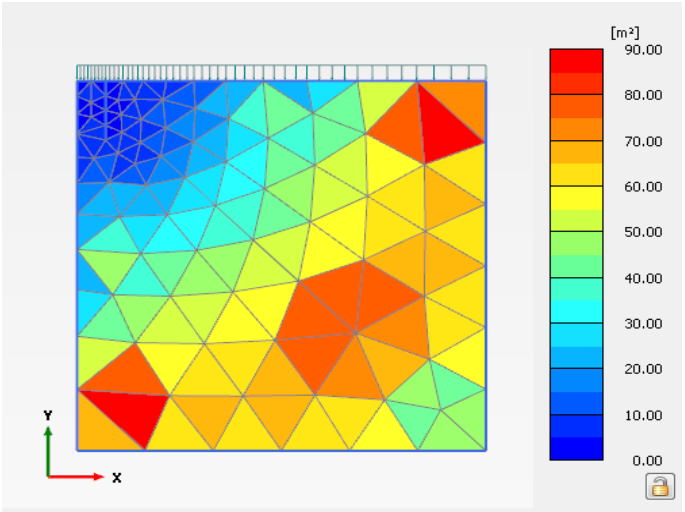

Figure 63 Very coarse mesh

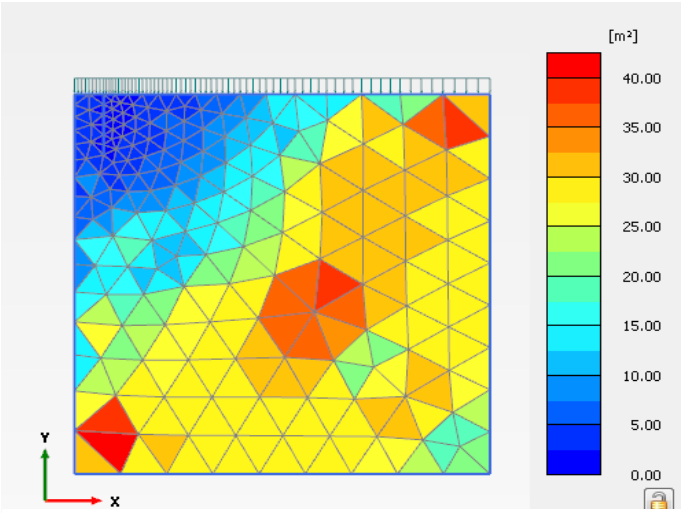

Figure 63 Coarse mesh

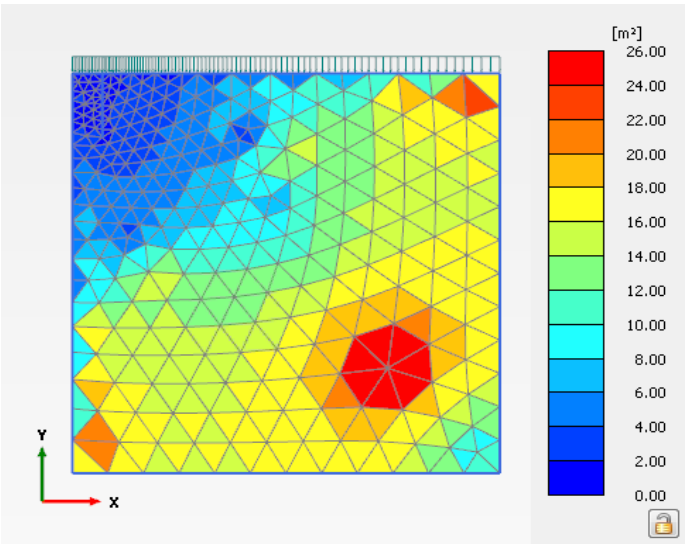

Figure 63 Medium mesh

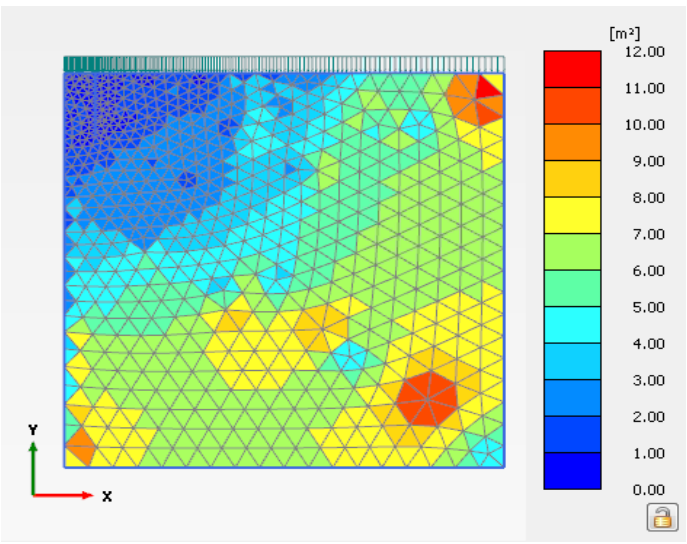

Figure 63 Fine mesh

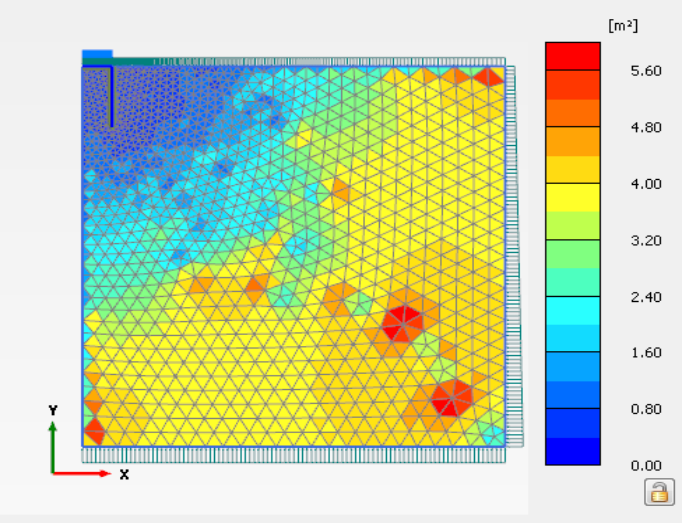

Figure 64 Very fine mesh

Appendix B

Phase-shift Method for SDOF system

▪ Analytical Background

The method to calculate the damping from phase shift for a SDOF system is derived below;

1. Equation of motion can be written as follows;

$$M\ddot{z} + C\dot{z} + Kz = F \tag{45}$$

2. The external force can be written as;

$$F = F_a e^{i\Omega t} \tag{46}$$

   - F_a : Force amplitude (real number)
   - Ω: Forcing frequency

3. The response z can be written as;

$$z = \widetilde{z_a} e^{i\Omega t} \tag{47}$$

   - $\widetilde{z_a}$: Response amplitude (complex number)

$$\widetilde{z_a} = z_a e^{i\varphi} \tag{48}$$

   Where φ is the phase shift.

   - Derivatives of z can be written as;

$$\dot{z} = i\Omega \widetilde{z_a} e^{i\Omega t} \tag{49}$$

$$\ddot{z} = -\Omega^2 \widetilde{z_a} e^{i\Omega t} \tag{50}$$

4. Substituting in the EOM, one gets;

$$M\left(-\Omega^2\widetilde{z_a}e^{i\Omega t}\right) + C\left(i\Omega\widetilde{z_a}e^{i\Omega t}\right) + K\left(\widetilde{z_a}e^{i\Omega t}\right) = F_a e^{i\Omega t} \quad (51)$$

$$(K - \Omega^2 M + Ci\Omega)\widetilde{z_a}e^{i\Omega t} = F_a e^{i\Omega t} \quad (52)$$

$$(K - \Omega^2 M + Ci\Omega) = \frac{F_a}{\widetilde{z_a}} \quad (53)$$

5. Separating the real and imaginary part of the equation;

$$Re\left(\frac{F_a}{\widetilde{z_a}}\right) = K - \Omega^2 M \qquad Im\left(\frac{F_a}{\widetilde{z_a}}\right) = Im(Ci\Omega) = C\Omega \quad (54)$$

6. The damping coefficient c can be written as;

$$C = \frac{Im\left(\frac{F_a}{\widetilde{z_a}}\right)}{\Omega} \quad (55)$$

▪ Matlab Script

```
% PHASE SHIFT METHOD
% This script calculates the damping coefficient for a single frequency by fitting the PLAXIS
% output (displacement v/s time ) into a sine curve and futhur calculates
% the coefficient from the phase shift.

clear all; close all; clc; format compact
% The input file data.mat consists of response data from PLAXIS in form of time and
displacement
load data.mat

%for single frequency
freq=0.25;
w=2*pi*freq;

%Forcing amplitude range : 5% 10% 20% 50% of the ultimate dynamic load
f=[-890000 -1780000 -3560000 -8900000]; % dynamic loading amplitude in N

%A pointer variable
v=1;

%To fit the output resposne into sine curve
ft = fittype('m+b*x+A*sin(w*x + p)','coefficients',{'m','b','A','p'},'problem',{'w'});

% Modification of the output response
% The output response from PLAXIS 2D is modified in a way that it fits a
```

```
% sine curve. This is done to get the steady state values of the phase
% shift,amplitude and mean shift.

%calculations

    T = time; % from data.mat
    figure('units','normalized','outerposition',[0 0 1 1])
    str=sprintf('Frequency %g  Hz\n',freq);
    suptitle(str)
    for i= 1:1:4     % for 4 cases of loading amplitudes


        R = responseV(:,v); % from data.mat
             F_i=fit(T,R,ft,'problem',w,...
            'StartPoint',[mean(R),mean(R)/10, (max(R)-min(R))/2,pi],...
            'Lower', [-Inf,-Inf, 0, 0]);

        F_ix=0:0.005:50;
        F_iy=F_i(F_ix);



        %graph plots
        subplot(2,2,i)
        plot(F_ix,F_iy,'b')
        str=sprintf('Force amplitude   %i  KN',-f(i)/1000);
        title(str)
        hold on
        plot(T,R,'r')
        xlabel('Time [s]')
        ylabel('Amplitude [m]')
        legend('fitted curve','original response')


        %Damping ratio calculation
        REAL_PART_1=F_i.A*cos(F_i.p);
        IMAG_PART_1=F_i.A*sin(F_i.p);
        C(i)=imag(f(i)/(REAL_PART_1+1i*IMAG_PART_1))/w;
        F(i)=real(f(i)/(REAL_PART_1+1i*IMAG_PART_1));

        %Response Amplitude
        A(i)=F_i.A;

        %Phase shift
        p(i)=F_i.p;

        %Mean shift
        m(i)=F_i.m;

        %v increases by 1
        v=v+1;

    end
```

- **Curve fit plots**

Frequency 0.2 Hz

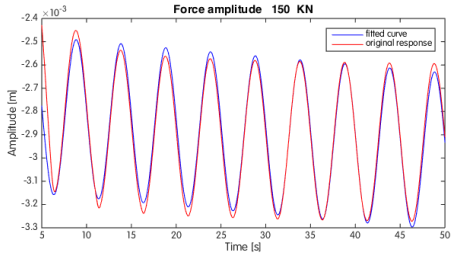

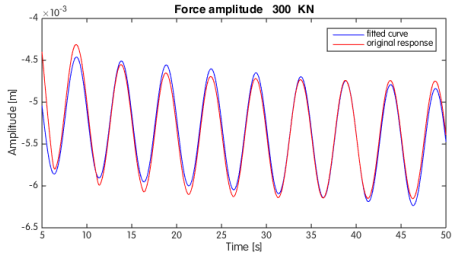

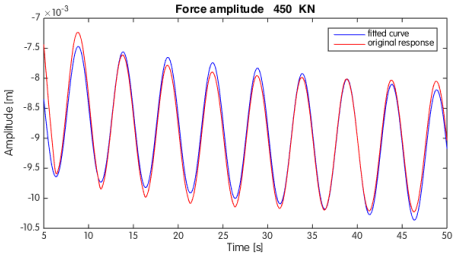

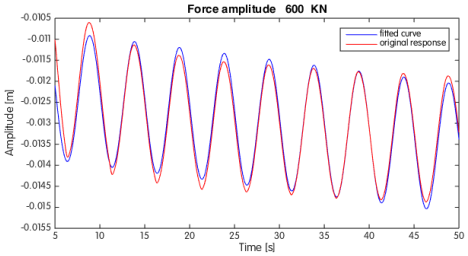

Frequency 0.4 Hz

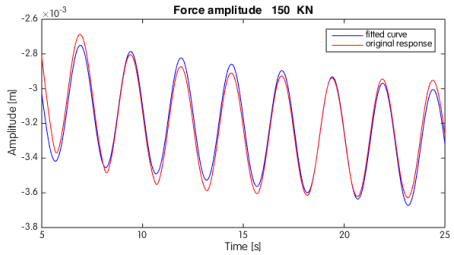

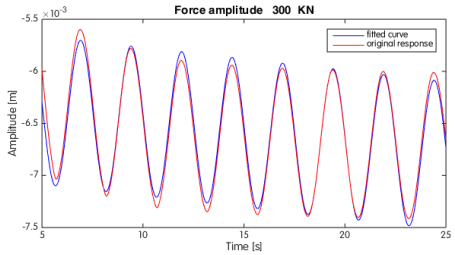

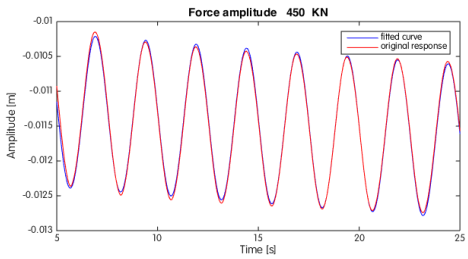

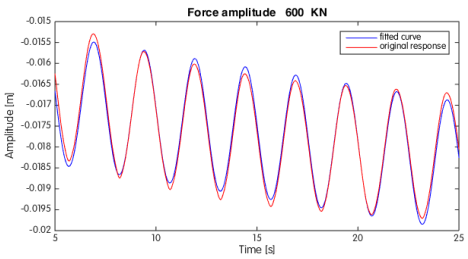

Frequency 0.6 Hz

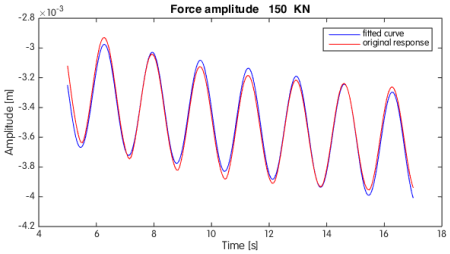

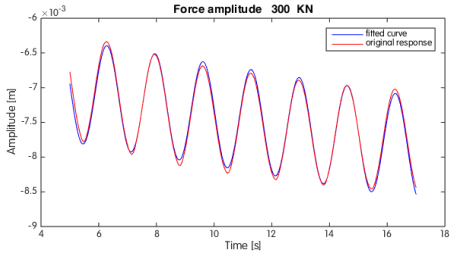

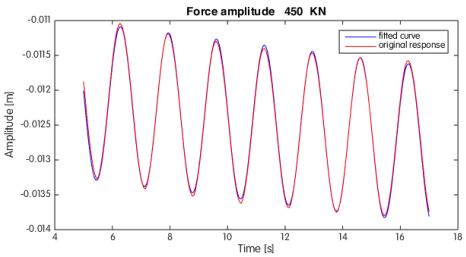

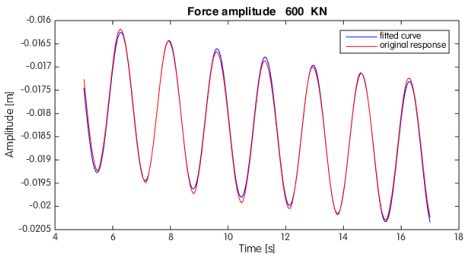

Frequency 0.8 Hz

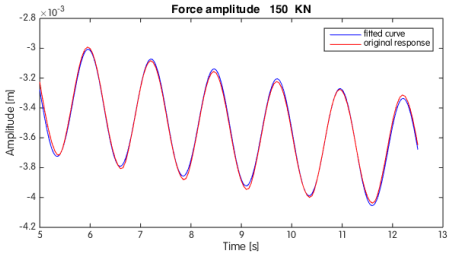

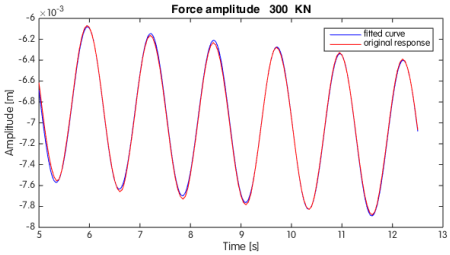

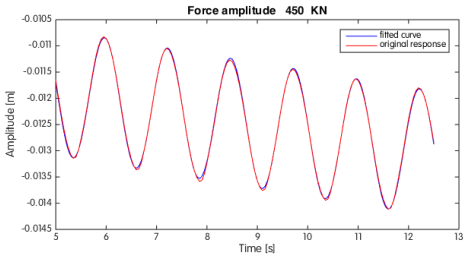

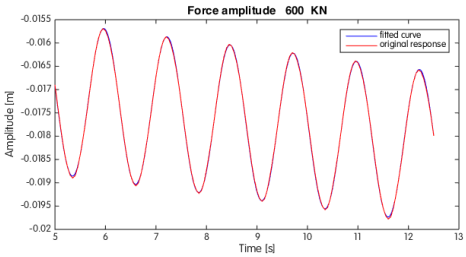

Appendix C

Calculating damping coefficient using Gazetas Charts

The parameters required for this calculation are as follows;

PARAMETER	VALUE/UNIT	COMMENT
Circumscribed rectangle dimensions (B & L)	3.5 m	Since the pile is circular, B=L. In this case it denotes the radius of the pile.
Embedment depth (D)	8 m	Gazetas also defines 'd' which is the height sidewall-soil contact surface. For the case of piles d= D.
Poisson's ratio (ν)	0.2	Project specific
Shear Modulus (G)	17.2e6 N/m^2	Gazetas method is very sensitive to the chosen shear modulus and stiffness of the foundation. The shear modulus for this case is chosen from the reduction curves of HSsmall soil model (PLAXIS generated) for the corresponding level of shear strain.
Soil density (ρ)	1.84e3 kg/m^3	Project specific
Soil hysteretic damping coefficient (β)	0.03	Generally used for clay (refer Figure 17)
Loading frequency (f)	0.2 -1.0 Hz	Project specific range

The calculated parameters are presented in the table below;

PARAMETER	VALUE/UNIT	CALCULATION
Area of the side wall (A_w)	3.5 m	$A_w = 2\pi BD$
Area of the base (A_b)	8 m	$A_b = \pi B^2$
Shear wave velocity (V_s)	96 m/s	$V_s = \sqrt{\frac{G}{\rho}}$

Lysmer's analog velocity (V_s)	17.2e6 N/m^2	$V_{La} = \frac{3.4 \times V_s}{\pi\,(1-v)}$
Cyclic loading frequency (ω)	1.26 - 6.28 rad/sec	$\omega = 2\pi f$
Dimensionless frequency (a_0)	0.0455 - 0.2273	$a_0 = \frac{\omega\, B}{V_s}$

With the specified parameters, the vertical damping coefficient $C_v(\equiv C_{total})$ is calculated from the formulae specified in Gazetas charts. The calculation for the case of 0.2 Hz is demonstrated below;

$$C_{total} = C_{rad} + C_{hsy} \tag{56}$$

$$C_{rad} = (\rho V_{La} A_b)\tilde{c}_z + \rho V_s A_s \tag{57}$$

Here $\tilde{c}_z = \tilde{c}_z(a_0; \frac{L}{B}, v)$ is taken from the graphs shown in Figure 65.

It is interesting to note that for the entire a_0 range (0.0455-0.2273), the value of $\tilde{c}_z$ is almost constant with $\tilde{c}_z \approx 0.9$. Hence for the entire frequency range, $C_{rad} \approx$ 3.95e7 Ns/m.

C_{hsy} on the other hand, varies inversely with the cyclic frequency (ω) according to the following equation;

$$C_{hys} = \frac{2\widetilde{K}}{\omega}\beta \tag{58}$$

Here $\widetilde{K}$=5.73e8 N/m is the dynamic stiffness of the pile which is also calculated from Gazetas charts. For f=0.2 Hz, C_{hys} =2.738e7 Ns/m.

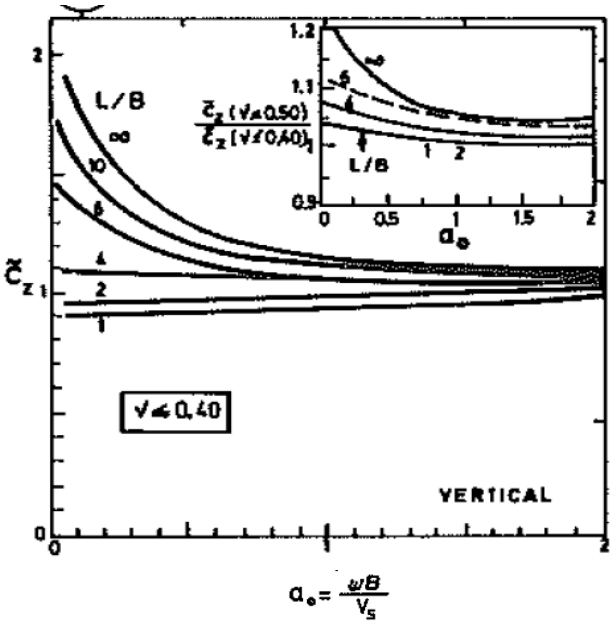

Figure 65 Dimensionless graph for determining dynamic damping coefficients ; Source:(Gazetas 1991)

The total vertical damping coefficient is then calculated as;

$$C_v = 3.95\text{e}7 + 2.738\text{e}7 = 6.69\text{e}7 \text{ Ns/m} \tag{59}$$

Similar procedure is applied for all the frequencies in order to calculate C_v. The calculated values have been plotted in Figure 66.

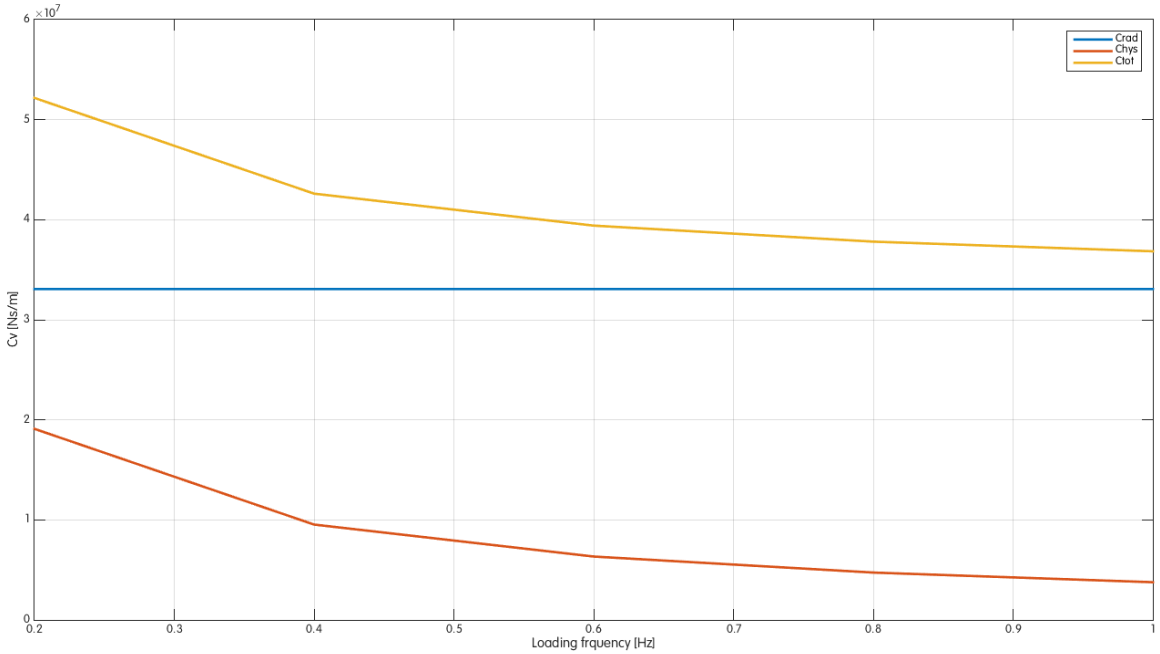

Figure 66 Vertical damping coefficient v/s loading frequency plot

Appendix D

Phase-shift Method for two degree of freedom system

- **Analytical Background**

The Phase-shift method for Two Degree of Freedom System can be derived as follows;

1. Let **u** and θ be the horizontal displacement and rotation respectively.

$$u = u_a e^{i\Omega t} \tag{60}$$

$$\theta = \theta_a e^{i\Omega t} \tag{61}$$

Where Ω is the frequency of prescribed displacement and u_a, θ_a are real valued.

2. The external loading is defined as a harmonic force (**F**) and a harmonic moment (**P**).

$$F = \bar{F}_a e^{i\Omega t} \tag{62}$$

Where $\bar{F}_a$ is a complex valued and φ is the phase shift w.r.t to **u**

$$\bar{F}_a = F_a e^{i\varphi} \tag{63}$$

Similarly, for P;

$$P = \bar{P}_a e^{i\Omega t} \tag{64}$$

Where $\bar{P}_a$ is a complex valued and α is the phase shift w.r.t to θ

$$\bar{P}_a = P_a e^{i\alpha} \tag{65}$$

3. The equation of motion can be formulated as;

$$\begin{bmatrix} M_H & M_{HM} \\ M_{HM} & M_M \end{bmatrix} \begin{bmatrix} \ddot{u} \\ \ddot{\theta} \end{bmatrix} + \begin{bmatrix} C_H & C_{HM} \\ C_{HM} & C_M \end{bmatrix} \begin{bmatrix} \dot{u} \\ \dot{\theta} \end{bmatrix} + \begin{bmatrix} K_H & K_{HM} \\ K_{HM} & K_M \end{bmatrix} \begin{bmatrix} u \\ \theta \end{bmatrix} = \begin{bmatrix} F \\ P \end{bmatrix} \tag{66}$$

$$= \begin{bmatrix} M_H & M_{HM} \\ M_{HM} & M_M \end{bmatrix} \begin{bmatrix} -\Omega^2 u_a \\ -\Omega^2 \theta_a \end{bmatrix} e^{i\Omega t} + \begin{bmatrix} C_H & C_{HM} \\ C_{HM} & C_M \end{bmatrix} \begin{bmatrix} i\Omega u_a \\ i\Omega \theta_a \end{bmatrix} e^{i\Omega t} + \begin{bmatrix} K_H & K_{HM} \\ K_{HM} & K_M \end{bmatrix} \begin{bmatrix} u_a \\ \theta_a \end{bmatrix} e^{i\Omega t} = \begin{bmatrix} F_a e^{i\varphi} \\ P_a e^{i\alpha} \end{bmatrix} e^{i\Omega t} \tag{67}$$

$$= \begin{bmatrix} -\Omega^2 M_H + i\Omega C_H + K_H & -\Omega^2 M_{HM} + i\Omega C_{HM} + K_{HM} \\ -\Omega^2 M_{HM} + i\Omega C_{HM} + K_{HM} & -\Omega^2 M_M + i\Omega C_M + K_M \end{bmatrix} \begin{bmatrix} u_a \\ \theta_a \end{bmatrix} = \begin{bmatrix} F_a e^{i\varphi} \\ P_a e^{i\alpha} \end{bmatrix} \quad (68)$$

4. Substituting $\theta_a = 0$ and comparing the imaginary parts in eq. 67;

$$\Omega C_H u_a = F_a \sin\varphi \quad (69)$$

$$C_H = \frac{F_a \sin\varphi}{u_a\, \Omega} \quad (70)$$

Similarly

$$C_{HM} = \frac{P_a \sin\alpha}{u_a\, \Omega} \quad (71)$$

This document ends here.